Stellar Oscillations:
Pulsations of Stars Throughout the H-R diagram

Mike Montgomery

Department of Astronomy and McDonald Observatory,
The University of Texas at Austin

January 15, 2013

Stellar Oscillations

Why study stars in the first place?

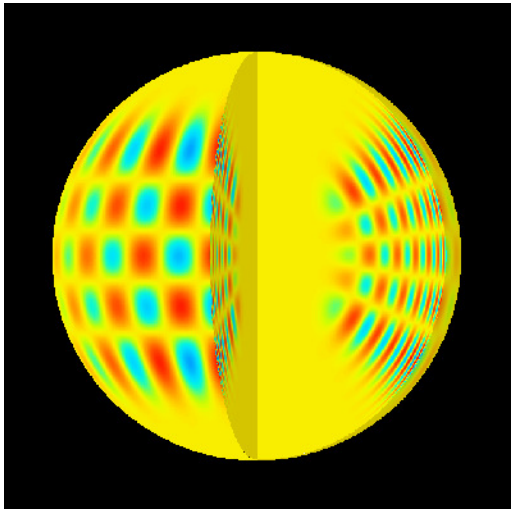

- Distance scales
  - Cepheids/RR Lyrae stars
  - Planetary Nebulae
  - Supernovae
- Ages
  - Main-Sequence turnoff
  - White Dwarf cooling
- Chemical Evolution
  - stellar nucleosynthesis
  - ISM enrichment

The Role of the Star in Astrophysics

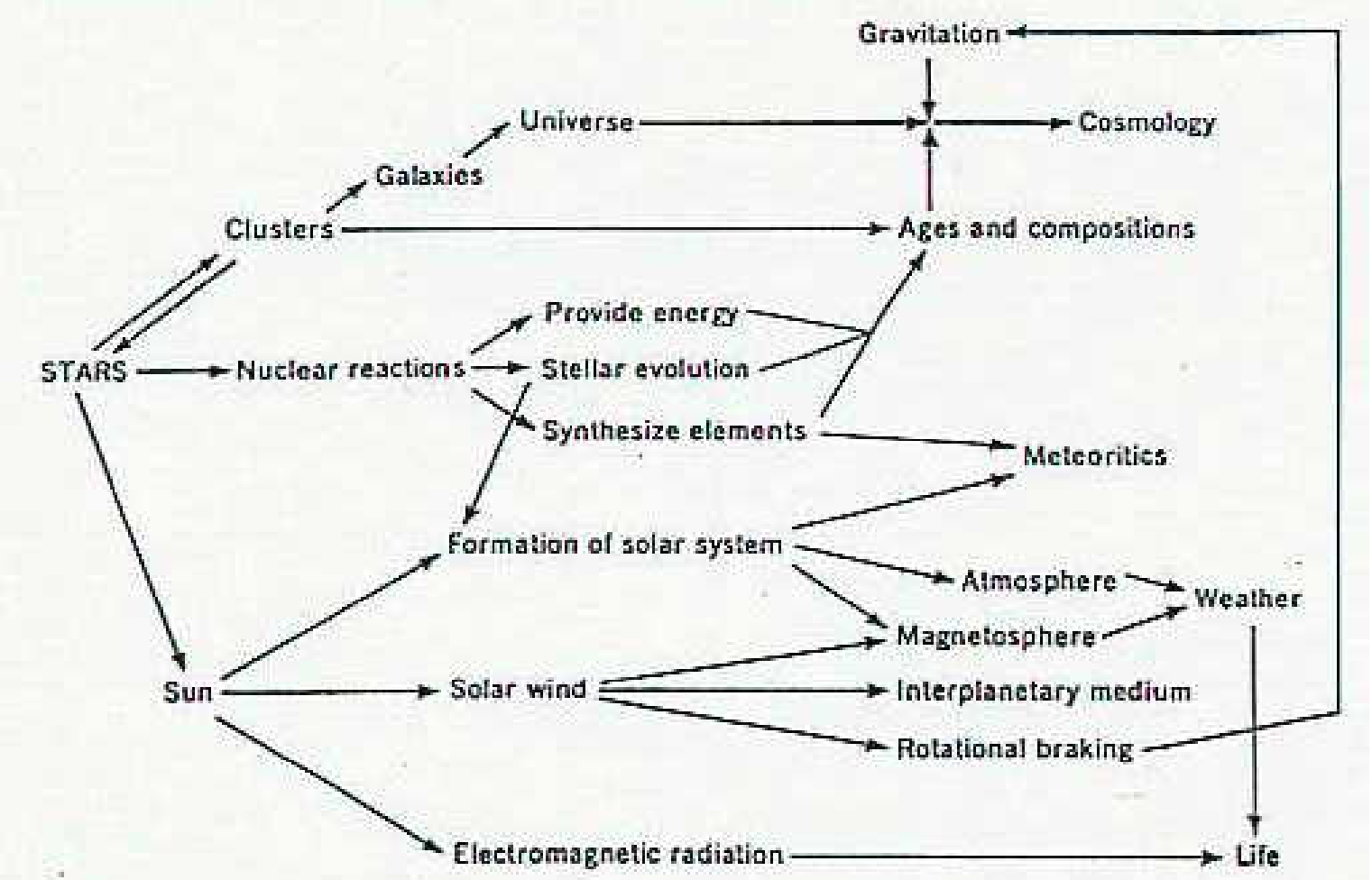

Figure 1.1. The role of the star in astrophysics. Almost every subject in astrophysics is influenced by our ideas about the structure and evolution of the stars. (From Clayton 1968).

The Role of the Star in Astrophysics

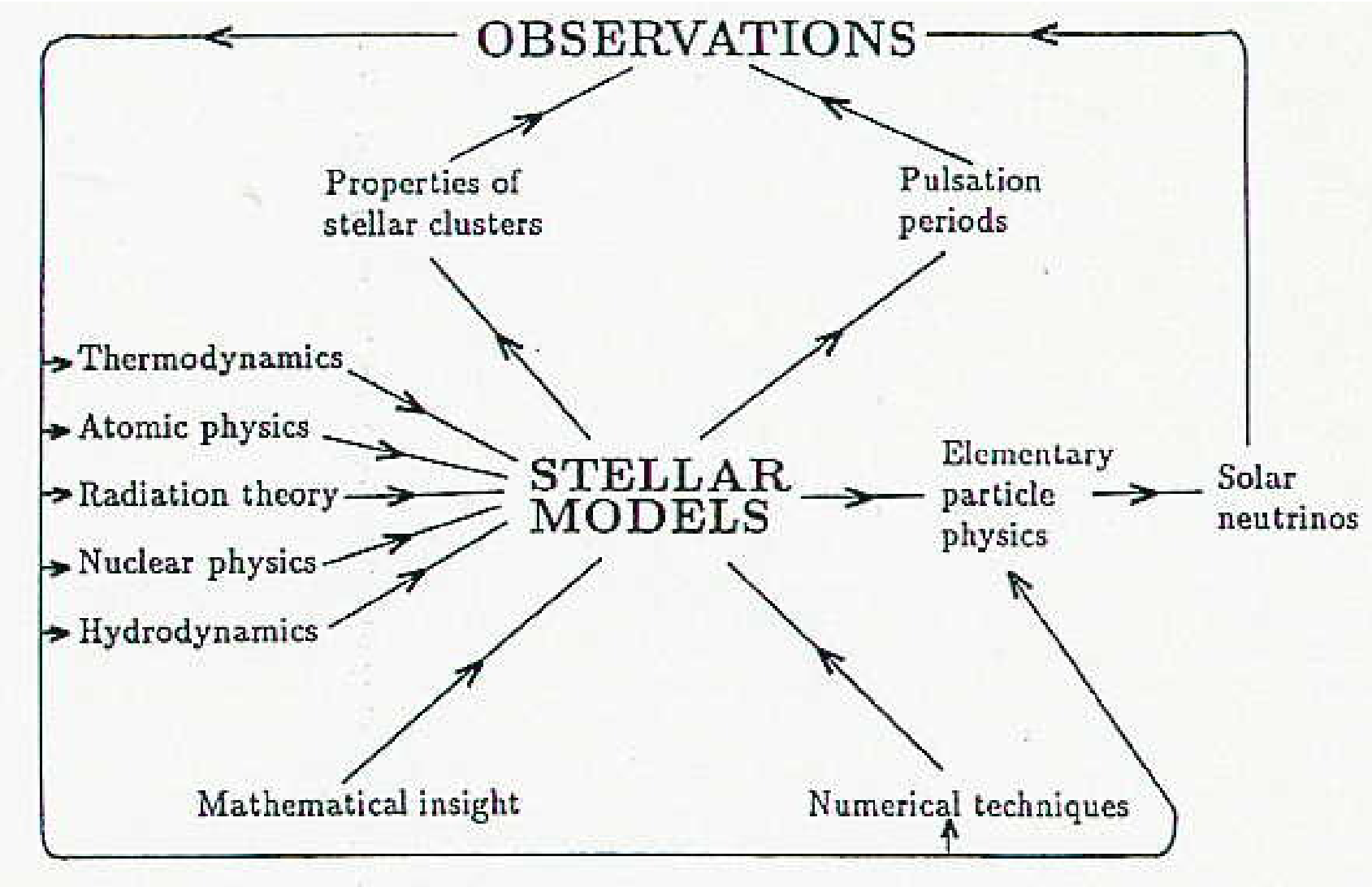

- Stars as laboratories for fundamental/exotic physics
  - General Relativity (binary NS)
  - Neutrino Physics (solar neutrinos, white dwarf cooling, SN neutrinos)
  - Degenerate Matter (white dwarfs, neutron stars, red giant cores)
  - convection
  - diffusion
  - hydrodynamics
  - magnetic fields
  - rotation

Ok, but why study *pulsating* stars?

Pulsations give us a *differential* view of a star:

- not limited to global quantities such as $T_{\rm eff}$ and $\log g$
- get a dynamic versus a static picture
- can 'see inside' the stars, study stellar interiors ('helio- and asteroseismology')
- potential to measure rotation (solid body and differential)
- find thickness of convection zones

A pulsational H-R diagram. The gold dashed curve shows the ZAMS, and the solid blue curve shows the white dwarf cooling curve. The classical instability strip is also indicated.

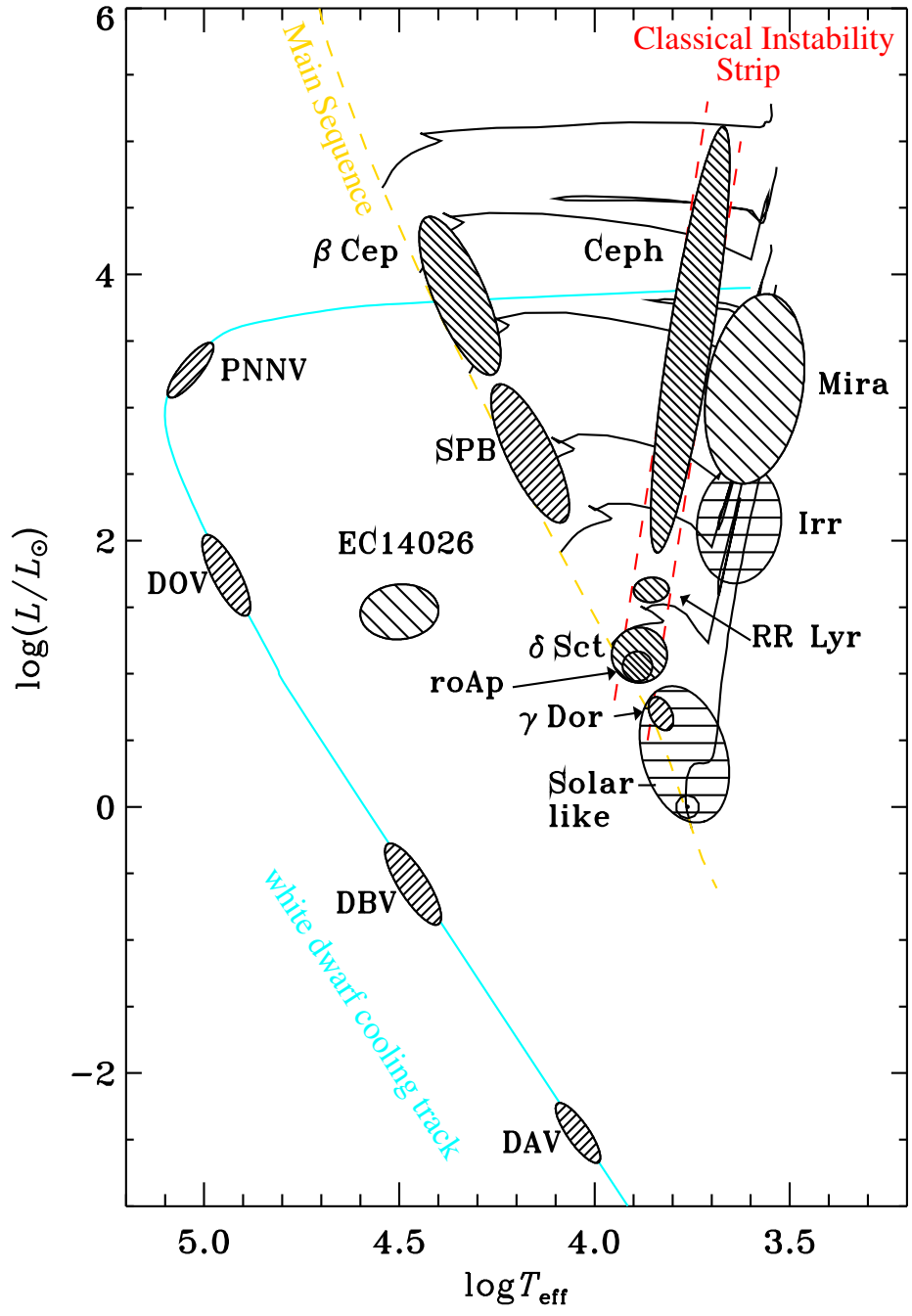

Theory of Stellar Pulsations

- Stellar pulsations are global eigenmodes
  Assuming they have “small” amplitudes,
  they are …
  - coherent fluid motions of the entire star
  - sinusoidal in time
  - the time-dependent quantities are characterized by small departures about the equilibrium state of the star
  - the angular dependence is $\propto Y_{\ell m}(\theta, \phi)$, if the equilibrium model is spherically symmetric

Review: the Vibrating String

$$\frac{\partial^2 \Psi}{\partial x^2} - \frac{1}{c^2}\frac{\partial^2 \Psi}{\partial t^2} = 0$$

Assuming $\Psi(x,t) = e^{i\omega t}\psi(x)$, this becomes

$$\frac{d^2\psi}{dx^2} - \frac{\omega^2}{c^2}\psi = 0,$$

which, together with the boundary conditions $\psi(0) = 0 = \psi(L)$, has the solution

$$\psi_n = A\sin(k_n x),$$

where

$$\omega_n = k_n c, \quad k_n = \tfrac{n\pi}{L}, \quad n = 1, 2, \ldots$$

Thus, we obtain a discrete set of eigenfrequencies, each of whose eigenfunctions has a different spatial structure.

Completely analogous to the case of pulsations of a star:
(Montgomery, Metcalfe, & Winget 2003, MNRAS, 344, 657)

vibrating string		**stellar pulsations**
wave equation	$\longleftrightarrow$	fluid equations (e.g., mass and momentum cons.)
frequencies (ω_n)	$\longleftrightarrow$	frequencies (ω_n)
vertical displacement	$\longleftrightarrow$	radial displacement (δr), or pressure (δp) eigenfunction
1D spatial eigenfunction	$\longleftrightarrow$	1D in radius $\times$ 2D in θ, ϕ ($Y_{\ell m}(\theta, \phi)$)

The time dependence ($e^{i\omega t}$) of both are identical

Stellar Hydrodynamics Equations

- mass conservation

$$\frac{\partial \rho}{\partial t} + \nabla \cdot (\rho \mathbf{v}) = 0$$

- momentum conservation

$$\rho \left(\frac{\partial}{\partial t} + \mathbf{v} \cdot \nabla \right) \mathbf{v} = -\nabla p - \rho \nabla \Phi$$

- energy conservation

$$\rho T \left(\frac{\partial}{\partial t} + \mathbf{v} \cdot \nabla \right) S = \rho \, \epsilon_N - \nabla \cdot \mathbf{F}$$

- Poisson's Equation

$$\nabla^2 \Phi = 4\pi G \rho$$

Definitions

ρ	density	T	temperature
$\mathbf{v}$	velocity	S	entropy
p	pressure	$\mathbf{F}$	radiative flux
Φ	gravitational potential	ϵ_N	nuclear energy generation rate

Stellar Hydrodynamics Equations

To obtain the equations describing linear pulsations (Unno et al. 1989, pp 87–104)

- perturb all quantities to first order (e.g., $p', \rho', \mathbf{v}' = \mathbf{v} = \partial\vec{\xi}/\partial t$)
- assume $p'(\mathbf{r}, t) = p(r)\, Y_{\ell m}(\theta, \phi)\, e^{i\omega t}$, and similarly for other perturbed quantities
- rewrite in terms of, say, $\xi_{\rm r}$ and p'

Technical Aside:
We use primes (e.g., p') to refer to *Eulerian* perturbations (perturbations of quantities at a fixed point in space) and delta's (δp) to refer to *Lagrangian* perturbations (evaluated in the frame of the moving fluid). The relationship between the two is

$$\delta p = p' + \vec{\xi} \cdot \nabla p,$$

where $\vec{\xi}$ is the displacement of the fluid.

In fact, if energy is conserved ("adiabatic") and the perturbations to the gravitational potential can be neglected ("Cowling approximation"), then the resulting 1-D equations may be written as a single 2nd-order equation (e.g., Gough 1993):

$$\frac{d^2}{dr^2}\Psi(r) + K^2\Psi(r) = 0,$$

where

$$K^2 \equiv \frac{\omega^2 - \omega_c^2}{c_s^2} - \frac{L^2}{r^2}\left(1 - \frac{N^2}{\omega^2}\right),$$

$$L^2 \equiv \ell(\ell+1), \qquad \Psi \equiv \rho^{-\frac{1}{2}}\,\delta p$$

$\Rightarrow$ the problem reduces mathematically to the (non-uniform) vibrating string problem:

$K^2 > 0:$ solution is oscillatory (propagating)

$K^2 < 0:$ solution is exponential (evanescent, damped)

Spatial structure of the eigenfunctions, in r, θ, and ϕ

m: number of vertical nodal great circles

ℓ: number of horizontal $+$ vertical nodal circles

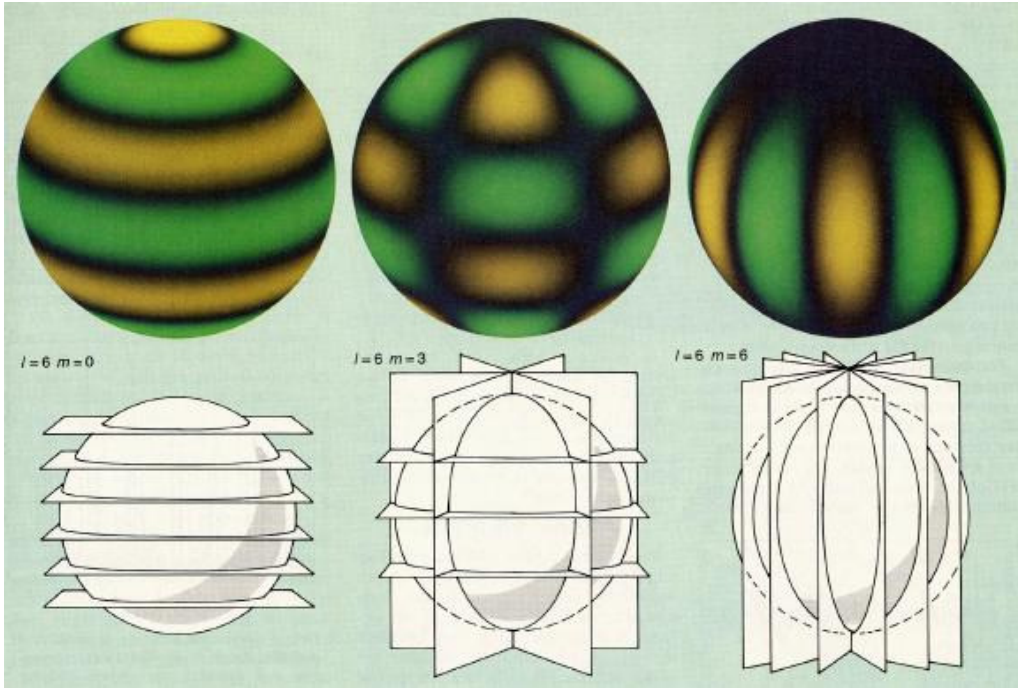

n: number of nodes in radial direction

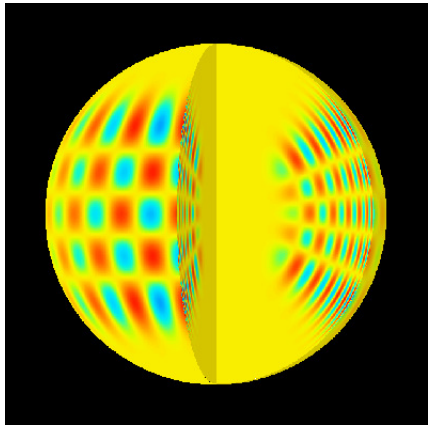

As a result of this analysis, we discover that there are two local quantities which are of fundamental importance: the Lamb frequency, $S_\ell = \frac{Lc_s}{r}$, and the Brunt-Väisälä frequency, N. These two quantities have to do with pressure and gravity, respectively.

Pressure waves:

- perturbations travel at the sound speed which is $c_s^2 \equiv \left(\frac{\partial P}{\partial \rho}\right)_{\rm ad} = \frac{\Gamma_1 P}{\rho}$
- perturbations are longitudinal

$\Rightarrow$ fluid velocity is in the direction of propagation

- disturbances propagate relatively quickly
- examples: sound waves in air or water

The Brunt-Väisälä frequency, N, is a local buoyancy frequency, which owes its existence to gravity.

Gravity waves:

- perturbations are transverse

$\Rightarrow$ fluid velocity is perpendicular to the direction of propagation of the wave

- disturbances propagate relatively slowly
- medium must be stratified (non-uniform)

Example: surface water waves

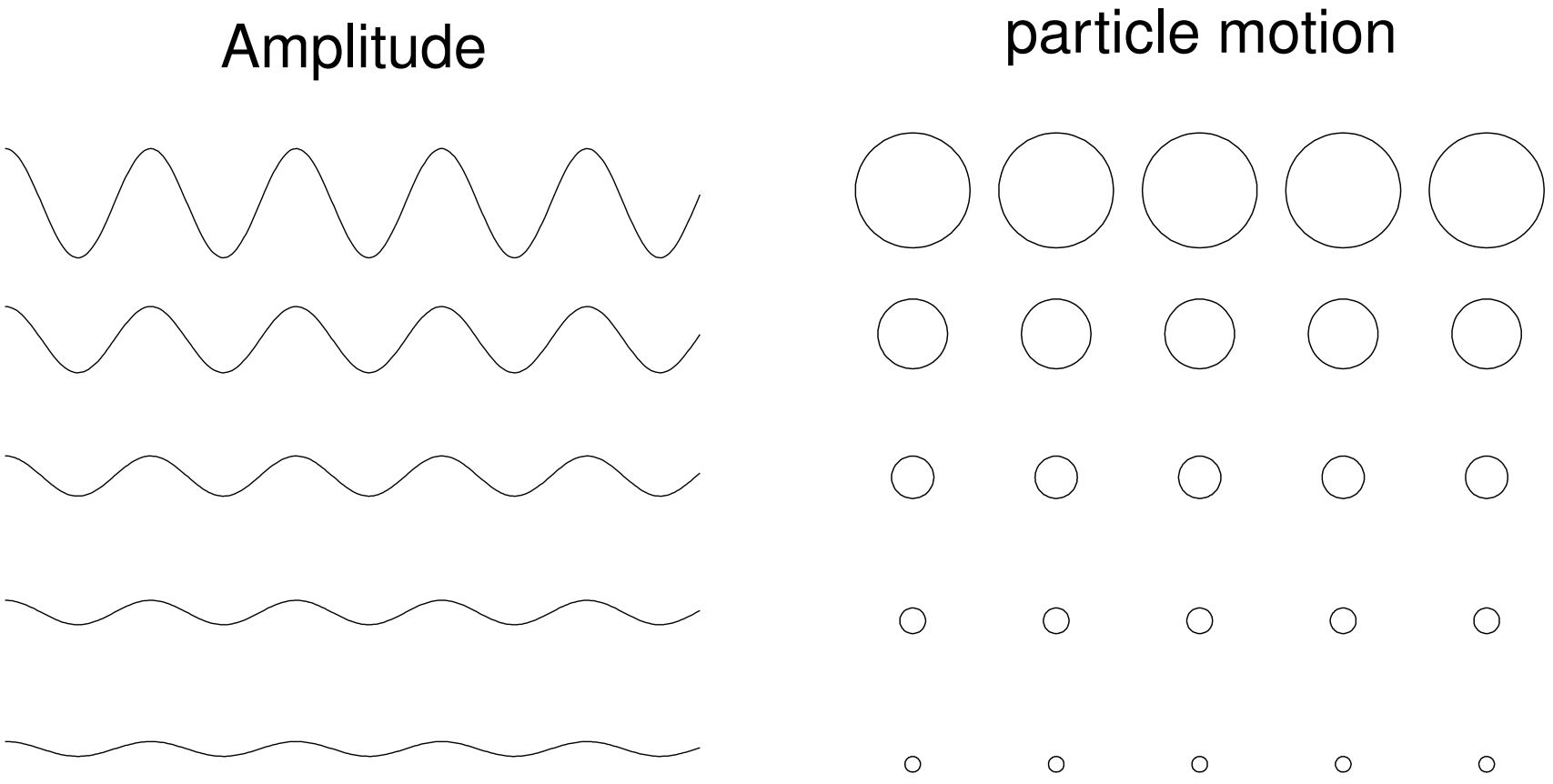

$$v = \frac{1}{2}\left(g\lambda\right)^{1/2}$$

Can we calculate N physically?

Fluid element is displaced from its equilibrium position.

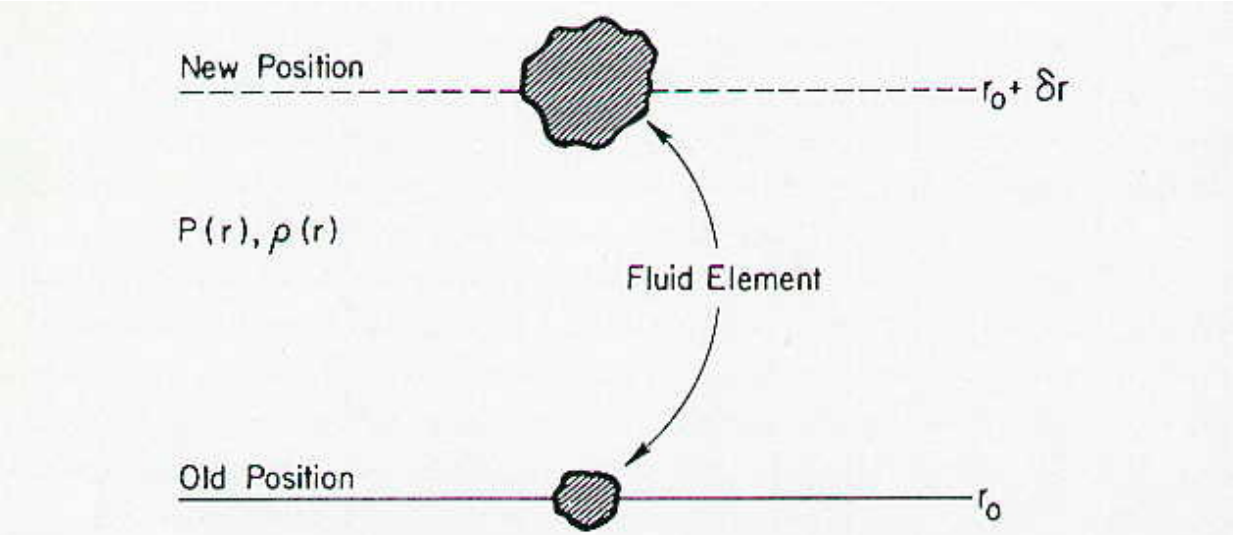

Figure 17.1. A displaced fluid element in a stratified fluid. The initial level is r_0 and the new level is $r_0 + \delta r$.

Assume

- pressure equilibrium
- no energy exchange ("adiabatic")

$$P(r+\delta r) = P(r) + \left(\frac{\partial P}{\partial \rho}\right)_{\rm ad} \delta\rho$$

$$\Rightarrow \delta\rho = \frac{\rho}{\Gamma_1 P}\frac{dP}{dr}\delta r$$

- density difference, $\Delta\rho$, with new surroundings:

$$\begin{aligned}\Delta\rho &= \rho(r) + \delta\rho - \rho(r+\delta r) \\ &= \frac{\rho}{\Gamma_1 P}\frac{dP}{dr}\,\delta r - \frac{d\rho}{dr}\delta r\end{aligned}$$

- applying $F = ma$ to this fluid element yields

$$\begin{aligned}\rho\frac{d^2\delta r}{dt^2} &= -g\Delta\rho \\ &= -\rho g\left(\frac{1}{\Gamma_1}\frac{d\ln P}{dr} - \frac{d\ln\rho}{dr}\right)\delta r \\ \frac{d^2\delta r}{dt^2} &= -\underbrace{g\left(\frac{1}{\Gamma_1}\frac{d\ln P}{dr} - \frac{d\ln\rho}{dr}\right)}_{N^2}\delta r\end{aligned}$$

  $N^2 > 0$: fluid element oscillates about equilibrium position with frequency N

  $N^2 < 0$: motion is unstable $\Rightarrow$ convection (Schwarzschild criterion)

Mode Classification

Depending upon whether pressure or gravity is the dominant restoring force, a given mode is said to be locally propagating like a p-mode or a g-mode. This is determined by the frequency of the mode, ω.

For

$$\frac{d^2}{dr^2}\Psi(r) + K^2\Psi(r) = 0,$$

Gough (1993) showed that K^2 could be written as

$$K^2 = \frac{1}{\omega^2 c^2}(\omega^2 - \omega_+^2)(\omega^2 - \omega_-^2),$$

where

$$\omega_+ \approx S_\ell \equiv \frac{Lc_s}{r}, \qquad \omega_- \approx N$$

Mode Classification

Whether a mode is locally propagating or evanescent is determined by its frequency relative to S_ℓ and N:

p-modes: $\omega^2 > S_\ell^2, N^2$ ("high-frequency")
$K^2 > 0$, mode is locally "propagating"

g-modes: $\omega^2 < S_\ell^2, N^2$ ("low-frequency")
$K^2 > 0$, mode is locally "propagating"

However, if

$$\min(N^2, S_\ell^2) < \omega^2 < \max(N^2, S_\ell^2),$$

then

$$K^2 < 0,$$

and the mode is *not* locally propagating, and is termed 'evanescent', 'exponential', or 'tunneling'.

The JWKB Approximation

$$\frac{d^2\Psi}{dr^2} + K^2\Psi = 0$$

If $K^2 > 0$, then the solution is oscillatory, having some spatial wavelength, $\lambda \sim 2\pi/K$. If K varies slowly over scales of order λ, i.e., $\frac{d\lambda}{dr} \ll 1$, then an approximate solution of this equation is

$$\Psi = A\,K(r)^{-1/2} \sin\left(\int^r K(r')dr' + C\right)$$

Although we required $\frac{d\lambda}{dr} \ll 1$, this approximation is frequently still good even if $\frac{d\lambda}{dr} \sim 0.5$

The JWKB method is useful in many cases, for instance, for describing the radial structure of tightly wound spiral arms in galaxies (Binney & Tremaine 1987) or for problems in quantum mechanics.

Asymptotic Analysis: The JWKB Approximation

Satisfying the boundary conditions for a mode propagating between r_1 and r_2 yields the following "quantization" condition:

$$\int_{r_1}^{r_2} dr\, K = n\,\pi.$$

For high frequencies, $K \sim \omega/c$, so this leads to

$$\omega = \frac{n\,\pi}{\int dr\, c^{-1}}$$

$\Rightarrow$ frequencies are evenly spaced as a function of radial overtone number n (just like the vibrating string).

Asymptotic Analysis: The JWKB Approximation

For low frequencies, $K \sim LN/\omega r$, so this leads to

$$\omega = \frac{L}{n\,\pi} \int dr\, N/r,$$

so

$$P = \frac{2\,n\,\pi^2}{L} \left[\int dr\, N/r \right]^{-1}.$$

$\Rightarrow$ periods are evenly spaced as a function of radial overtone number n.

Example: propagation diagram for a white dwarf model

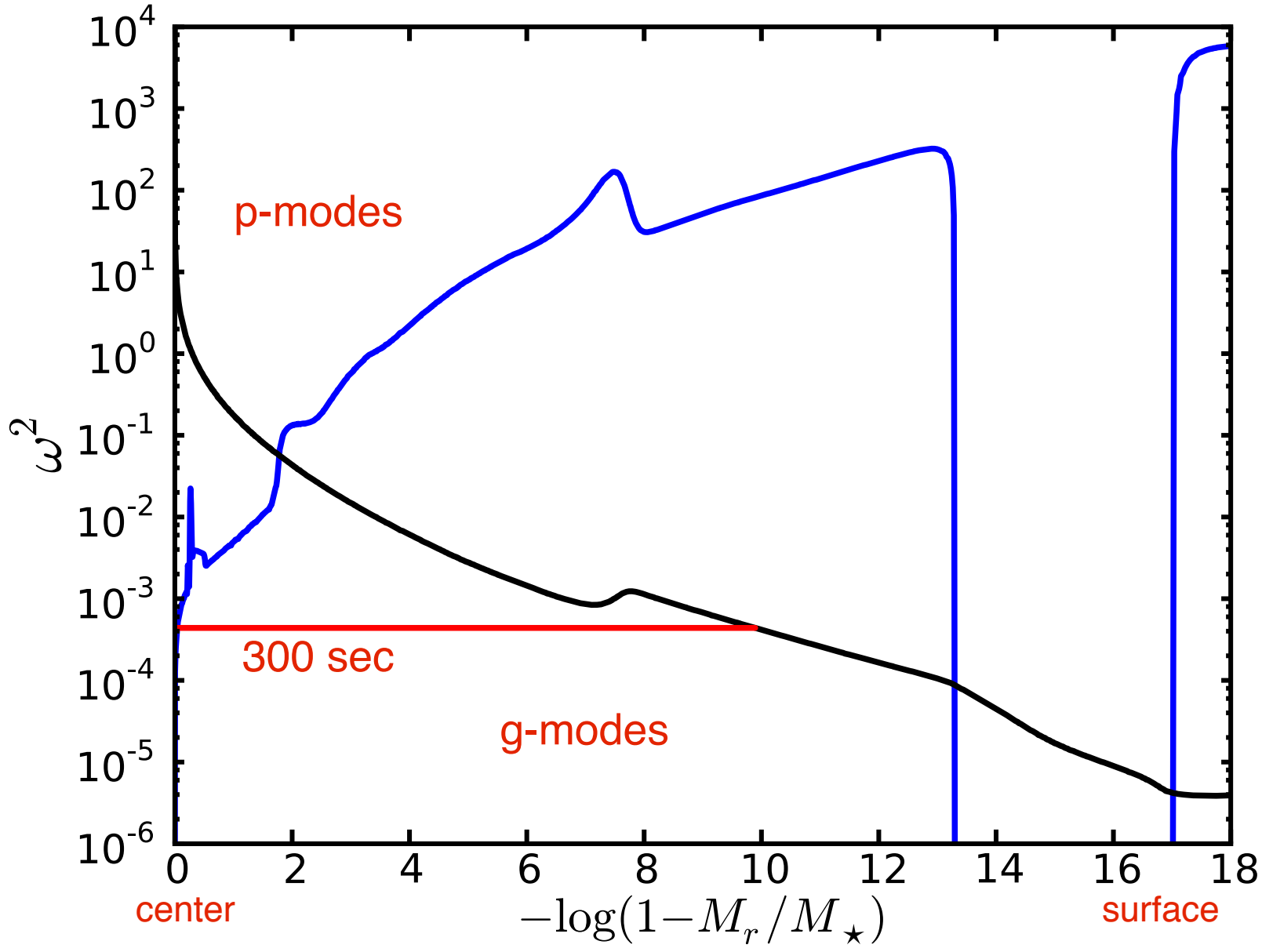

Driving Pulsations: The Adiabatic Assumption

Adiabatic: No heat gain or loss during a pulsation cycle, i.e., $\frac{dq}{dt} = 0$

One way to quantify this is to compare the energy content "stored" in the layers in the star above a certain point, Δq_s, with the energy which passes through these layers in one pulsation period, Δq_l:

$$\Delta q_s \sim C_V \, T \, \Delta M_r$$

Here $\Delta M_r \equiv M_\star - M_r$ is the envelope mass. The energy passing through this layer in one pulsation period, Π, is

$$\Delta q_l \sim L_r \, \Pi,$$

where L_r is the luminosity at radius r.

Driving Pulsations: The Adiabatic Assumption

In order for the adiabatic approximation to be valid we need $\Delta q_l \ll \Delta q_s$, which implies that

$$\eta \equiv \frac{L_r \, \Pi}{C_V \, T \, \Delta M_r} \ll 1$$

In general, $C_V \sim 10^9$ ergs/g-K, and for solar p-modes, $\Pi \sim 300$ sec. Using solar values for L_r and M_r we find

- $\eta \sim 10^{-16}$ in the inner regions of the sun
- $\eta \sim 1$ at $\Delta M_r / M_\odot \sim 10^{-10}$

In other words, $\eta \ll 1$ throughout the vast majority of the Sun.

Driving Pulsations: Mechanisms

Without some mechanism to drive the pulsations, finite amplitude eigenmodes would not be observed in stars
Two classes of driven modes:

linearly unstable: Mode amplitudes grow exponentially in time until quenched by nonlinear effects ("large amplitude pulsators"), e.g., modes radiatively driven by the "Kappa-gamma mechanism".

stochastically driven: Modes are intrinsically stable, but are dynamically excited ("hit") by the convective motions, and then decay away ("solar-like, low amplitude pulsators"), e.g., driven by turbulent motions of the convection zone.

Linear Driving/Amplification

- A mode which is linearly unstable will increase its amplitude with time
  - infinitesimal perturbations are linearly amplified ("self-amplified"), grow exponentially
  - Example: the harmonic oscillator

$$\ddot{x} + \gamma\,\dot{x} + \omega_0^2\,x = 0$$

$$\Rightarrow \quad x(t) = A\,e^{\gamma\,t/2}\cos\omega\,t,$$

where

$$\omega = \sqrt{\omega_0^2 - \gamma^2/4}.$$

So amplitude grows in time as $e^{\gamma\,t/2}$.

Linear Driving/Amplification

Several mechanisms exist which can do this:

nuclear driving: "the epsilon mechanism"

radiative driving: "the kappa mechanism"

- In order to drive locally, energy must be flowing into a region at maximum compression
- Typically, only a few regions of a star can drive a mode, but the mode is radiatively damped everywhere else. For a mode to grow, the total driving has to exceed the total damping

Phasing of the Driving

Driving region: A region which acts to *increase* the local amplitude:
Driving $\Longleftrightarrow t_{P(\max)} > t_{\rho(\max)}$

Damping region: A region which acts to *decrease* the local amplitude:
Damping $\Longleftrightarrow t_{P(\max)} < t_{\rho(\max)}$

To see when this can happen we consider the equation

$$\frac{1}{P}\frac{d\,\delta P}{dt} = \frac{\Gamma_1}{\rho}\frac{d\,\delta\rho}{dt} + \frac{\rho(\Gamma_3 - 1)}{P}\,\delta\left(\epsilon - \frac{1}{\rho}\nabla\cdot F\right)$$

At density maximum, $d\,\delta\rho/dt = 0$, so

$$\frac{1}{P}\frac{d\,\delta P}{dt} = \frac{\rho(\Gamma_3 - 1)}{P}\,\delta\left(\epsilon - \frac{1}{\rho}\nabla\cdot F\right)$$

Phasing of the Driving

If $\delta\left(\epsilon - \frac{1}{\rho}\nabla \cdot F\right) > 0$ then the pressure is still increasing and we will have $t_{P(\max)} > t_{\rho(\max)}$. This is the condition for the mass element to still be gaining energy. Energy gain will lead to a more forceful expansion, leading to local driving.

If $\delta\left(\epsilon - \frac{1}{\rho}\nabla \cdot F\right) < 0$ then the pressure is decreasing and we have $t_{P(\max)} < t_{\rho(\max)}$. This is the condition for the mass element to be losing energy. Energy loss will lead to a less forceful expansion, leading to local damping.

Of course, if $\delta\left(\epsilon - \frac{1}{\rho}\nabla \cdot F\right) \approx 0$, then $t_{P(\max)} \approx t_{\rho(\max)}$ and there is no driving or damping. This is the adiabatic case.

The Kappa-gamma Mechanism

Consider a temperature perturbation $\delta T/T$ which is independent of position:

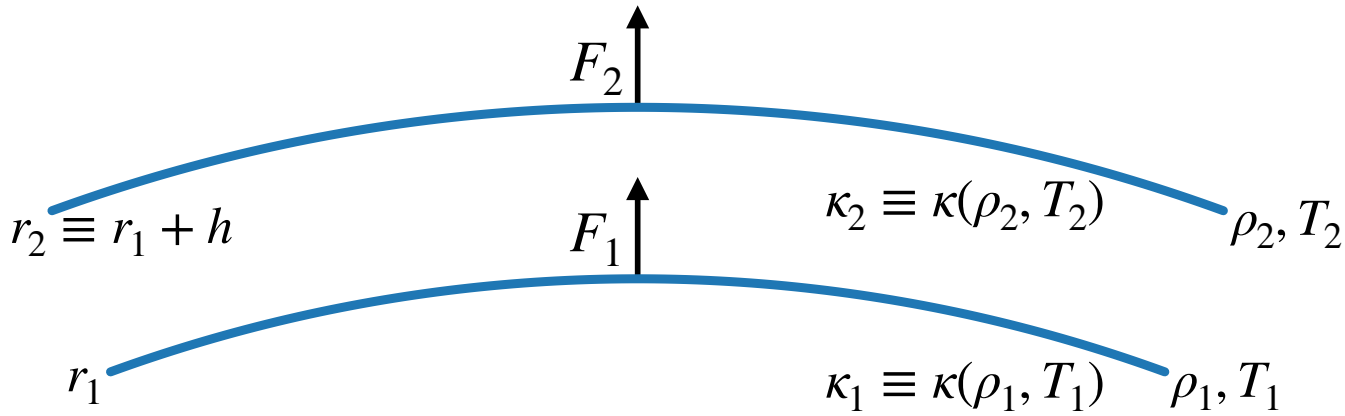

In equilibrium, $F_1 = F_2$. Now consider perturbations only to the opacity due to the temperature perturbation. Since

$$F = -\frac{4ac}{3\kappa\rho} T^3 \nabla T \propto 1/\kappa,$$

we have $\delta F = -F \dfrac{\delta\kappa}{\kappa} = -F\delta \ln \kappa = -F \dfrac{\partial \ln \kappa}{\partial \ln T} \dfrac{\delta T}{T}$

The flux going in minus the flux leaving is

$$\begin{aligned}\Delta F &\equiv F_1 + \delta F_1 - (F_2 + \delta F_2) \\ &= -F\,\frac{\delta T}{T}\left[\left(\frac{\partial \ln \kappa}{\partial \ln T}\right)_{r1} - \left(\frac{\partial \ln \kappa}{\partial \ln T}\right)_{r2}\right] \\ &= F\,\frac{\delta T}{T} h \left(\frac{d}{dr}\kappa_T\right),\end{aligned}$$

where

$$\kappa_T \equiv \left(\frac{\partial \ln \kappa}{\partial \ln T}\right)_{\rho}.$$

Thus, we have local driving if

$$\frac{d}{dr}\kappa_T > 0$$

This condition is fulfilled in the outer partial ionization zones of many stars.

A more careful derivation (including density perturbations in the quasi-adiabatic approximation) shows that the condition for local driving due to the Kappa-gamma mechanism is actually

$$\frac{d}{dr}\left[\kappa_T + \kappa_\rho/(\Gamma_3 - 1)\right] > 0,$$

where $\Gamma_3 - 1 \equiv \left(\frac{\partial \ln T}{\partial \ln \rho}\right)_S$.

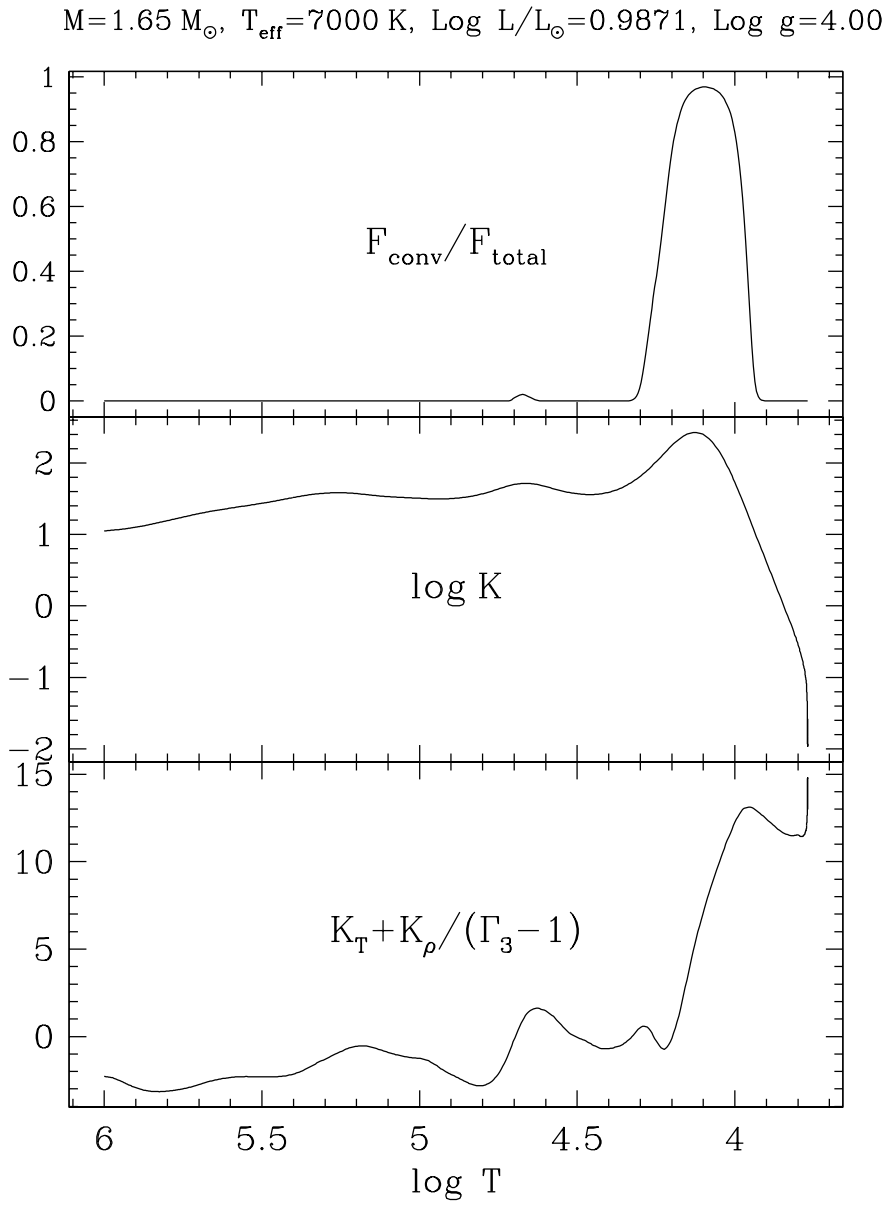

Timescales and Driving

A region which can locally drive modes (e.g., He II partial ionization) most effectively drives modes whose periods are close to the thermal timescale of the region:

$$\tau_{\rm thermal} \sim \frac{\Delta M_r c_V T}{L_{\rm tot}} \sim P \text{ (mode period)}$$

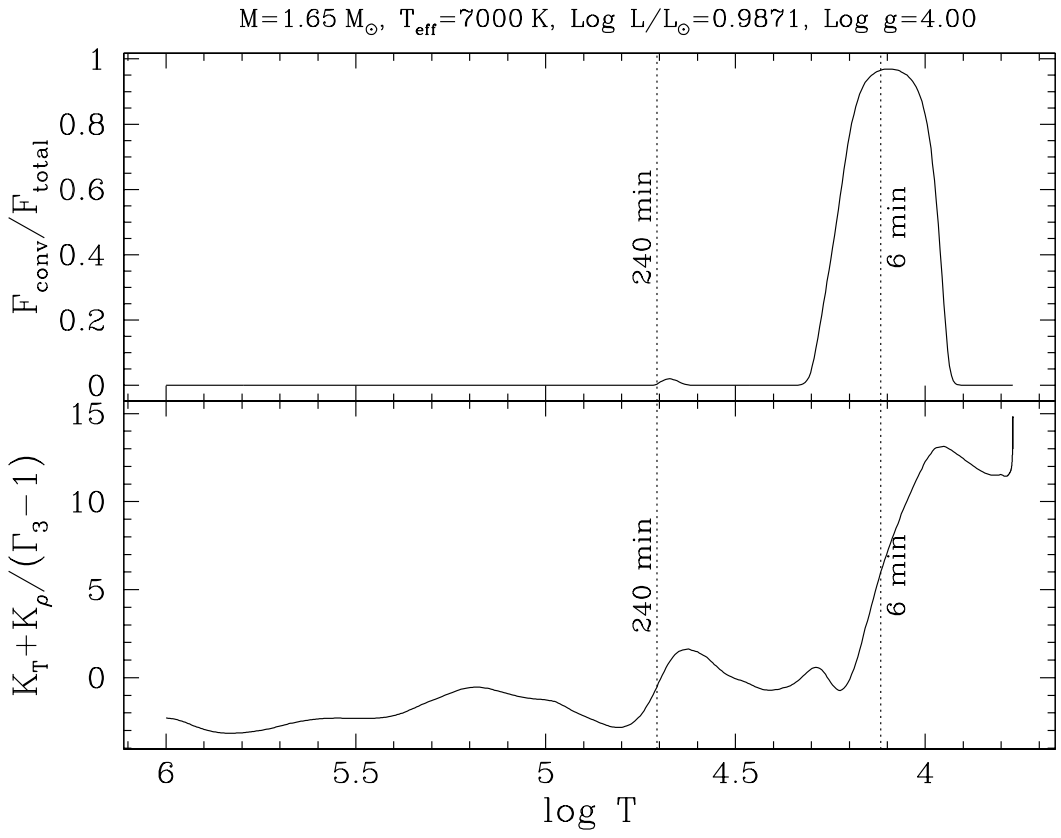

Timescales

The thermal timescale $\tau_{\rm thermal}$ increases with increasing depth

$\Rightarrow$ longer period modes are driven by deeper layers than short period modes

In the model shown above, the possibility exists to drive modes with periods of

$\sim$ 4 hours, due to He II ionization

$\sim$ 6 minutes, due to H I ionization

The energy gained by the mode in the driving regions has to be greater than the radiative damping which it experiences everywhere else. Thus, the above conditions are necessary but not sufficient to insure linear instability.

A More Detailed (but still qualitative) Calculation of κ-γ Driving

$$\rho\, T\, \frac{ds}{dt} = \rho\, \epsilon - \nabla \cdot \vec{F}$$

Again, let's assume a perturbation with $\delta T/T$ constant in space. For a region in the envelope, $\epsilon = 0$, and let's qualitatively write $T\, ds \approx c_V\, dT/T$, so

$$\rho\, c_V\, \frac{dT}{dt} = -\nabla \cdot \vec{F} = -\frac{\partial F_r}{\partial r}$$

Ignoring differences between δ and $'$, we consider the effect of a perturbation in δT:

$$\rho\, c_V\, \frac{d\,\delta T}{dt} = -\frac{\partial\, \delta F_r}{\partial r}$$

$$F_r \propto -\frac{\nabla T^4}{\kappa} \qquad \Rightarrow \qquad \frac{\delta F_r}{F_r} = -\frac{\delta \kappa}{\kappa} + 4\frac{\delta T}{T}$$

Calculation of κ-γ Driving

$$\text{So} \quad \delta F_r = F_r \left(-\frac{\delta\kappa}{\kappa} + 4\frac{\delta T}{T} \right)$$

Since F_r is constant in the outer envelope (plane parallel approximation),

$$\frac{\partial\, \delta F_r}{\partial r} = -F_r \frac{\partial}{\partial r}\left(\frac{\delta\kappa}{\kappa}\right)$$

$$\frac{\delta\kappa}{\kappa} = \kappa_T \frac{\delta T}{T} + \kappa_\rho \frac{\delta\rho}{\rho}$$

Assuming quasi-adiabatic perturbations,

$$\frac{\delta\rho}{\rho} = \frac{1}{\Gamma_3 - 1}\frac{\delta T}{T}, \qquad \text{where} \quad \Gamma_3 - 1 = \left(\frac{\partial \ln T}{\partial \ln \rho}\right)_s$$

$$\frac{\delta\kappa}{\kappa} = \frac{\delta T}{T}\left(\kappa_T + \frac{\kappa_\rho}{\Gamma_3 - 1}\right)$$

Calculation of κ-γ Driving

$$\rho\, c_V \frac{d\,\delta T}{dt} = F_r \frac{\delta T}{T} \frac{\partial}{\partial r}\left(\kappa_T + \frac{\kappa_\rho}{\Gamma_3 - 1}\right)$$

$$\frac{d}{dt}\left(\frac{\delta T}{T}\right) = \left[\frac{F_r}{\rho\, c_V\, T} \frac{d}{dr}\left(\kappa_T + \frac{\kappa_\rho}{\Gamma_3 - 1}\right)\right]\left(\frac{\delta T}{T}\right)$$

Assuming $\delta T/T = A\, e^{\gamma\, t}$, then

$$\begin{aligned}\gamma &= \frac{F_r}{\rho\, c_V\, T} \frac{d}{dr}\left(\kappa_T + \frac{\kappa_\rho}{\Gamma_3 - 1}\right) \\ &= \frac{L_r}{4\pi r^2\, \rho\, c_V\, T} \frac{d}{dr}\left(\kappa_T + \frac{\kappa_\rho}{\Gamma_3 - 1}\right)\end{aligned}$$

Letting H_p be a pressure scale height, $4\pi r^2 H_P \rho \approx \Delta M_r$, so

$$\gamma = \frac{L_r}{\Delta M_r\, c_V\, T}\left[H_P \frac{d}{dr}\left(\kappa_T + \frac{\kappa_\rho}{\Gamma_3 - 1}\right)\right]$$

Calculation of κ-γ Driving

In terms of the thermal timescale this is

$$\gamma = \tau_{\rm th}^{-1} \left[H_P \frac{d}{dr} \left(\kappa_T + \frac{\kappa_\rho}{\Gamma_3 - 1} \right) \right]$$

The term in brackets is $\mathcal{O}(1)$, although it can be as large as 10. Thus, the *local* growth rate can be as large as $\tau_{\rm th}^{-1}$, and we again see that

$$\frac{d}{dr} \left(\kappa_T + \frac{\kappa_\rho}{\Gamma_3 - 1} \right) > 0$$

is the criterion for local driving to occur. In practice, this always occurs in a partial ionization (PI) zone of some element.

Of course, the total growth rate for a mode is summed over the entire star, which includes driving *and* damping regions, and it is typically much smaller than this.

Incidentally, I have saved you from the derivation in Unno et al. (1989), which is somewhat less transparent:

$$\alpha_1 \equiv 4 - \frac{1}{\nabla_{ad}} - \kappa_T - \frac{\kappa_\rho}{\Gamma_3 - 1} + \left(1 - \frac{L_l^2}{\Gamma_1 \sigma^2}\right)\left(\frac{c_1\omega^2 - U}{\alpha_0 \nabla_{ad}}\right). \quad (26.12)$$

Substituting these equations and disregarding Φ', we obtain, after lengthy manipulations, an approximate expression for W_F:

$$\frac{\sigma}{\pi} W_F \simeq -\frac{1}{2}\left[\alpha_1 L_R \left(\frac{\delta T}{T}\right)^2\right]_{r=R} - \frac{1}{2}\int_0^R dr \left(\frac{\delta T}{T}\right)^2 \frac{d}{dr}(\alpha_1 L_R)$$

$$+ \int_0^R dr L_R \frac{H_p}{\nabla_{ad}} \left(\frac{\nabla - \nabla_{ad}}{\nabla} - \frac{c_1\omega^2 - U}{\alpha_0}\right)\left\{\left[\frac{d}{dr}\left(\frac{\delta T}{T}\right)\right]^2 + \frac{l(l+1)}{r^2}\left(\frac{\delta T}{T}\right)^2\right\}$$

$$+ l(l+1)\int_0^R dr \left(\frac{\delta T}{T}\right)^2 \frac{1}{\nabla_{ad}}\left[\frac{4 - V}{\alpha_0 V}\left(\frac{1}{c_1\omega^2}\frac{dL_r}{dr} - \frac{L_R}{r}\right)\right.$$

$$\left. + \frac{c_1\omega^2 - U}{c_1\omega^2 \alpha_0 V}\frac{dL_r}{dr} + \frac{1}{2}\frac{d}{dr}\left(\frac{c_1\omega^2 L_R - dL_r/d\ln r}{c_1\omega^2 \alpha_0 V}\right)\right], \quad (26.13)$$

where L_r and L_R are, respectively, the total and the radiative

Which periods are most strongly driven?

The transition region between adiabatic and nonadiabatic for a mode is by

$$\frac{c_V\, T\, \Delta M_r}{L\, P} \sim 1$$

Deeper than this (larger ΔM_r) the mode is adiabatic, and higher than this (smaller ΔM_r) the mode is strongly nonadiabatic.

If the transition region for a given mode lies *above* the PI zone, then the oscillation is nearly adiabatic in the PI zone so very little driving or damping can occur.

If the transition region for a given mode lies *below* the PI zone, then energy leaks out of the region too quickly for driving to occur, i.e., the luminosity is “frozen in.”

Which periods are most strongly driven?

Thus, the modes that are most strongly driven are the ones whose adiabatic/nonadiabatic transition region lies on top of the PI zone. The period of these modes is given by

$$P \sim \tau_{\rm th} \approx \frac{c_V T \Delta M_r}{L}.$$

This is a necessary but not sufficient condition for a mode to be globally driven.

Convective Driving

If we are honest with ourselves (and we often are not), the κ-γ mechanism is often less applicable than one would imagine.

This is because PI zones are usually coupled to large rises in the opacity, and these large opacities often lead to convection.

If flux is predominantly transported by convection, not radiation, then modulating the opacity does nothing, so the κ-γ mechanism cannot operate.

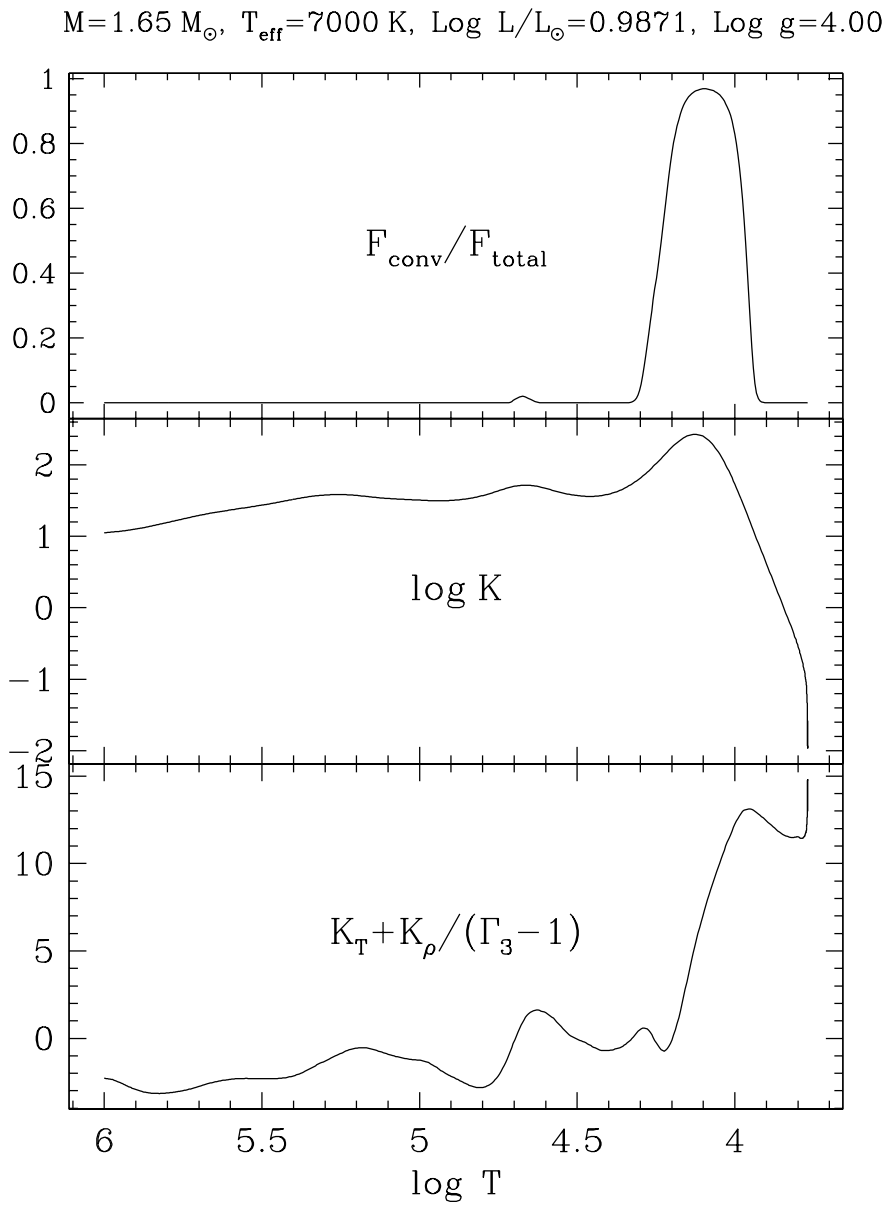

Convective Driving

Fortunately, work by Brickhill (1991,1992) and Goldreich & Wu (1999) has shown that a convection zone can naturally drive pulsations if the convective turnover timescale, $t_{\rm conv}$, is much shorter than the pulsation period, P, i.e., $t_{\rm conv} \ll P$:

THE ASTROPHYSICAL JOURNAL, 511:904–915, 1999 February 1

GRAVITY MODES IN ZZ CETI STARS. I. QUASI-ADIABATIC ANALYSIS OF OVERSTABILITY

PETER GOLDREICH[1] AND YANQIN WU[1,2]
Received 1998 April 28; accepted 1998 September 3

ABSTRACT

We analyze the stability of g-modes in white dwarfs with hydrogen envelopes. All relevant physical processes take place in the outer layer of hydrogen-rich material, which consists of a radiative layer overlaid by a convective envelope. The radiative layer contributes to mode damping, because its opacity decreases upon compression and the amplitude of the Lagrangian pressure perturbation increases outward. The convective envelope is the seat of mode excitation, because it acts as an insulating blanket with respect to the perturbed flux that enters it from below. A crucial point is that the convective motions respond to the instantaneous pulsational state. Driving exceeds damping by as much as a factor of 2 provided $\omega\tau_c \geq 1$, where ω is the radian frequency of the mode and $\tau_c \approx 4\tau_{\rm th}$, with $\tau_{\rm th}$ being the thermal time constant evaluated at the base of the convective envelope. As a white dwarf cools, its con-

Convective Driving

As a convection zone is heated from below its entropy rises. This requires heat/energy, so less energy is radiated out the top of the convection zone than enters at its base.

It is possible (but not easy) to show that this energy gain occurs at maximum density during the pulsations, so this naturally leads to driving.

This explains the driving in pulsating white dwarfs (DAs and DBs), and possibly also Gamma Doradus and other stars.

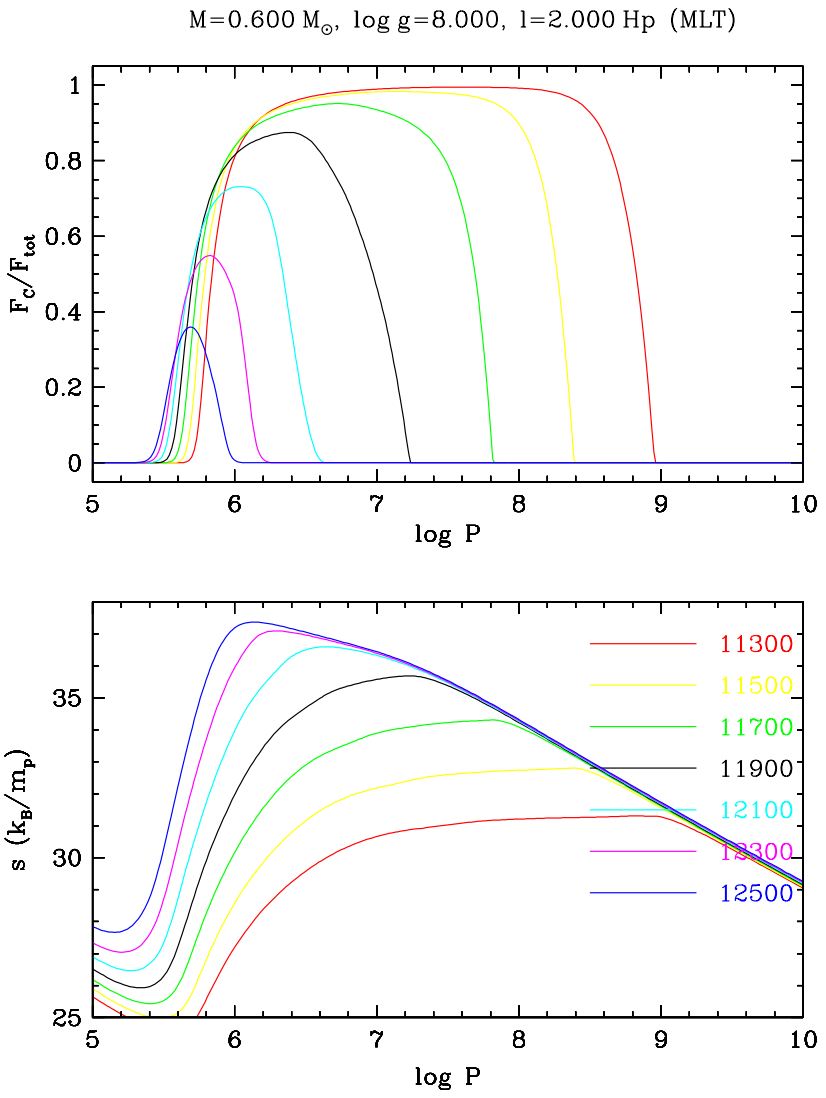

Stochastic Driving

Stochastic driving is *not* the linear driving we have been considering. It is driving due to the turbulent fluid motions of a star's convection zone. The modes are intrinsically damped but excited by a broad spectrum driving force. This is completely analogous to the damped harmonic oscillator with time-dependent forcing:

$$\ddot{x} + \gamma\,\dot{x} + \omega_0^2\,x = f(t)$$

If we do an FT, we find

$$x(\omega) = \frac{f(\omega)}{\omega_0^2 - \omega^2 + i\omega\gamma}$$

In terms of power this is

$$|x(\omega)|^2 = \frac{|f(\omega)|^2}{\left(\omega_0^2 - \omega^2\right)^2 + \omega^2\gamma^2}$$

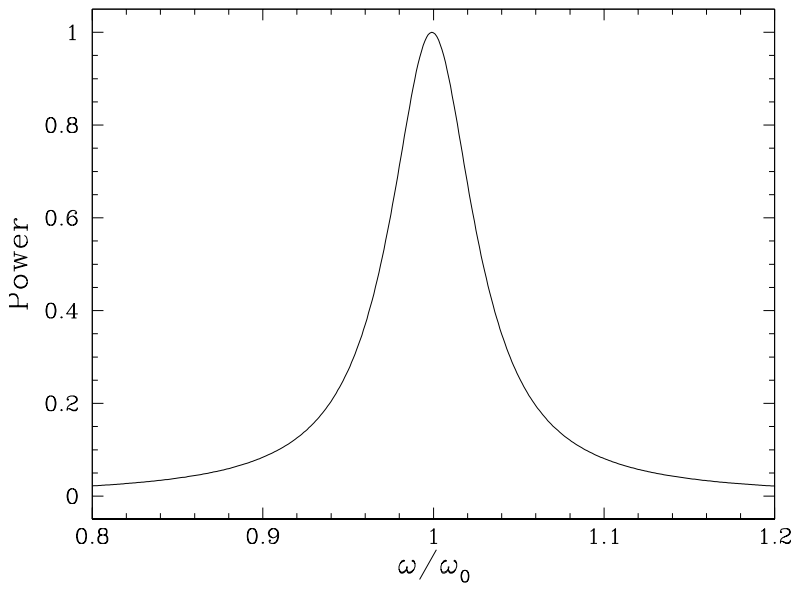

Stochastic Driving

Now let's consider a system with more than one degree of freedom, the vibrating string (with damping):

$$\frac{\partial^2 \psi}{\partial x^2} - \frac{1}{c^2}\frac{\partial^2 \psi}{\partial t^2} + \frac{\gamma}{c^2}\frac{\partial \psi}{\partial t} = g(x)\, f(t)$$

The right-hand side (RHS) contains the external forcing. If we Fourier Transform (FT) this equation with respect to time, we get

$$\frac{\partial^2 \bar{\psi}}{\partial x^2} + \frac{\omega^2}{c^2}\,\bar{\psi} + \frac{i\,\omega\,\gamma}{c^2}\,\bar{\psi} = g(x)\, f(\omega),$$

where $\bar{\psi}(x,\omega) = FT[\psi(x,t)]$, and $f(\omega) = FT[f(t)]$. Our string has length L, and our boundary conditions for this problem are

$$\psi(0,t) = 0 \quad \text{and} \quad \left(\frac{\partial \psi(x,t)}{\partial x}\right)_{x=L} = 0.$$

Stochastic Driving

We can expand ψ in basis functions of the unperturbed problem:

$$\bar{\psi}(x,\omega) = \sum_n \left[A_n(\omega)\, \sin k_n x + B_n(\omega)\, \cos k_n x\right]$$

Our BCs lead to $B_n = 0$, and $k_n\, L = \pi(n + 1/2)$. We further assume that the driving occurs only at $x = L$, i.e., $g(x) = \delta(x - L)$. Substituting this in our equation and multiplying and integrating by $\sin k_n x$ allows us to solve for A_m:

$$A_m(L/2c^2)\left[-k_m^2 c^2 + \omega^2 + i\gamma\omega\right] = \sin k_m L\, f(\omega)$$

$$A_m(\omega) = \frac{2\,c^2\, \sin k_m L}{L} \frac{f(\omega)}{\omega^2 - \omega_{0,m}^2 + i\gamma\omega}$$

where $\omega_{0,m} \equiv k_m\, c$.

Stochastic Driving

Thus, we find that ψ at $x = L$ is

$$\begin{aligned}\bar{\psi}(L,\omega) &= \sum_n \frac{c^2}{2L}\frac{f(\omega)\,\sin^2 k_n L}{\omega^2 - \omega_{0,n}^2 + i\gamma\omega} \\ &= \frac{c^2}{2L} f(\omega) \sum_n \frac{1}{\omega^2 - \omega_{0,n}^2 + i\gamma\omega}.\end{aligned}$$

The power spectrum of the FT is therefore given by

$$\begin{aligned}POWER &\equiv \left|\bar{\psi}(L,\omega)\right|^2 \\ &\propto |f(\omega)|^2 \left|\sum_n \frac{1}{\omega^2 - \omega_{0,n}^2 + i\gamma\omega}\right|^2 \\ &\approx |f(\omega)|^2 \sum_n \frac{1}{\left|\omega^2 - \omega_{0,n}^2 + i\gamma\omega\right|^2}\end{aligned}$$

- In the Sun, the driving $f(\omega)$ due to the convection zone is a fairly flat function of ω.
- Although there is power at “all” frequencies (continuous), the discrete peaks in the power spectrum correspond to the linear eigenfrequencies of the Sun.

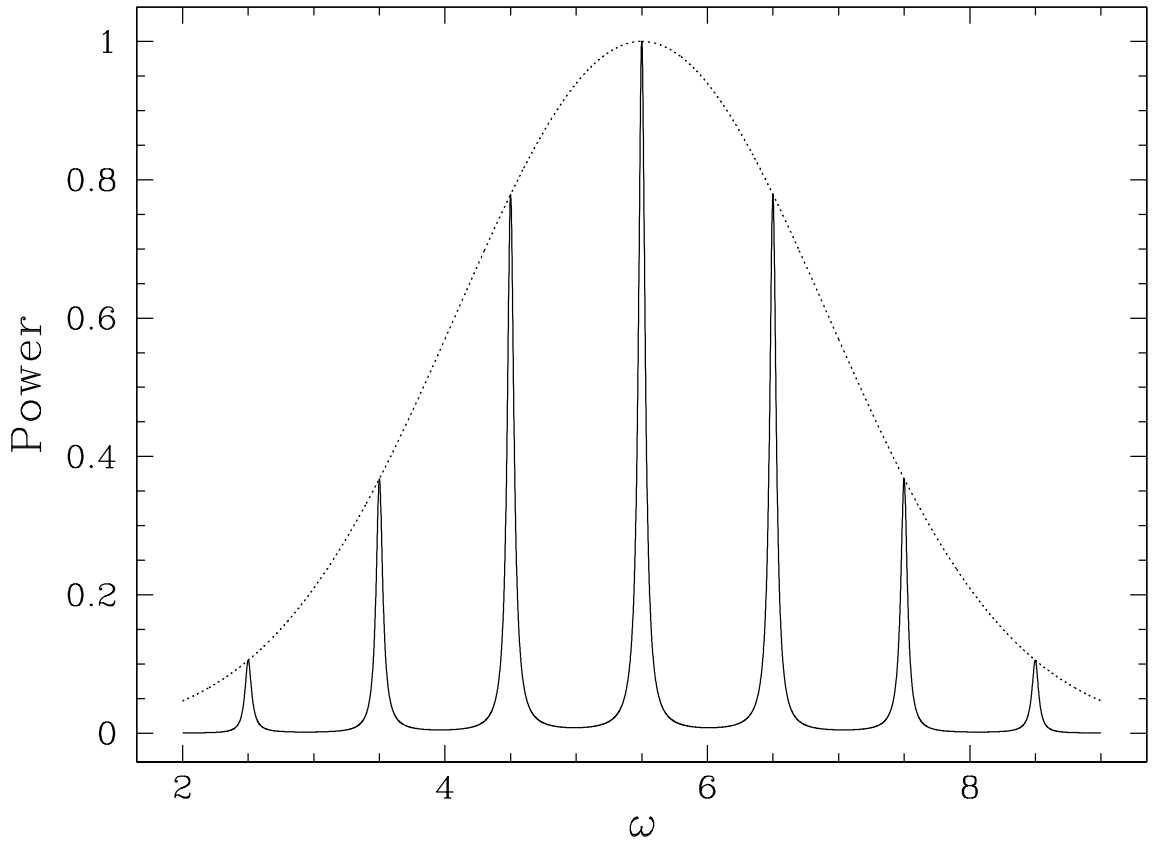

A “real” solar spectrum obtained from Doppler observations:

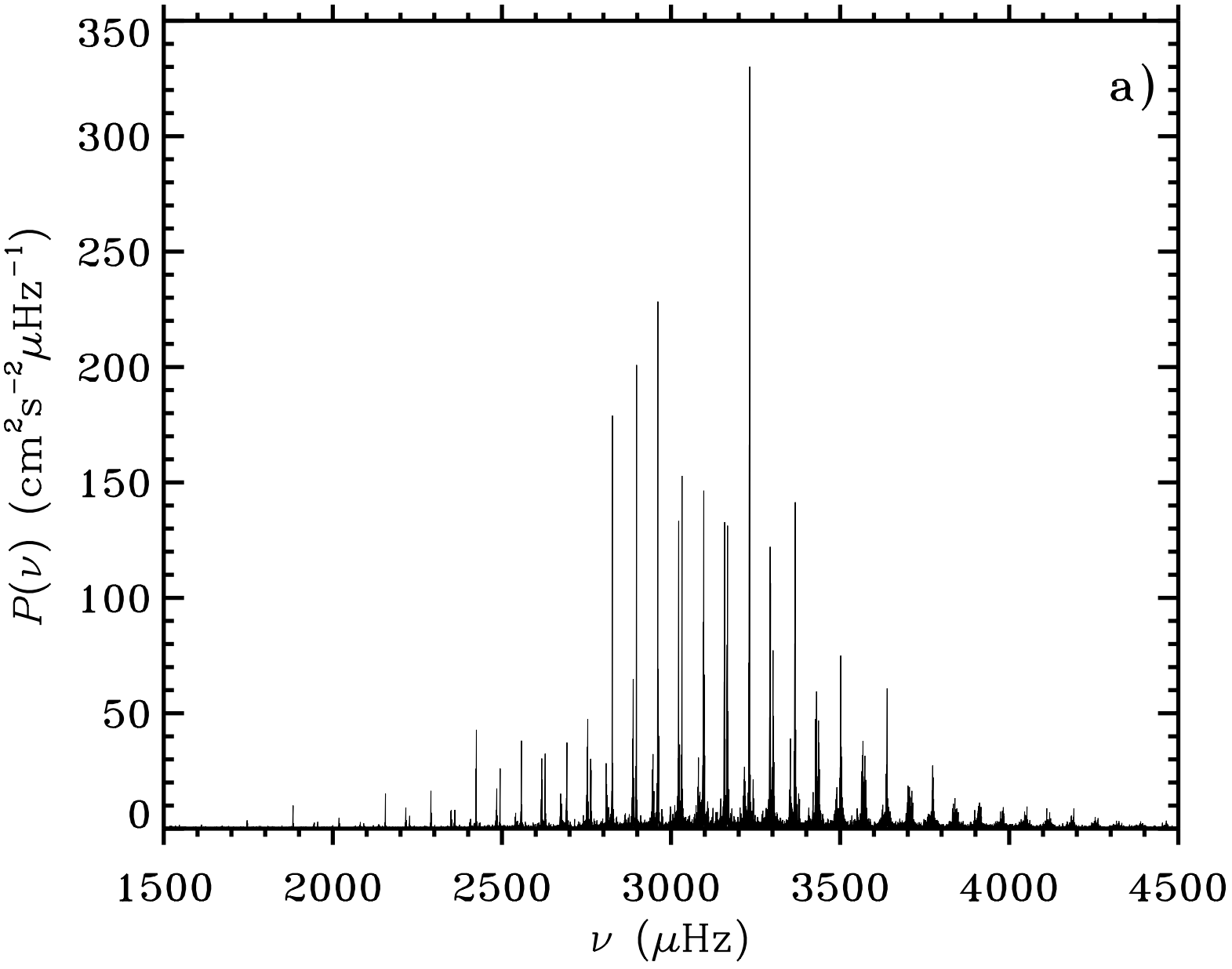

Good News:

- "All" the modes in a broad frequency range, with many values of ℓ, are observed to be excited in the Sun

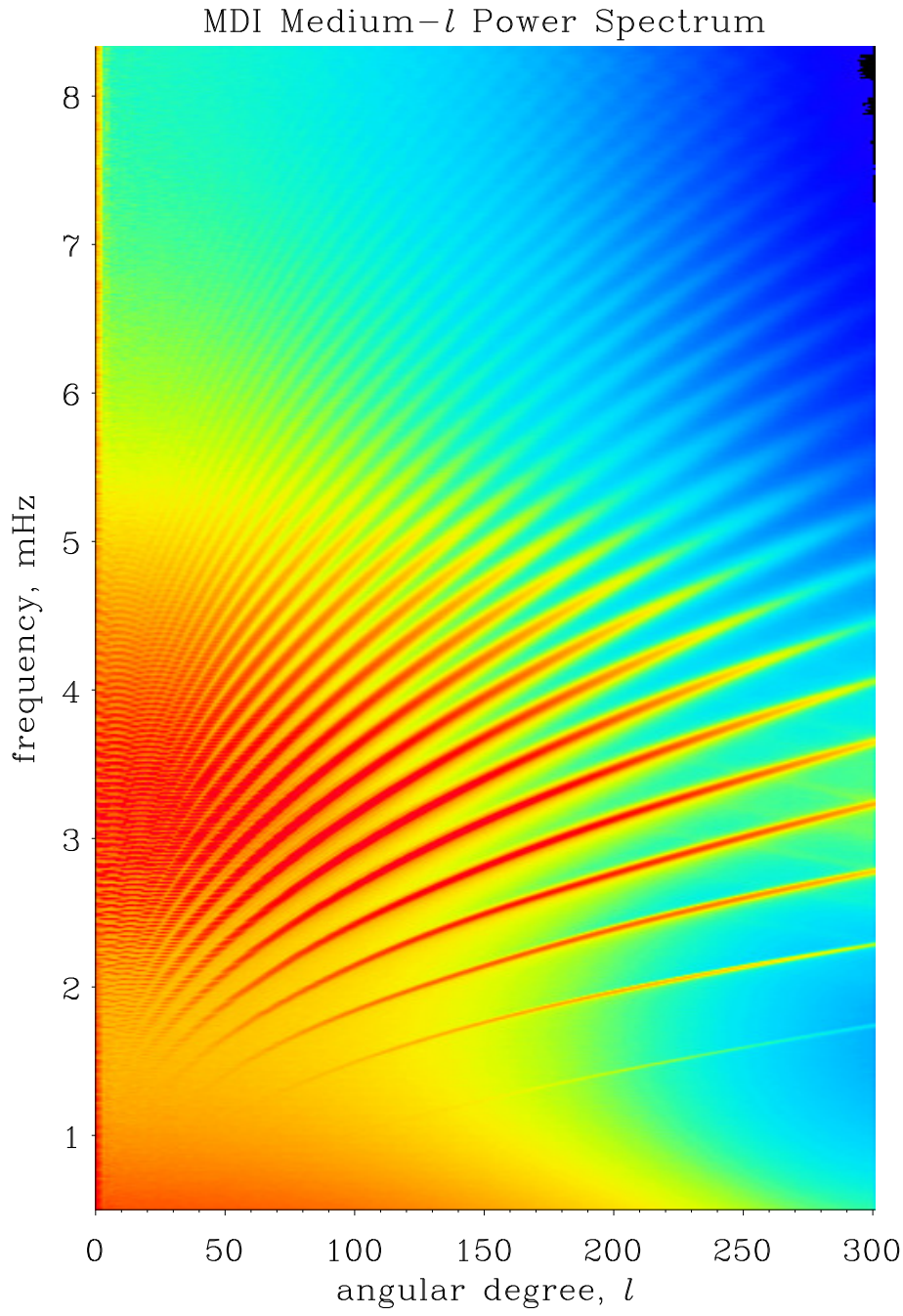

Bad News:

- The amplitudes are very small. For a given mode, the flux variations $\Delta I/I \sim 10^{-6}$, and the velocity variations are ~ 15 cm/s

The Sun is so close that these variations are detectable (both from the ground and from space).

In the last 12 years convincing evidence has been found for Solar-like oscillations in other stars. The principal drivers for this progress are the satellite missions COROT and Kepler.

$\Rightarrow$ solar-like oscillations appear to be a generic feature of stars with convection zones

Asteroseismology — how does it work?

"Using the observed oscillation frequencies of a star to infer its interior structure"

- If the structure of our model is "close" to the actual structure of the star, then the small differences between the observed frequencies and the model frequencies give us specific information about the internal structure of the star

This can be illustrated with a simple physical example: The Vibrating String.

$$\frac{1}{c^2}\frac{\partial^2\psi}{\partial t^2} = \frac{\partial^2\psi}{\partial x^2} \quad \Rightarrow \quad \omega_n = n\pi c/L, \quad n = 1, 2, 3\ldots$$

Now perturb the "sound speed" c at the point x, $\delta c(x)$

location of perturbation $\delta c(x)$

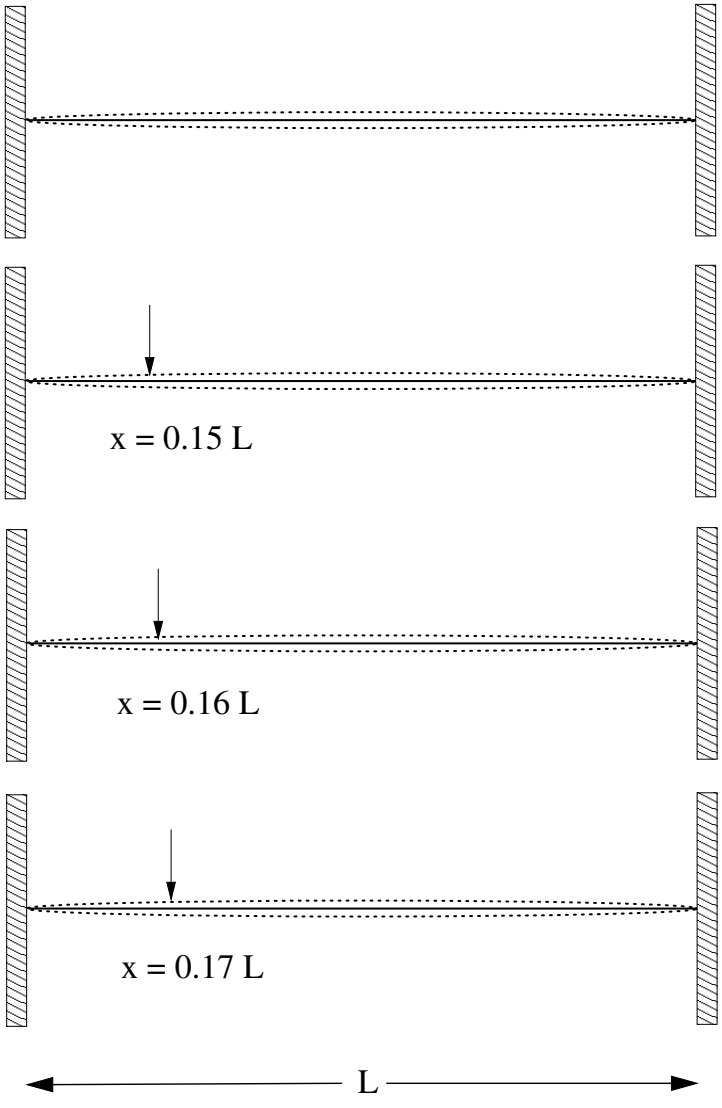

$\Delta\omega_n \equiv \omega_{n+1} - \omega_n - \pi c/L$

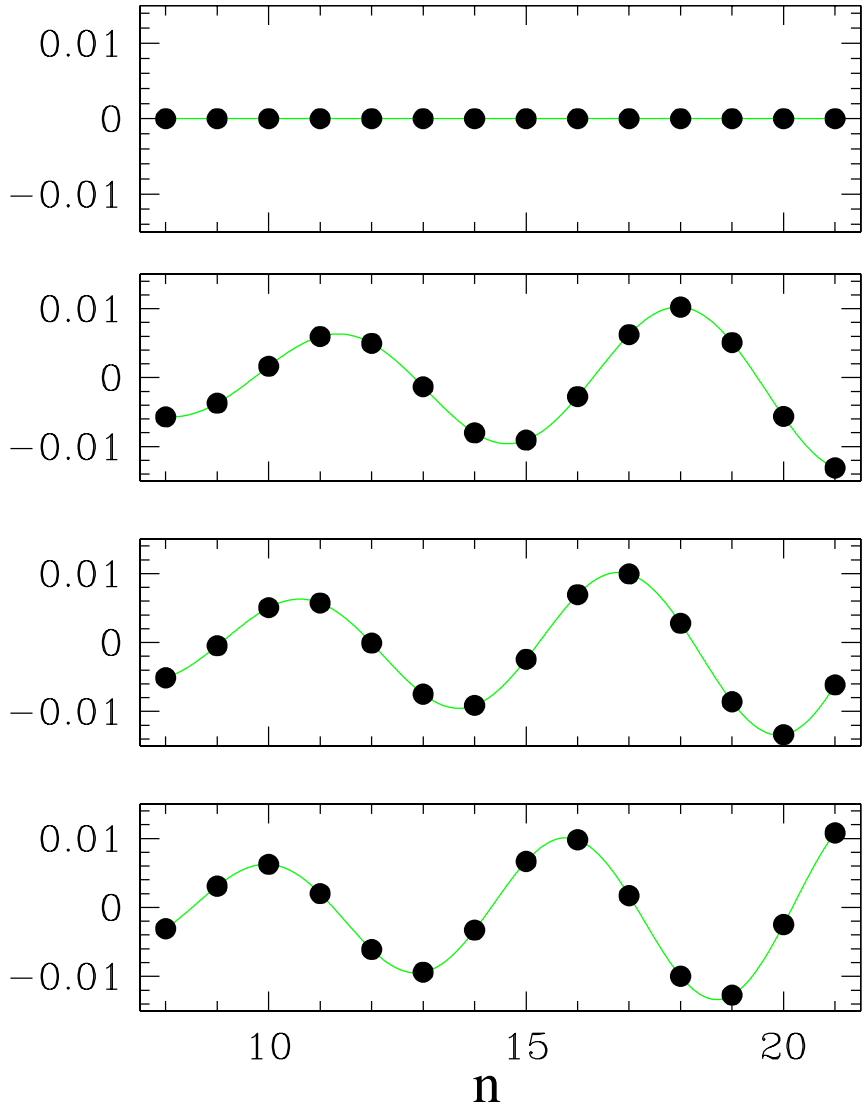

Pattern of $\Delta\omega_n$ vs n gives location of $\delta c(x)$

Amplitude of $\Delta\omega_n$ vs n gives magnitude of $\delta c(x)$

How this works mathematically…

It can be shown that the string equation,

$$\frac{d^2\psi}{dx^2} + \frac{\omega^2}{c^2}\psi = 0,$$

can be derived from a variational principle for ω^2:

$$\omega^2[\psi] = \frac{\int_0^L dx \, \left(\frac{d\psi}{dx}\right)^2}{\int_0^L dx \, \frac{1}{c^2}\psi^2}.$$

If $\omega^2[\psi]$ is an extremum with respect to ψ, then

$$\delta\omega^2[\psi] \equiv \omega^2[\psi + \delta\psi] - \omega^2[\psi] = 0$$

$$\propto \int_0^L dx \, \delta\psi \left(\frac{d^2\psi}{dx^2} + \frac{\omega^2}{c^2}\psi\right).$$

For $\delta\omega^2$ to be zero for arbitrary variations $\delta\psi$ requires that

$$\Rightarrow \frac{d^2\psi}{dx^2} + \frac{\omega^2}{c^2}\psi = 0$$

Keeping this in mind, consider a small change in $c(x)$, $\delta c(x)$, and the effect which it has on the frequencies, ω_n:

- produces a small change in ψ, $\delta\psi$, and in ω, $\delta\omega$
- due to variational principle, $\delta\psi$ does not contribute to the perturbed integral, to first order in δc, so we can effectively treat ψ as unchanged

$$\begin{aligned}
\frac{\delta\omega_n}{\omega_n} &= \frac{2}{A^2 L}\int_0^L dx \left(\frac{\delta c}{c}\right)\psi_n^2 \\
&\equiv \int_0^L dx \left(\frac{\delta c}{c}\right) K_c \\
&\equiv \frac{2}{L}\int_0^L dx \left(\frac{\delta c}{c}\right)\sin^2(k_n x)
\end{aligned}$$

- Note: K_c is called the *kernel* of c for the n^{th} eigenfunction

As an example, if

$$\delta c = 0.06\, L\, c\, \delta(x - x_0),$$

then we find the following perturbations to the frequencies:

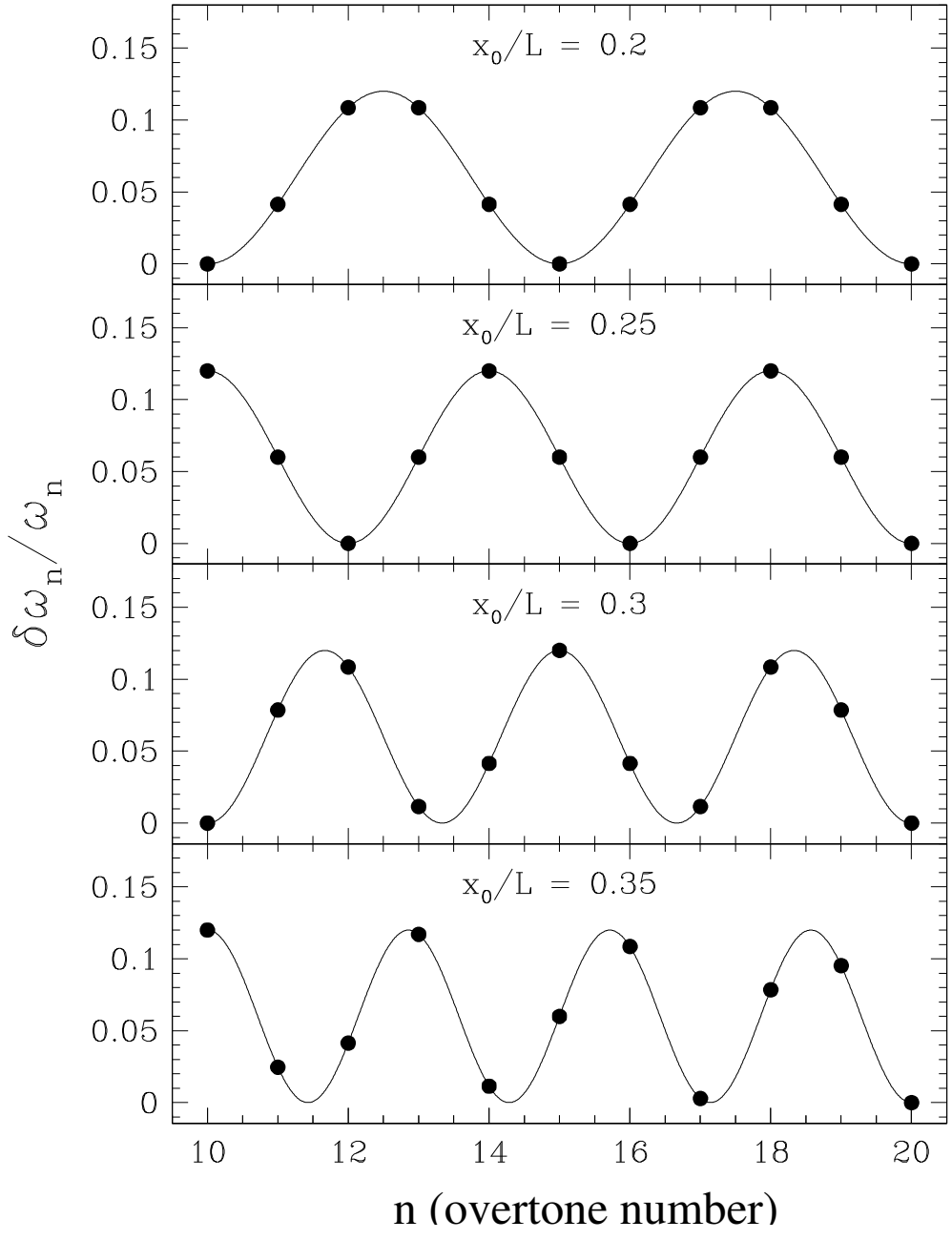

This is because the different modes show different sensitivities to the perturbation because they have different kernels (eigenfunctions):

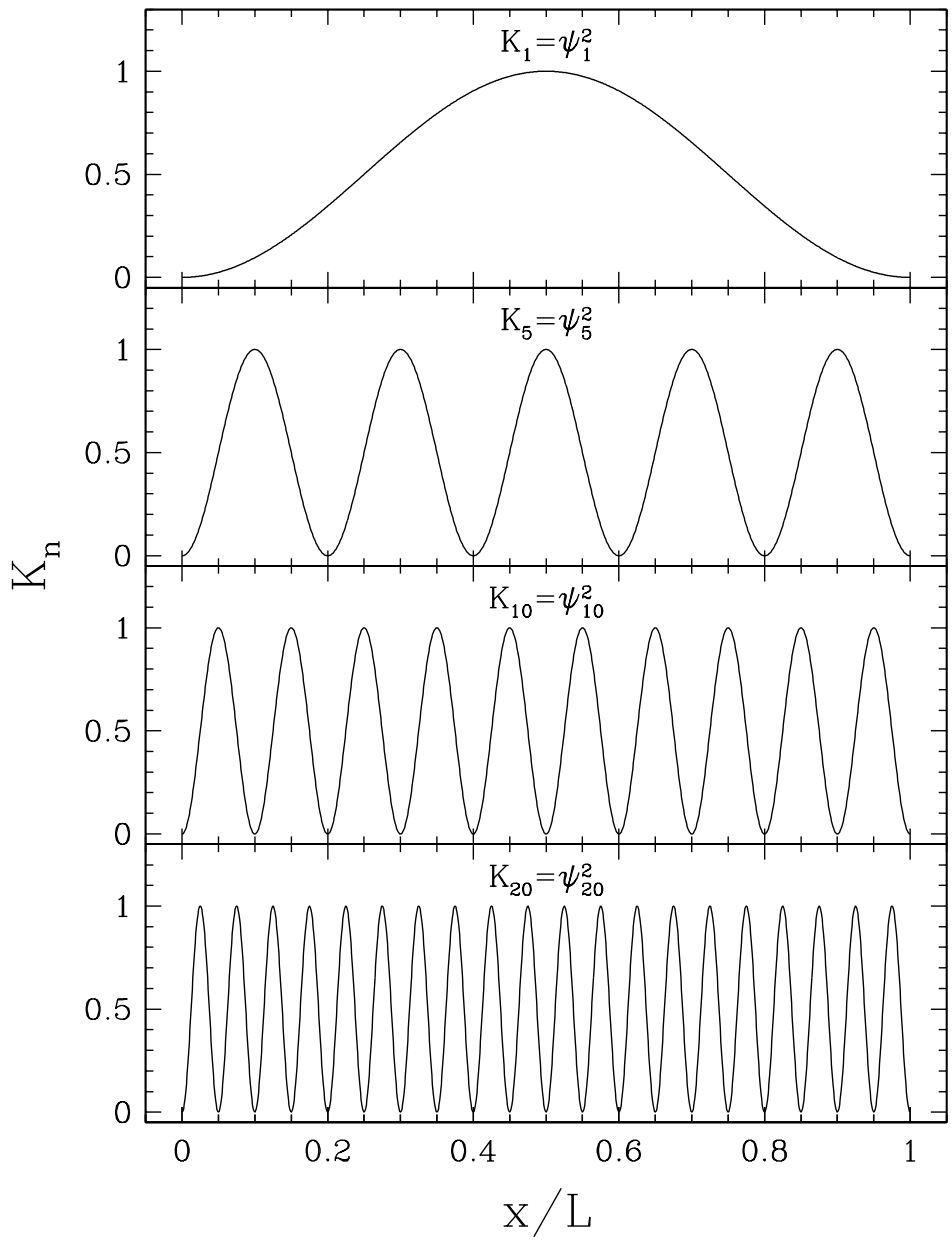

Example: specially chosen bumps for the string

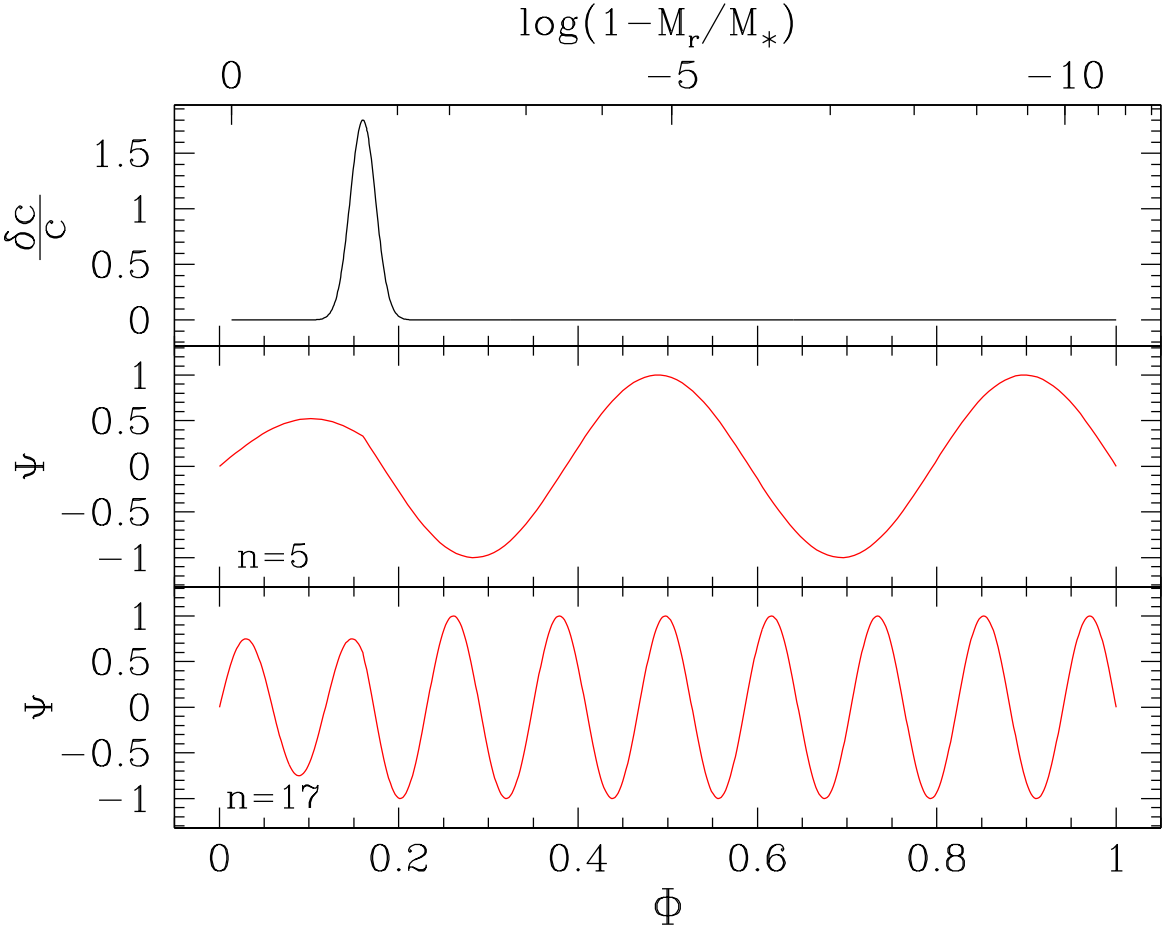

(Montgomery 2005, ASP, 334, 553)

The bump/bead introduces “kinks” into the eigenfunctions. Sharp bumps produce larger kinks than broader ones.

Example: specially chosen bumps for the string

The bumps also introduce patterns into the frequency and/or period spacings:

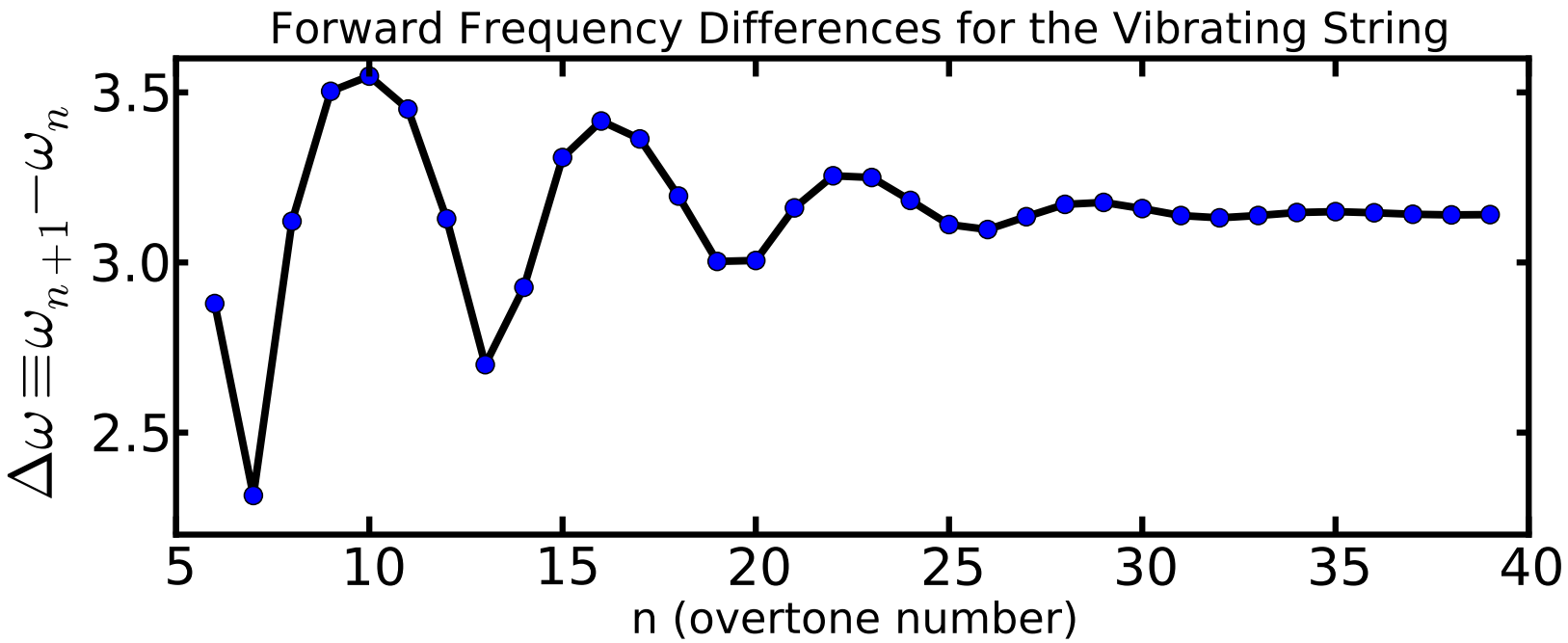

Example: specially chosen bumps for the string

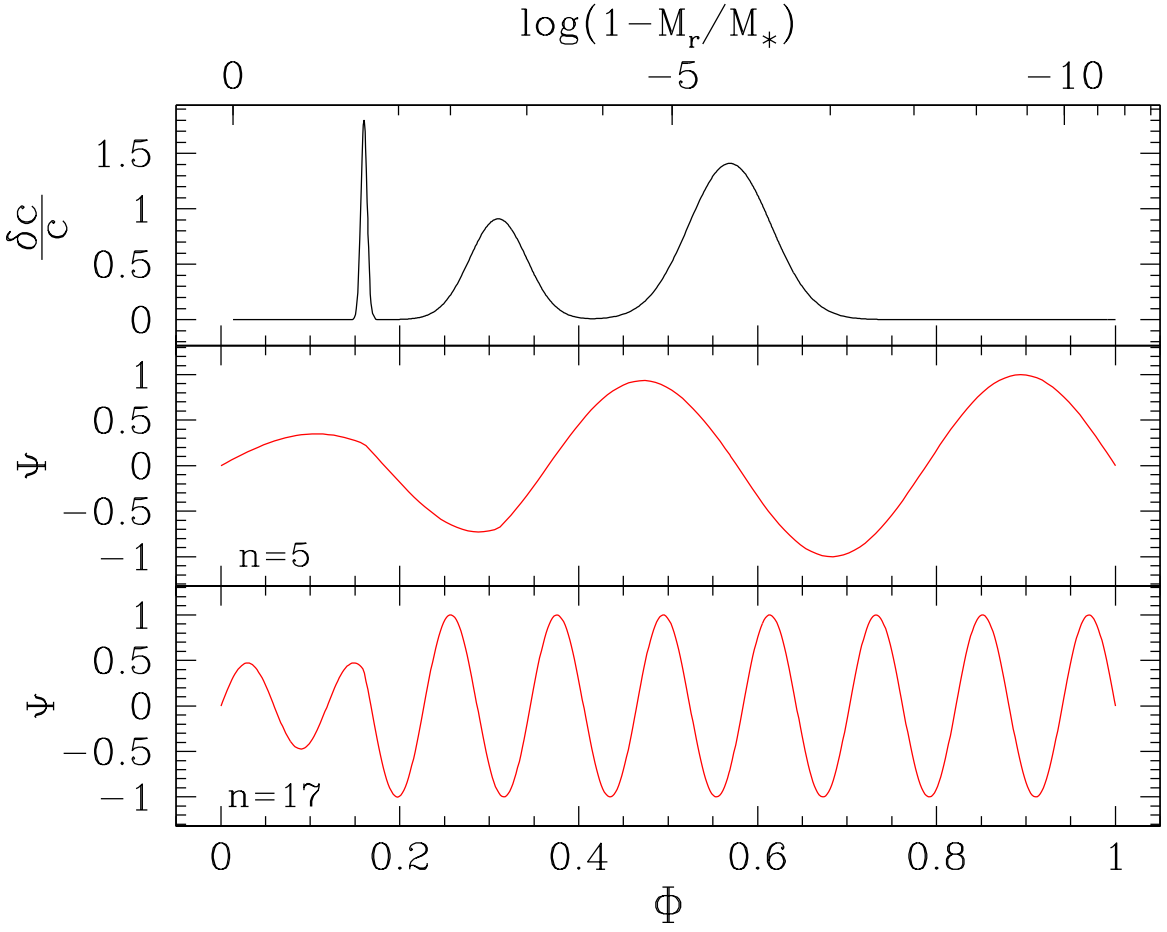

(Montgomery 2005, ASP, 334, 553)

Three beads introduce three “kinks” into the eigenfunctions. Sharp bumps produce larger kinks than broader ones. Note the amplitude difference across the bumps due to partial reflection of the waves.

Example: specially chosen bumps for the string

The pattern in the frequency spacing is a superposition (in the linear limit) of the patterns introduced by the individual beads:

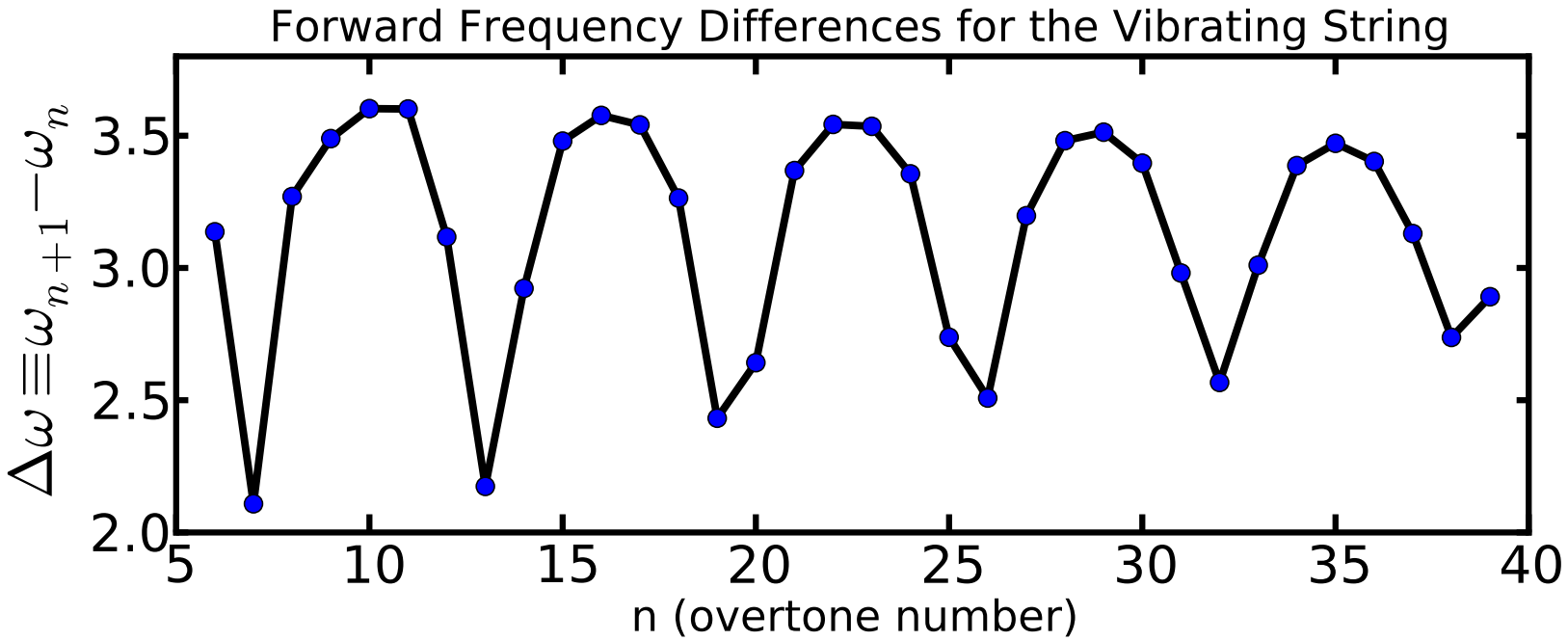

The perturbations assumed here in $\delta c/c$ are *not* in the small/linear limit.

Why do we care? Because beads on a string are like bumps in a stellar model

Changes in the chemical profiles (in a WD) produce bumps in the Brunt-Väisälä frequency. These bumps produce mode trapping in exactly they way that beads on a string do. This allows us to learn about the location and width of chemical transition zones in stars.

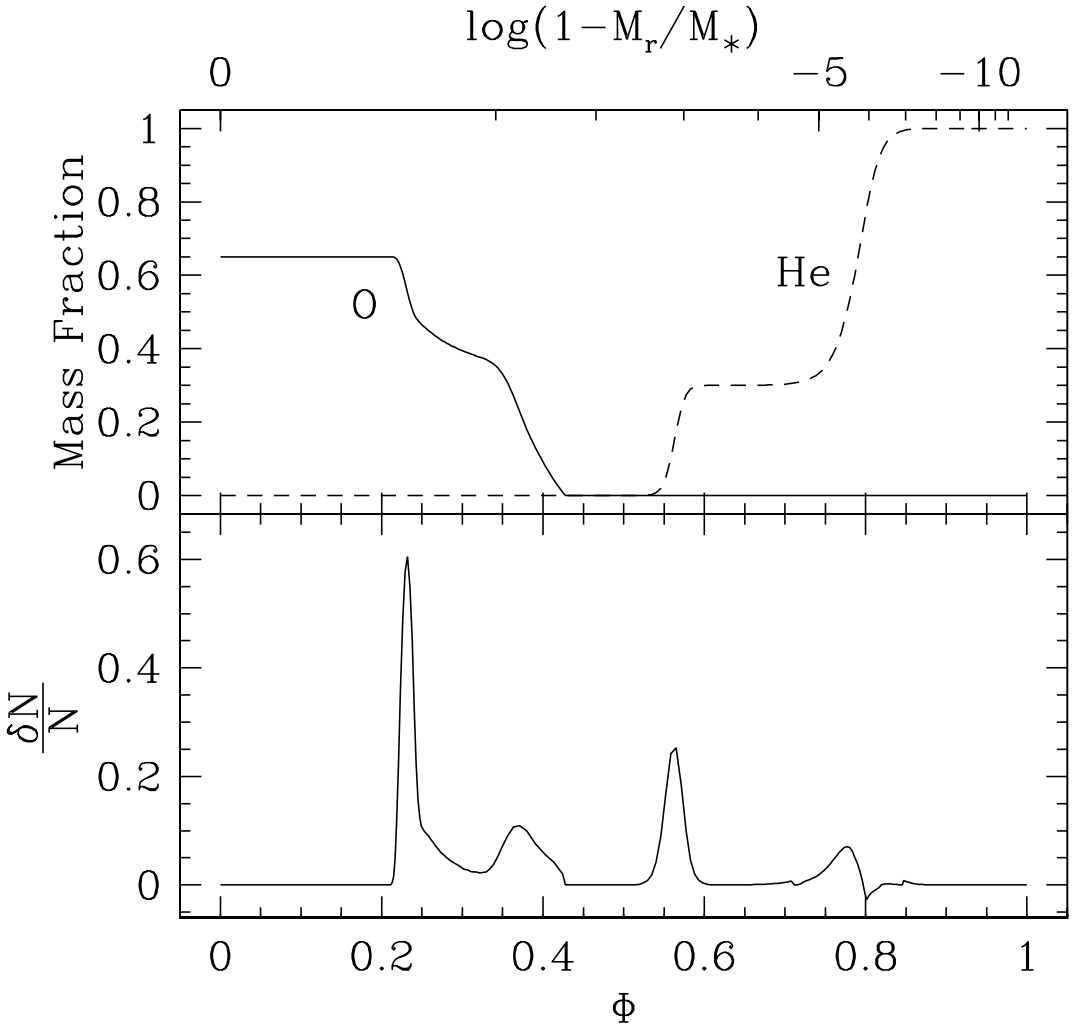

$\Phi \equiv$ "normalized buoyancy radius" $\propto \int_0^r dr|N|/r$

Mode trapping of eigenfunctions in a WD model due to the composition transition zones.

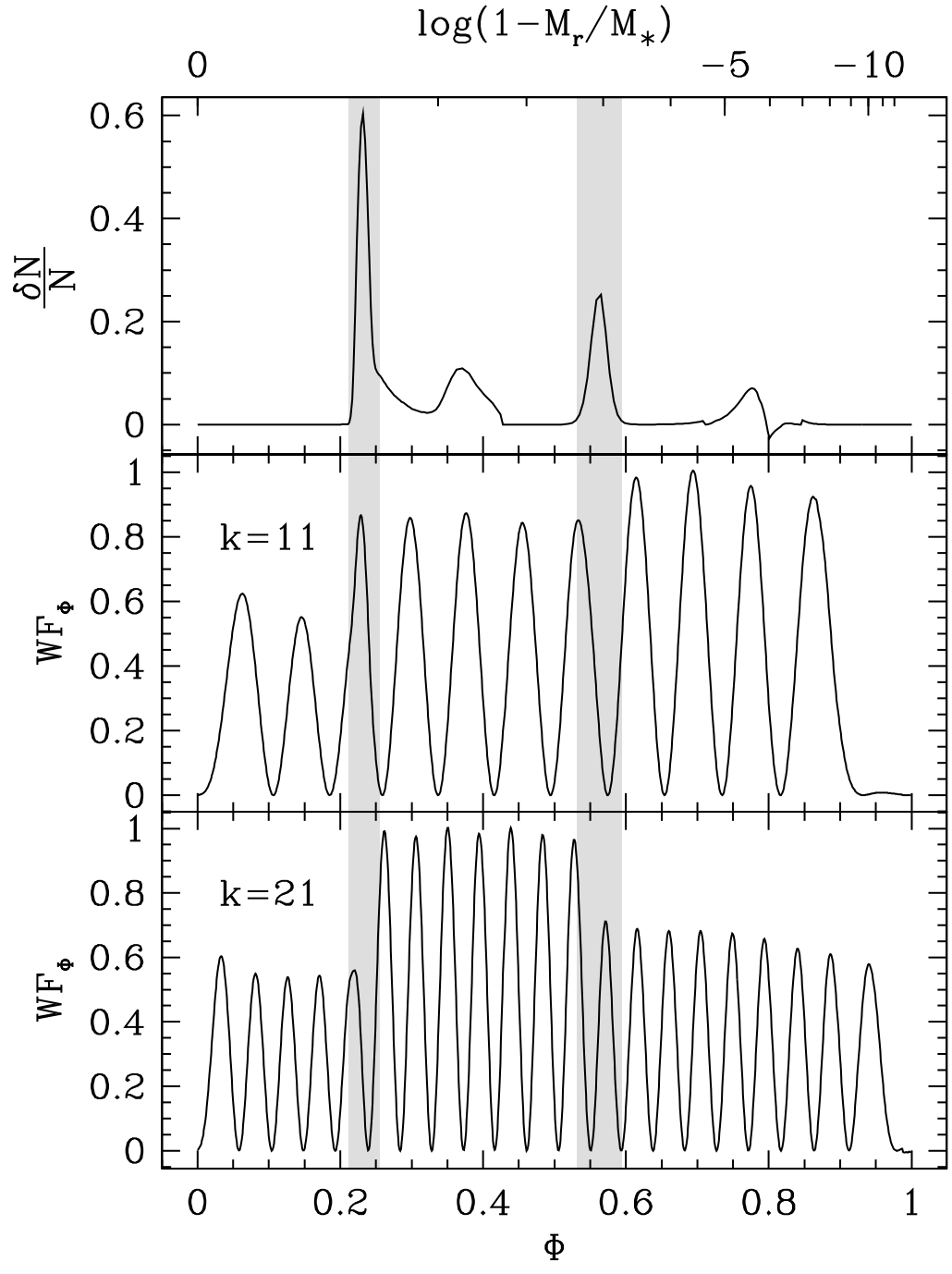

Mode trapping also affects the period spacings…

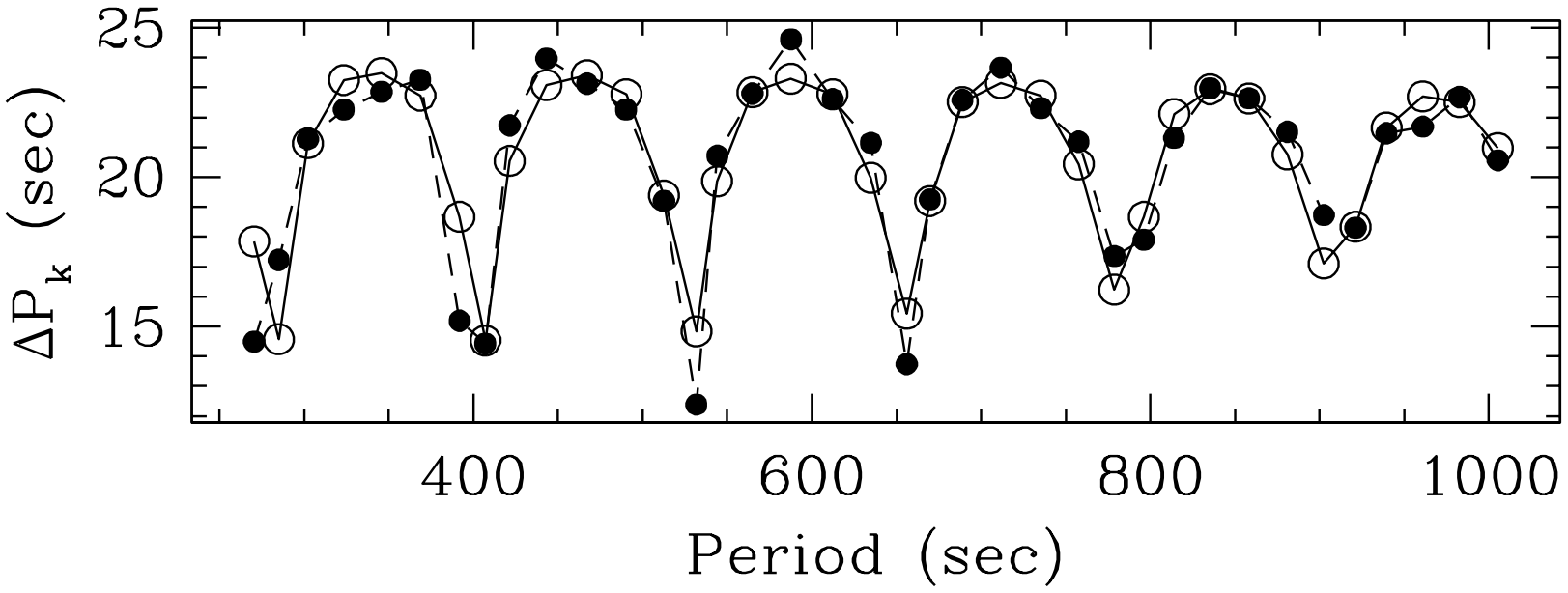

(Córsico, Althaus, Montgomery, García–Berro, & Isern, 2005, A&A, 429, 277)

The open circles/solid lines are the mode trapping seen in a full WD model and the filled circles/dashed lines are the result of applying the simple beaded string approach. This shows that the string analogy captures much of the physics of the full problem.

The Core/Envelope Symmetry

For the vibrating string, a bump near one end of the string produces the same set of frequencies as a bump the same distance from the other end of the string.

In the same way, a “bump” in the buoyancy frequency in the deep interior of a WD can mimic a bump in its envelope.

So a bump at $M_r \approx 0.5\, M_\star$ can mimic a bump at $\log(1 - M_r/M_\star) \approx -5.5$ and vice versa.

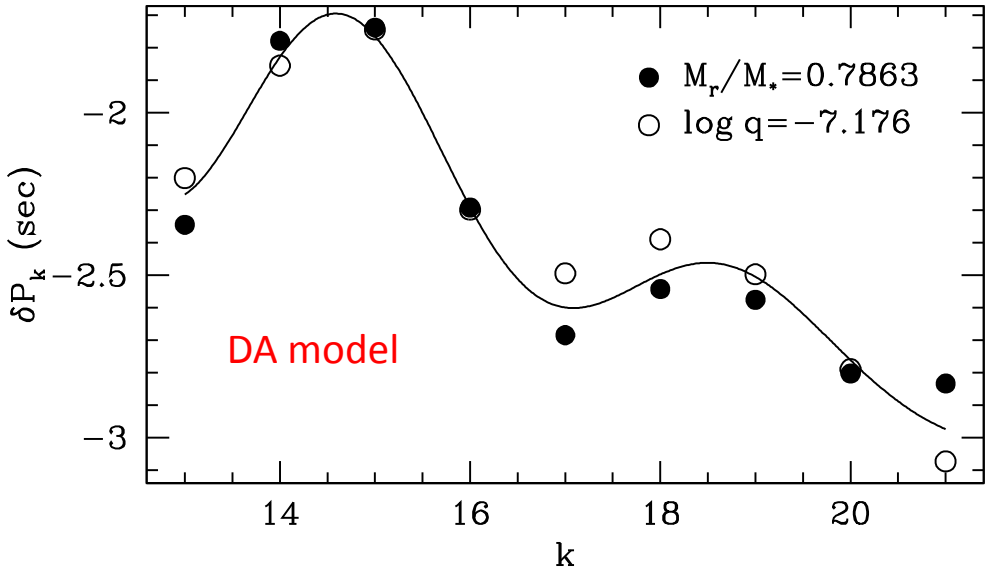

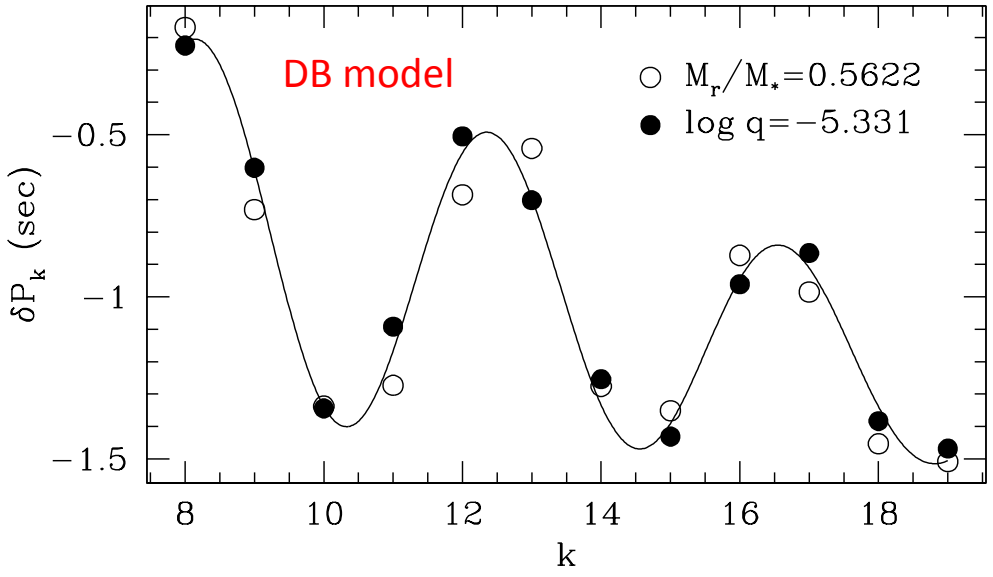

The Core/Envelope Symmetry

We can map the connection between these “reflection” points, points in the envelope that produce qualitatively the same signature as points in the core:

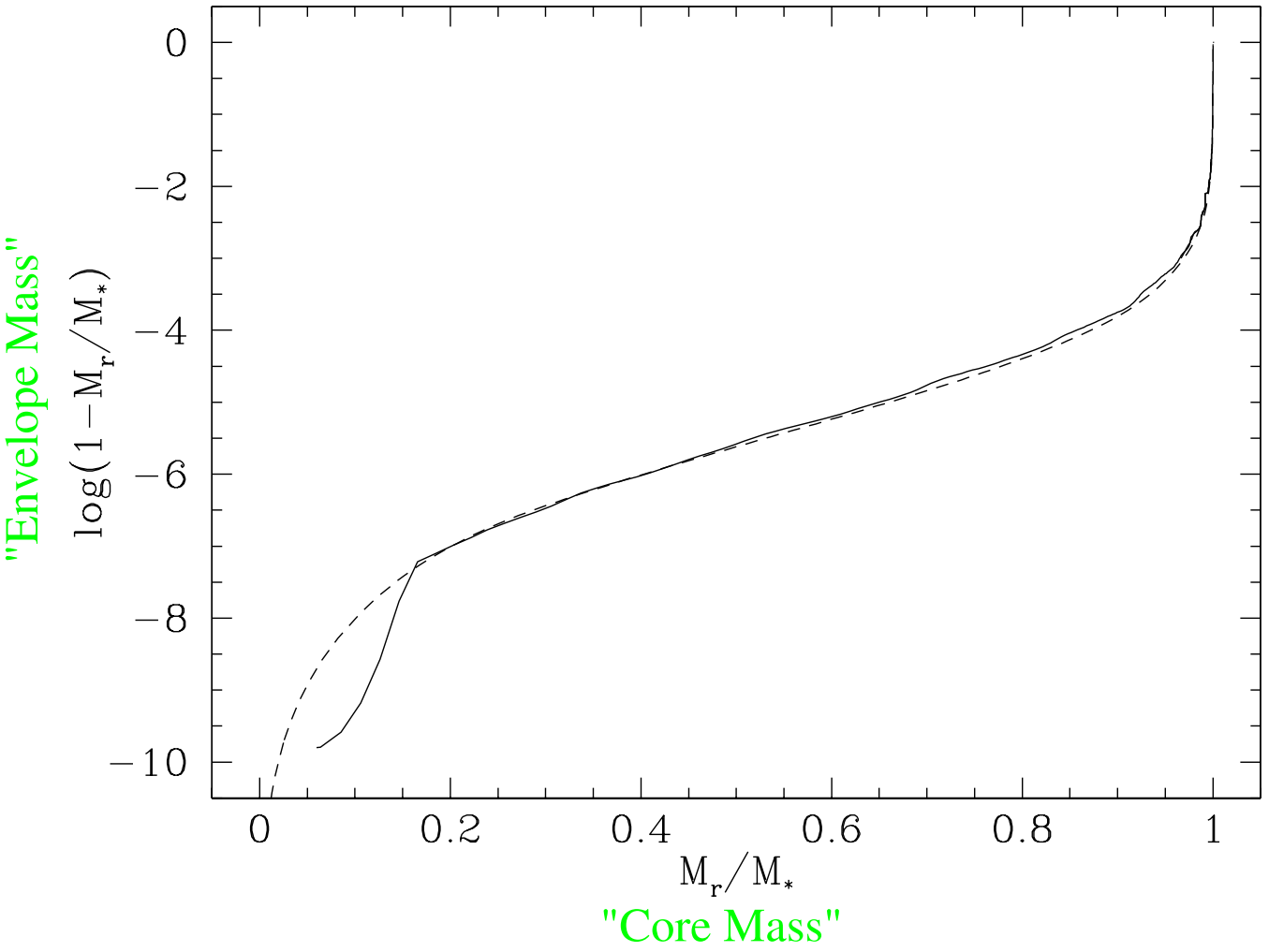

Observations and Time Series Data

Pulsations are observed by time series measurements of

- intensity variations
- radial velocity variations

Only for the case of the Sun can we obtain disc-resolved measurements of the perturbations.
For other stars, we observe the light integrated over the observed disc of the star, although the techniques of Doppler Imaging can be used to provide information about the spatial structure of the perturbations on the stellar surface.

Sampling and Aliasing

In trying to recover frequencies from data, it is important for any gaps in the data to be as small as possible

- This is because data gaps introduce false peaks into the Fourier transform
  - these peaks are called “aliases” of the true frequency
  - *a priori*, one cannot tell which peaks are the “true” peaks and which are the aliases (especially if several frequencies are simultaneously present)

For instance, if one observes a star from a single observatory, one might obtain 8 hours of data per night with a 16-hour gap until the next night’s observations.

Sampling and Aliasing (cont.)

Taking the Fourier Transform of such a signal, we find that

$$|A(\omega)| =$$

$$\frac{\sin[N\, t_D(\omega - \omega_0)/2]}{\sin[t_D(\omega - \omega_0)/2]} \cdot \frac{\sin[t_N(\omega - \omega_0)/2]}{t_N(\omega - \omega_0)/2}$$

where, t_D is the length of a day in seconds, t_N is the length of time observed per night, ω_0 is the angular frequency of the input signal, and N is the number of nights observed.

The alias structure of a single frequency, sampled in the same way as the data, is called the “spectral window”, or just the “window”. The closer this is to a delta function, the better.

Sampling and Aliasing (cont.)

five 8-hour nights with
16-hour gaps

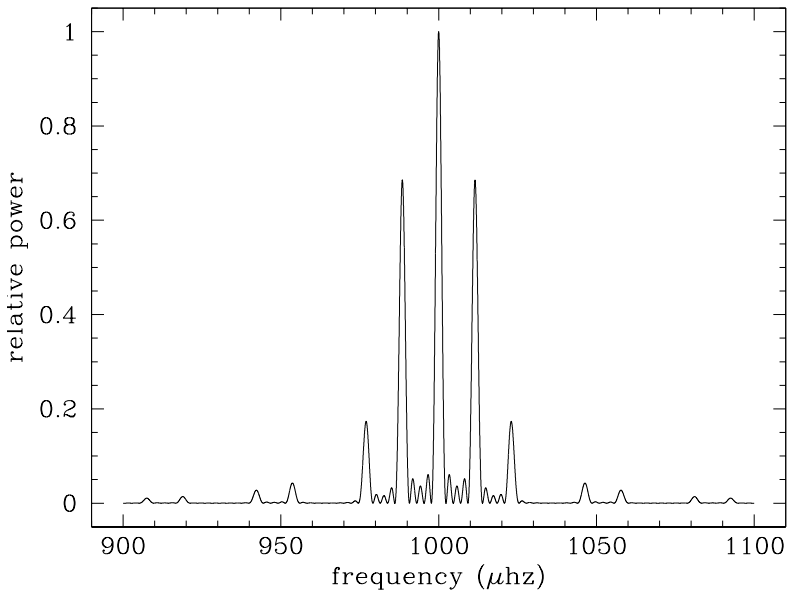

five days continuous data

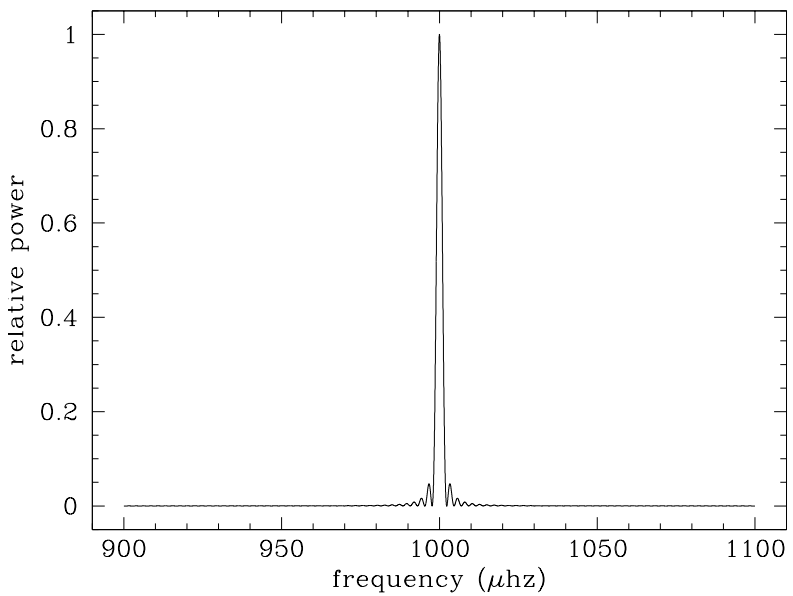

Sampling and Aliasing (cont.)

Two obvious solutions to this problem:

- observe target continuously from space
  - SOHO (Solar Heliospheric Observatory)
  - *Kepler* satellite
- observe target continuously from the ground…using a network of observatories
  - WET (Whole Earth Telescope)
  - BISON (Birmingham Solar Oscillations Network)
  - GONG (Global Oscillations Network Group)

Spectral window for WET observations of the white dwarf GD 358

(Winget, D. E. et al. 1994, ApJ, 430, 839)

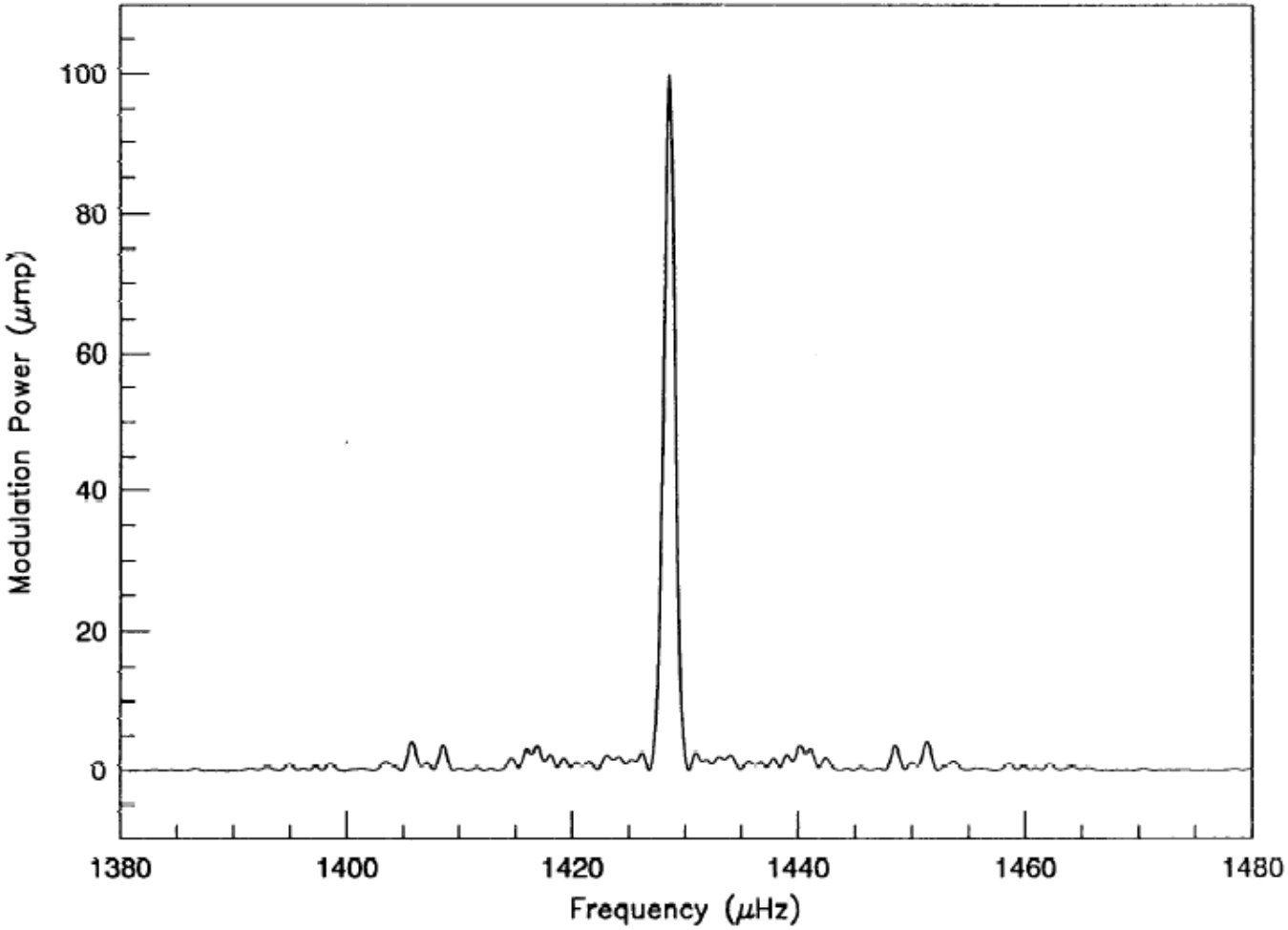

FIG. 2.—Spectral window for the complete GD 358 data set, showing the pattern of peaks that will result from the presence of a single frequency in the power spectrum, in units of micromodulation power (μmp).

Power spectrum of the white dwarf GD 358

(Winget, D. E. et al. 1994, ApJ, 430, 839)

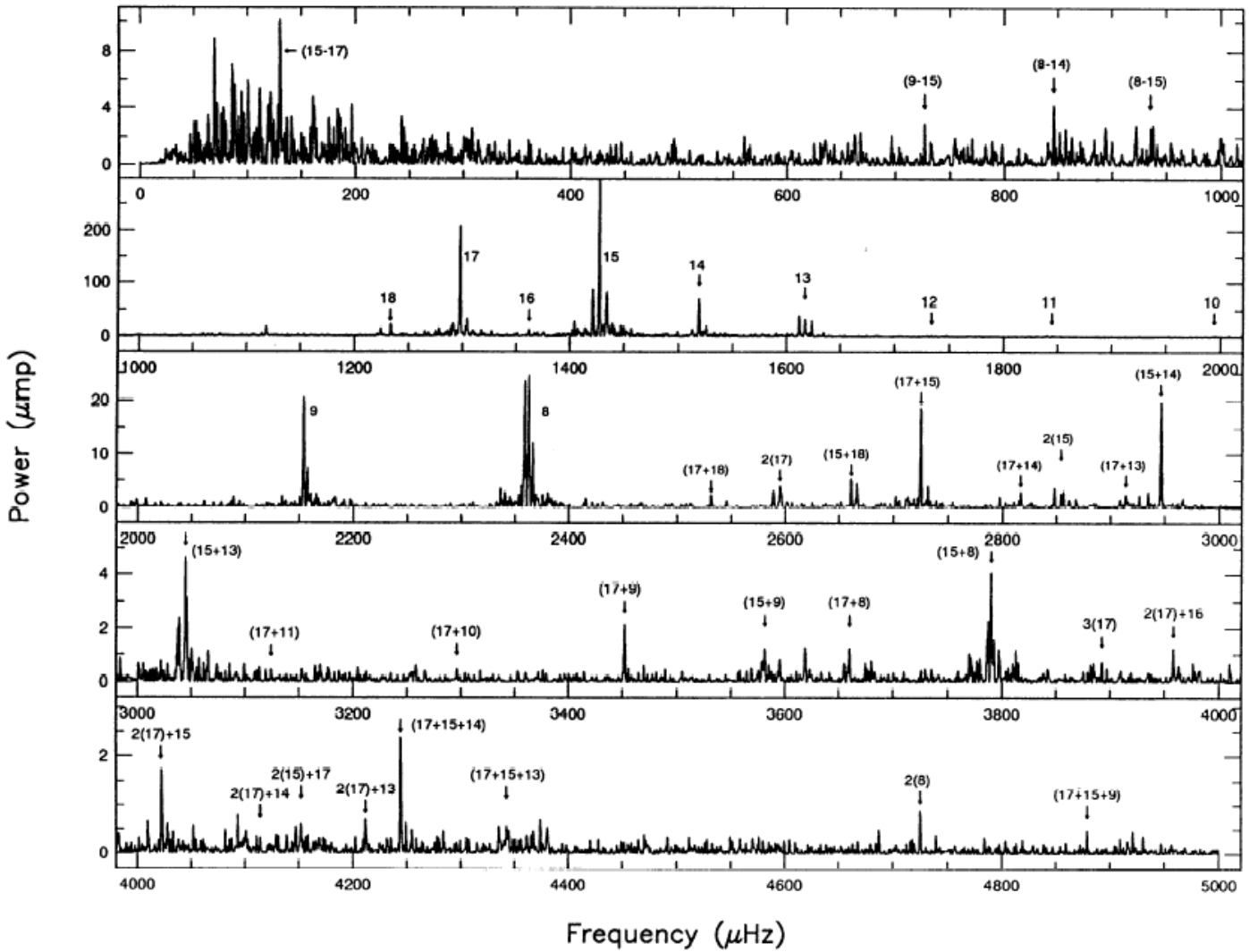

FIG. 7.—Full power spectrum of GD 358. The different scales for each panel attempt to accommodate the large dynamic range present. Triplets are labeled with their corresponding *k*-value, and the sum and difference frequencies are labeled with the *k*-values for the triplets which combine to form them.

Helioseismology: Asymptotic relation for p-mode frequencies

A more systematic analysis of the adiabatic equations for the n *and* ℓ dependence of p-mode frequencies gives

$$\nu_{n\ell} \simeq \underbrace{\left(n + \frac{\ell}{2} + \frac{1}{4} + \alpha\right)\Delta\nu}_{\text{dominant, “large separation”}} - \underbrace{(AL^2 - \delta)\frac{\Delta\nu^2}{\nu_{n\ell}}}_{\text{“small separation”}}$$

- valid in high-n, low-ℓ limit

$$\Delta\nu = \left[2\int_0^R \frac{dr}{c}\right]^{-1} = \text{inverse sound crossing time}$$

- near degeneracy of modes: $\nu_{n\ell} \simeq \nu_{n-1,\ell+2}$
- *deviations* from this near degeneracy give us information about the radial structure of the Sun or other stars

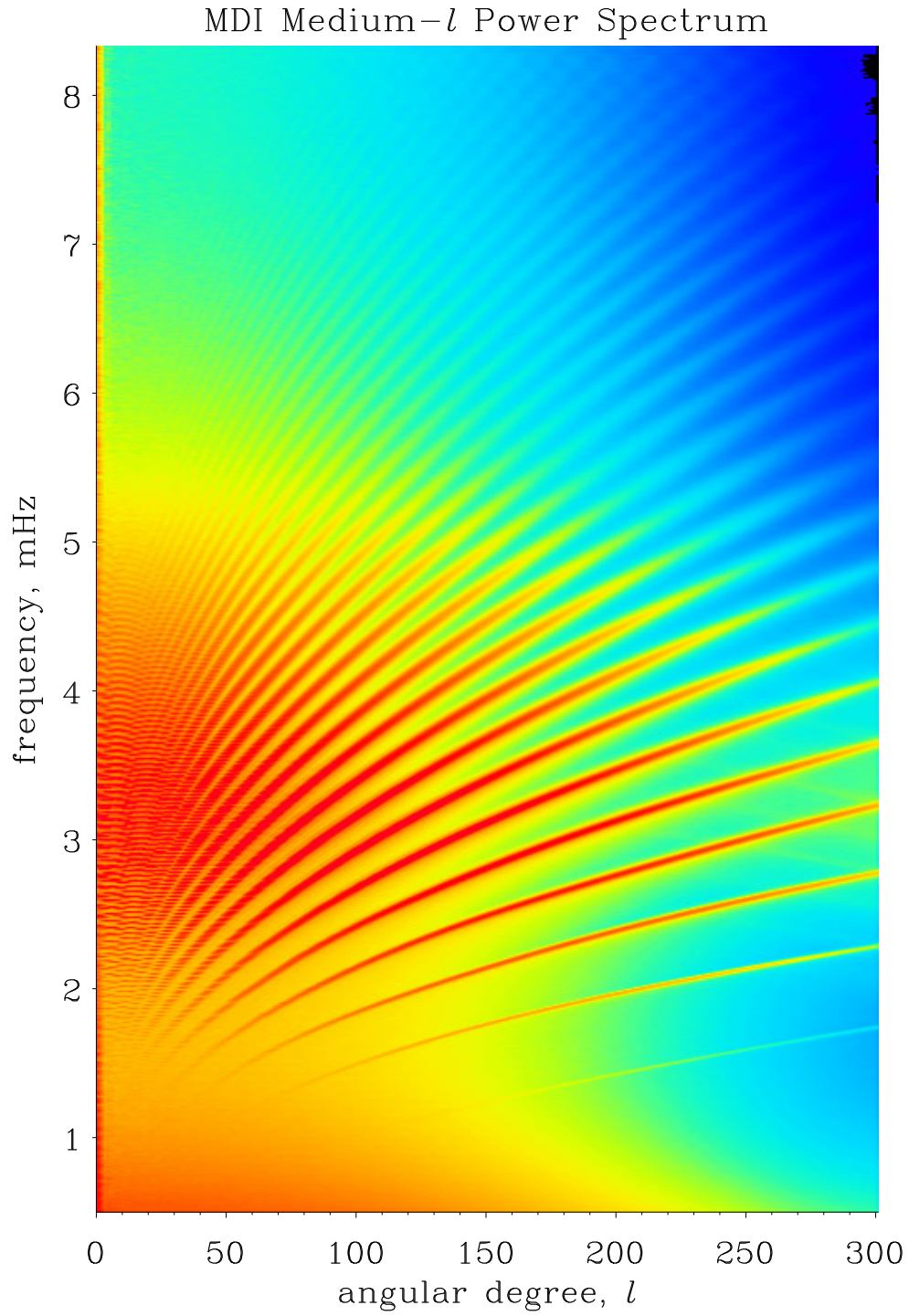
MDI Medium−l Power Spectrum
frequency, mHz
1
2
3
4
5
6
7
8
0
50
100
150
200
250
300
angular degree, l

Helioseismology

Helioseismology is the application of exactly these principles to the oscillations in the Sun:

$$\frac{\delta\omega_{n\ell}}{\omega_{n\ell}} = \int_0^R \left[K_{c^2}^{n\ell} \frac{\delta c^2}{c^2} + K_{\rho}^{n\ell} \frac{\delta\rho}{\rho} \right] dr$$

In the above formula, we have defined

$$\begin{aligned}
\delta\omega_{n\ell} &\equiv \omega_{n\ell}(\text{observed}) - \omega_{n\ell}(\text{model}) \\
\delta c^2 &\equiv c^2(\text{Sun}) - c^2(\text{model}) \\
\delta\rho &\equiv \rho(\text{Sun}) - \rho(\text{model}) \\
K_{c^2}^{n\ell} &\equiv \text{the sampling kernel for } c^2 \\
&\quad \text{for eigenmode } \{n, \ell\} \\
K_{\rho}^{n\ell} &\equiv \text{the sampling kernel for } \rho \\
&\quad \text{for eigenmode } \{n, \ell\}
\end{aligned}$$

Given the large number of observed modes in the Sun (millions, literally), we can hope to construct "locally optimized kernels" by looking at the appropriate linear combinations of the frequency differences, $\delta\omega_{n\ell}$:

$$\sum_{n,\ell} A_{n\ell} \frac{\delta\omega_{n\ell}}{\omega_{n\ell}} =$$

$$\int_0^R \left[\frac{\delta c^2}{c^2} \underbrace{\sum_{n,\ell} A_{n\ell} K_{c^2}^{n\ell}}_{\equiv K_{c^2}^{\rm opt}} + \frac{\delta\rho}{\rho} \underbrace{\sum_{n,\ell} A_{n\ell} K_{\rho}^{n\ell}}_{\equiv K_{\rho}^{\rm opt}} \right] dr$$

Since the original kernels are oscillatory, such as individual terms in a Fourier series, by choosing the $\{A_i\}$ appropriately we can make the optimized kernels, $K_x^{\rm opt}$ have any functional form we choose. In particular, …

Inversions

The $A_{n\ell}$ can be chosen such that

- $K^{\rm opt}_{c^2}$ is strongly peaked at $r = 0.75\,R_\odot$, say
- $K^{\rm opt}_{\rho}$ is negligibly small everywhere (is suppressed)

The result: a helioseismic inversion for the sound speed in the Sun

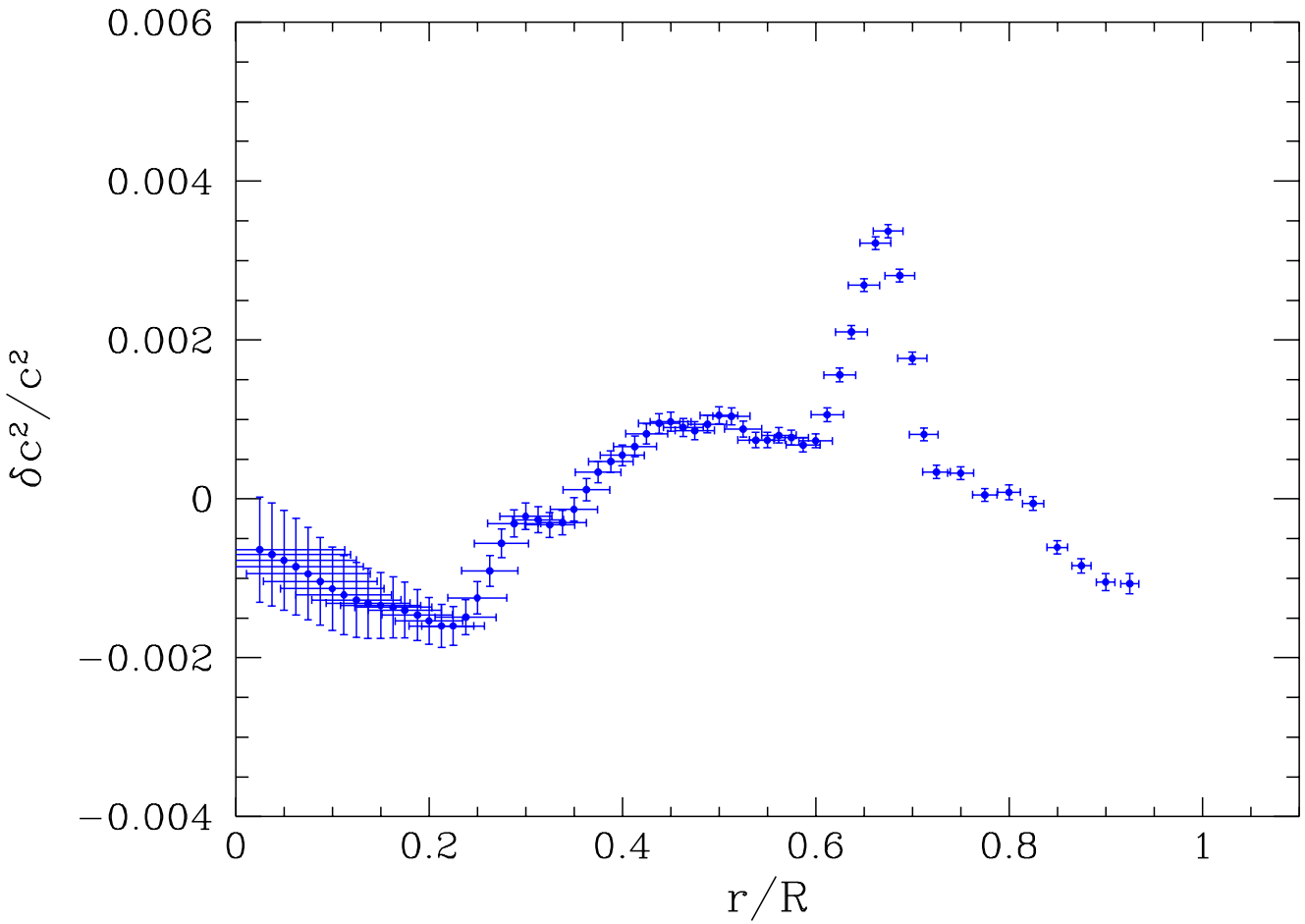

The most conspicuous feature of this inversion is the bump at $r \sim 0.65\, R_\odot$, where

$$\delta c^2 \equiv c^2(\mathrm{Sun}) - c^2(\mathrm{model})$$

- most likely explanation has to do with He settling (diffusion)
  - the model includes He settling, which enhances the He concentration in this region
  - overshooting of the convection zone may inhibit He settling

  $\Rightarrow$ Sun has lower He concentration than model at this point
  - since $c^2 \propto \Gamma_1 T/\mu$, and model has higher μ than Sun, this produces a positive bump in δc^2

Why do inversions work so well for solar p-modes?

- solar p-modes can be thought of as sound waves which refract off the deeper layers
- depth of penetration depends on ℓ

  low-ℓ: penetrate deeply, sample the core

  high-ℓ: do not penetrate deeply, sample only the envelope

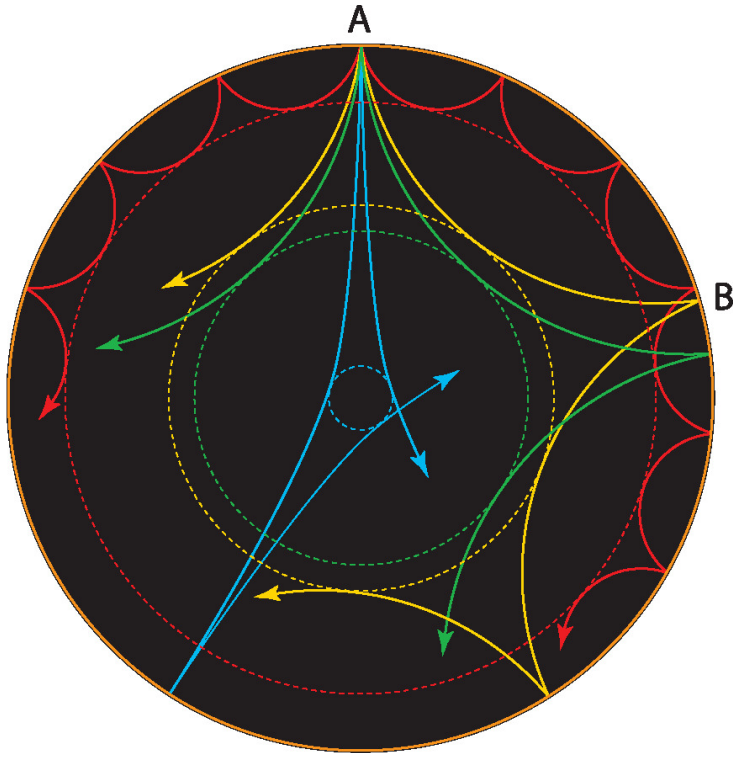

$\Rightarrow$ different ℓ's are very linearly independent

$\Rightarrow$ relatively easy to construct localized kernels

Refraction of p-modes

- p-modes are essentially sound waves
- $c_s^2 \sim k_B T/m$

$\Rightarrow$ c_s^2 is a decreasing function of r

- wavefront is refracted upward
  - "mirage" or "hot road" effect

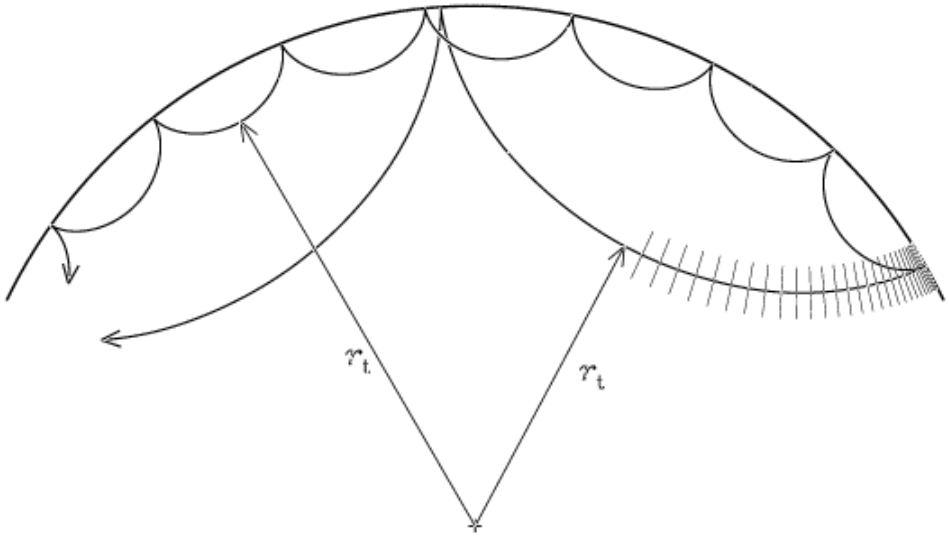

Figure 5.4. Propagation of acoustic waves, corresponding to modes with $l = 30$, $\nu = 3\,\mathrm{mHz}$ (deeply penetrating rays) and $l = 100$, $\nu = 3\,\mathrm{mHz}$ (shallowly penetrating rays). The lines orthogonal to the former path of propagation illustrate the wave fronts.

Major Results of Helioseismology

- depth of the convection zone measured
  - found to be ~ 3 times deeper than previously thought (models in the 1970's had been "tweaked" to minimize the Solar neutrino problem)

In addition, Houdek and Gough (2007, MNRAS, 375, 861) have recently shown that, by looking at second differences of low-ℓ modes only, one could derive the depth of the convection zone:

Major Results of Helioseismology (cont.)

$$(\Delta_2\nu \equiv \nu_{n+1,\ell} - 2\,\nu_{n,\ell} + \nu_{n-1,\ell})$$

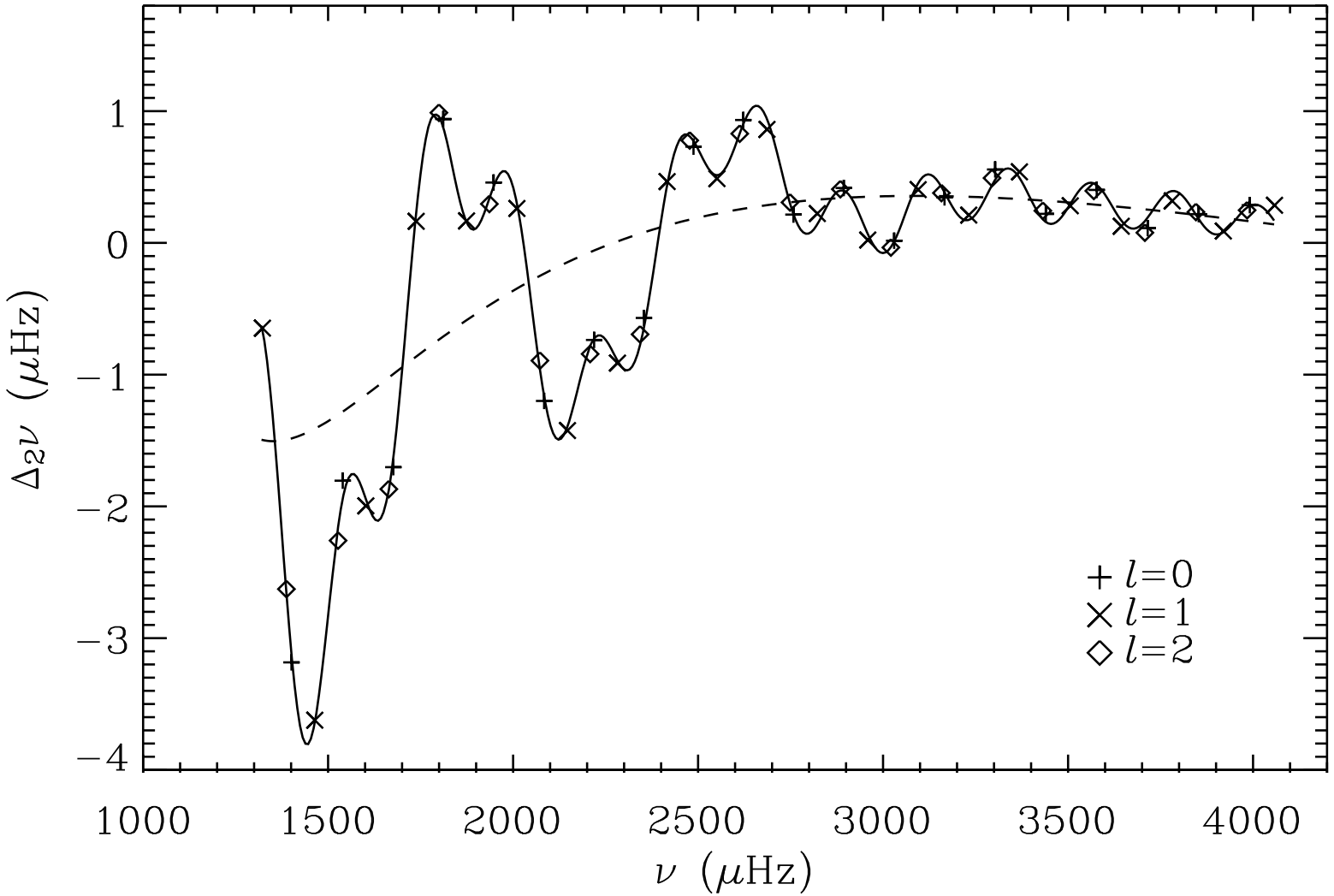

$$r_C/R_\odot \simeq 0.7$$

Major Results of Helioseismology (cont.)

- the standard opacities used up to the late 1980's were found to be ~ 3 too small

  the effects of metals needed to be added
  - this led to the:

    OPAL opacity project (Iglesias & Rogers 1996, ApJ, 464, 943)
    OP opacity project (Seaton et al. 1994, MNRAS, 266, 805)
  - this had effects throughout the H-R diagram:
    e.g., with new higher opacities, the pulsations of B stars could now be explained (bump in opacity due to partial ionization of metals — Dziembowski & Pamyatnykh 1993, MNRAS, 262, 204)

Major Results of Helioseismology (cont.)

- detection of differential rotation in the Sun
  - rotation profile different from what was theoretically expected
- discovery of a shear layer near the base of the Solar convection zone (the “tachocline”)

Both of these effects have to do with rotation.

How does rotation affect a pulsating object?

The Effect of Rotation

- breaks spherical symmetry
  - analogous to an H atom in an external magnetic field
- lifts degeneracy of frequencies of modes with the same $\{n, \ell\}$ but different m
  - again analogous to an H atom (Zeeman splitting)
- frequencies are perturbed by the non-zero fluid velocities of the equilibrium state (e.g., to linear order by the “Coriolis force” and to second order by the “centrifugal force”)

The Effect of Rotation (cont.)

- if rotation may be treated as a perturbation ("slow rotation"), then we can calculate kernels which give the frequency perturbations as an average over the rotation profile $\Omega(r, \theta)$:

$$\delta\omega_{n\ell m} = \int_0^R dr \int_0^\pi r d\theta \, K_{n\ell m}(r, \theta) \, \Omega(r, \theta)$$

- for uniform ("solid body") rotation

$$\delta\omega_{n\ell m} = m \, \beta_{n\ell} \, \Omega_{\rm solid}$$

  $\Rightarrow$ $\delta\omega$ is linearly proportional to m, the azimuthal quantum number

- for more general (differential) rotation, e.g., $\Omega = \Omega(r, \theta)$, $\delta\omega$ is no longer a linear function of m

  $\Rightarrow$ departures from linearity give information about $\Omega(r, \theta)$

Rotational Inversion for the Sun

- radiative interior rotates rigidly
- convection zone rotates differentially
  - faster at equator
  - slower at poles

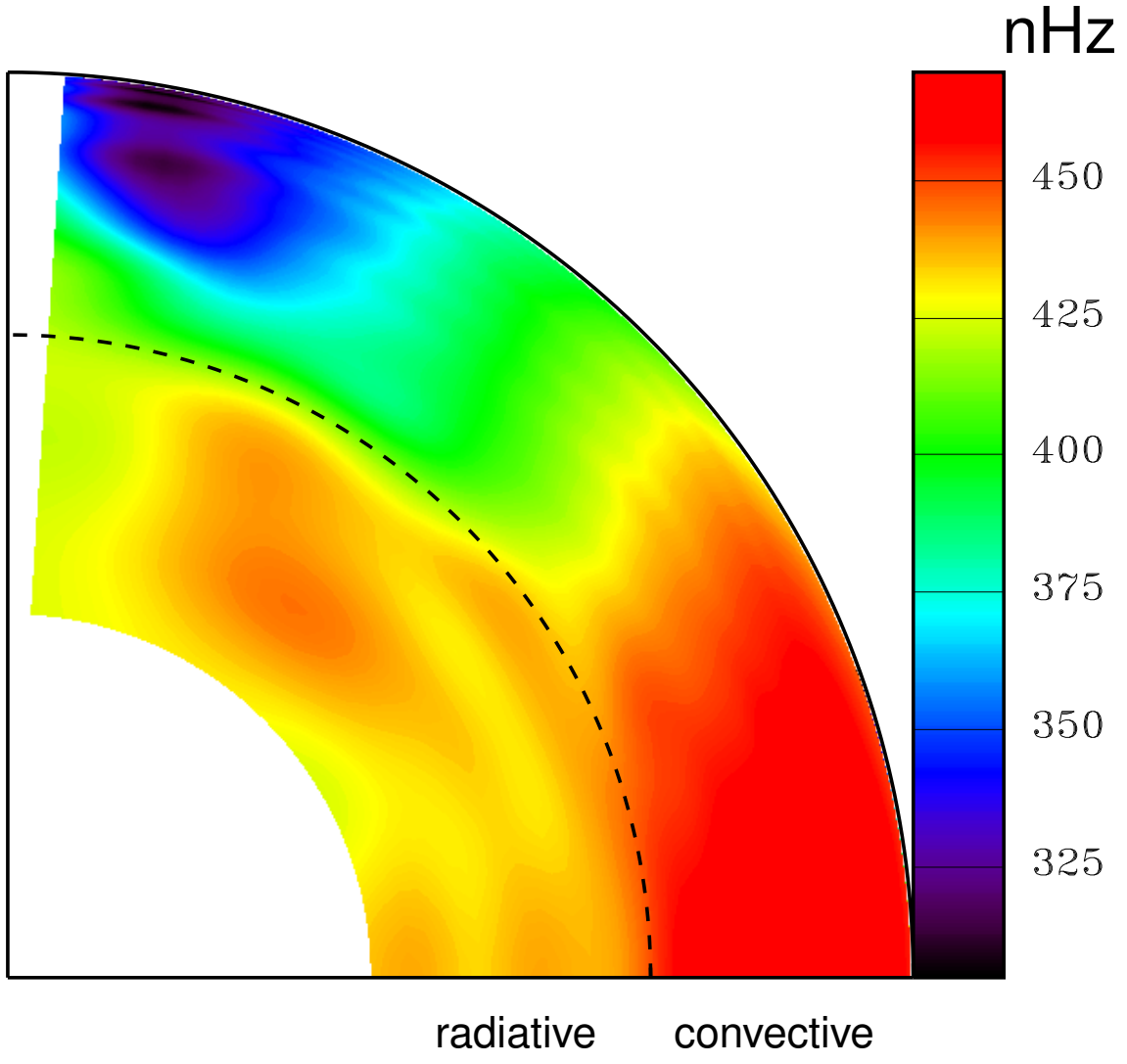

- naive models predict “constant rotation on cylinders”
  - in contrast, in the convective region, we find that the rotation rate is mainly a function of latitude, $\Omega \approx \Omega(\theta)$

  $\Rightarrow$ little radial shear in the convection zone
- nearly rigid rotation of radiative region implies additional processes are at work
  - e.g., a magnetic field could help these layers to rotate rigidly
- **The tachocline:** the region of shear between the rigidly rotating radiative region and the differentially rotating convective region

The Solar Tachocline

(from Charbonneau et al. 1999, Apj, 527, 445)

- location: $r \approx 0.70\, R_\odot$
- thickness: $w \approx 0.04\, R_\odot$
- prolate in shape:

$$\begin{aligned} r_t &\approx 0.69\, R_\odot \quad \text{(equator)} \\ r_t &\approx 0.71\, R_\odot \quad \text{(latitude } 60^\circ\text{)} \end{aligned}$$

- likely seat for the Solar dynamo
  - magnetic field + shear

LETTER

doi:10.1038/nature10612

Fast core rotation in red-giant stars as revealed by gravity-dominated mixed modes

Paul G. Beck[1], Josefina Montalban[2], Thomas Kallinger[1,3], Joris De Ridder[1], Conny Aerts[1,4], Rafael A. García[5], Saskia Hekker[6,7], Marc-Antoine Dupret[2], Benoit Mosser[8], Patrick Eggenberger[9], Dennis Stello[10], Yvonne Elsworth[7], Søren Frandsen[11], Fabien Carrier[1], Michel Hillen[1], Michael Gruberbauer[12], Jørgen Christensen-Dalsgaard[11], Andrea Miglio[7], Marica Valentini[2], Timothy R. Bedding[10], Hans Kjeldsen[11], Forrest R. Girouard[13], Jennifer R. Hall[13] & Khadeejah A. Ibrahim[13]

When the core hydrogen is exhausted during stellar evolution, the central region of a star contracts and the outer envelope expands and cools, giving rise to a red giant. Convection takes place over much of the star's radius. Conservation of angular momentum requires that the cores of these stars rotate faster than their envelopes; indirect evidence supports this[1,2]. Information about the angular-momentum distribution is inaccessible to direct observations, but it can be extracted from the effect of rotation on oscillation modes that probe the stellar interior. Here we report an increasing rotation rate from the surface of the star to the stellar core in the interiors of red giants, obtained using the rotational frequency splitting of recently detected 'mixed modes'[3,4]. By comparison with theoretical stellar models, we conclude that the core must rotate at least ten times faster than the surface. This observational result confirms the theoretical prediction of a steep gradient in the rotation profile towards the deep stellar interior[1,5,6].

because that would not lead to a consistent multiplet appearance over several orders such as that shown in Fig. 1. The spacings in period between the multiplet components (Supplementary Fig. 7) are too small to be attributable to consecutive unsplit mixed modes[4] and do not follow the characteristic frequency pattern of unsplit mixed modes[3]. Finally, the projected surface velocity, $v \sin i$, obtained from ground-based spectroscopy (Table 1), is consistent with the rotational velocity measured from the frequency splitting of the mixed mode that predominantly probes the outer layers. We are thus left with rotation as the only cause of the detected splittings.

The observed rotational splitting is not constant for consecutive dipole modes, even within a given dipole forest (Fig. 1b and Supplementary Figs 3b and 5b). The lowest splitting is generally present for the mode at the centre of the dipole forest, which is the mode with the largest amplitude in the outer layers. Splitting increases for modes with a larger gravity component, towards the wings of the dipole mode

Rotation in Red Giants

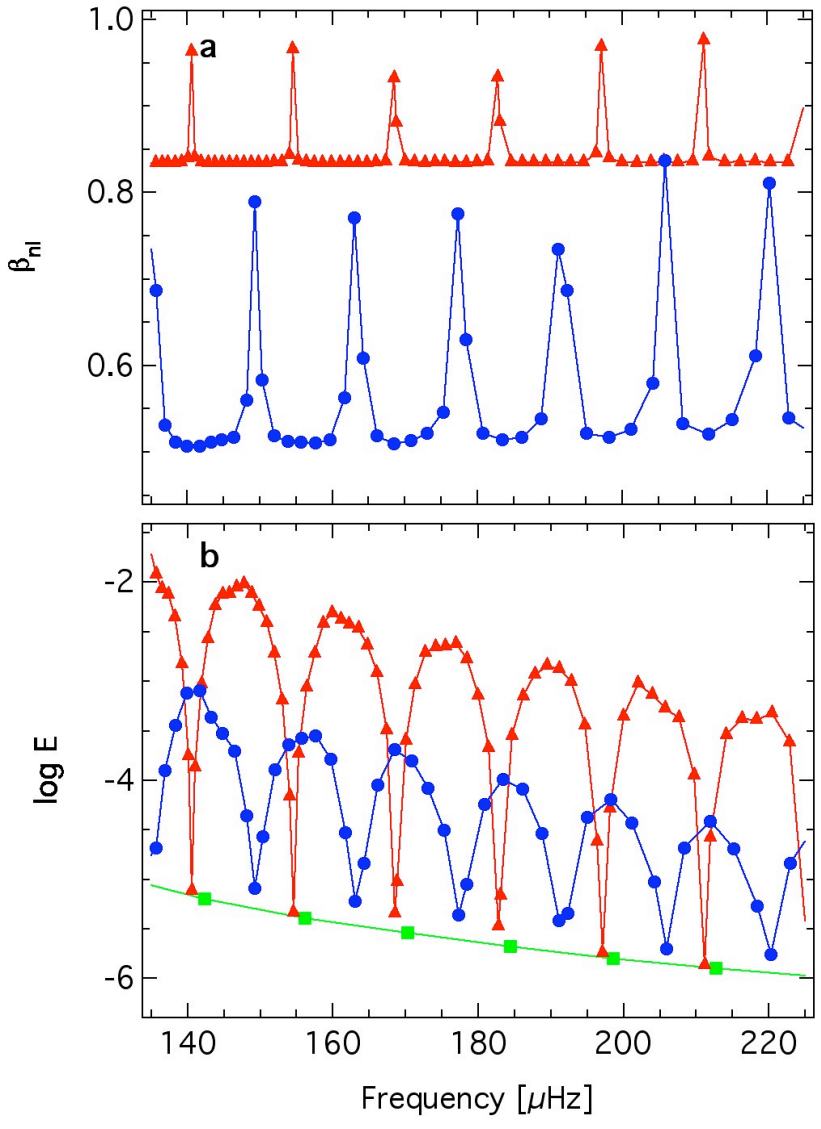

Supplementary Figure 8. The value β_{nl} and mode inertia for a representative stellar model of KIC 8366239. a, β_{nl} as a function of mode frequency for oscillation modes of spherical degree ℓ=1 and ℓ=2 **b,** The corresponding mode inertia log(E) of these modes. Modes of degree ℓ=0, ℓ=1, ℓ=2 are drawn in green, blue, and red, respectively.

A&A 548, A10 (2012)
DOI: 10.1051/0004-6361/201220106

Astronomy & Astrophysics

Spin down of the core rotation in red giants⋆

B. Mosser[1], M. J. Goupil[1], K. Belkacem[1], J. P. Marques[2], P. G. Beck[3], S. Bloemen[3], J. De Ridder[3], C. Barban[1], S. Deheuvels[4], Y. Elsworth[5], S. Hekker[6,5], T. Kallinger[3], R. M. Ouazzani[7,1], M. Pinsonneault[8], R. Samadi[1], D. Stello[9], R. A. García[10], T. C. Klaus[11], J. Li[12], S. Mathur[13], and R. L. Morris[12]

ABSTRACT

Context. The space mission *Kepler* provides us with long and uninterrupted photometric time series of red giants. We are now able to probe the rotational behaviour in their deep interiors using the observations of mixed modes.
Aims. We aim to measure the rotational splittings in red giants and to derive scaling relations for rotation related to seismic and fundamental stellar parameters.
Methods. We have developed a dedicated method for automated measurements of the rotational splittings in a large number of red giants. Ensemble asteroseismology, namely the examination of a large number of red giants at different stages of their evolution, allows us to derive global information on stellar evolution.
Results. We have measured rotational splittings in a sample of about 300 red giants. We have also shown that these splittings are dominated by the core rotation. Under the assumption that a linear analysis can provide the rotational splitting, we observe a small increase of the core rotation of stars ascending the red giant branch. Alternatively, an important slow down is observed for red-clump stars compared to the red giant branch. We also show that, at fixed stellar radius, the specific angular momentum increases with increasing stellar mass.
Conclusions. Ensemble asteroseismology indicates what has been indirectly suspected for a while: our interpretation of the observed rotational splittings leads to the conclusion that the mean core rotation significantly slows down during the red giant phase. The slow-down occurs in the last stages of the red giant branch. This spinning down explains, for instance, the long rotation periods measured in white dwarfs.

Rotation in Red Giants

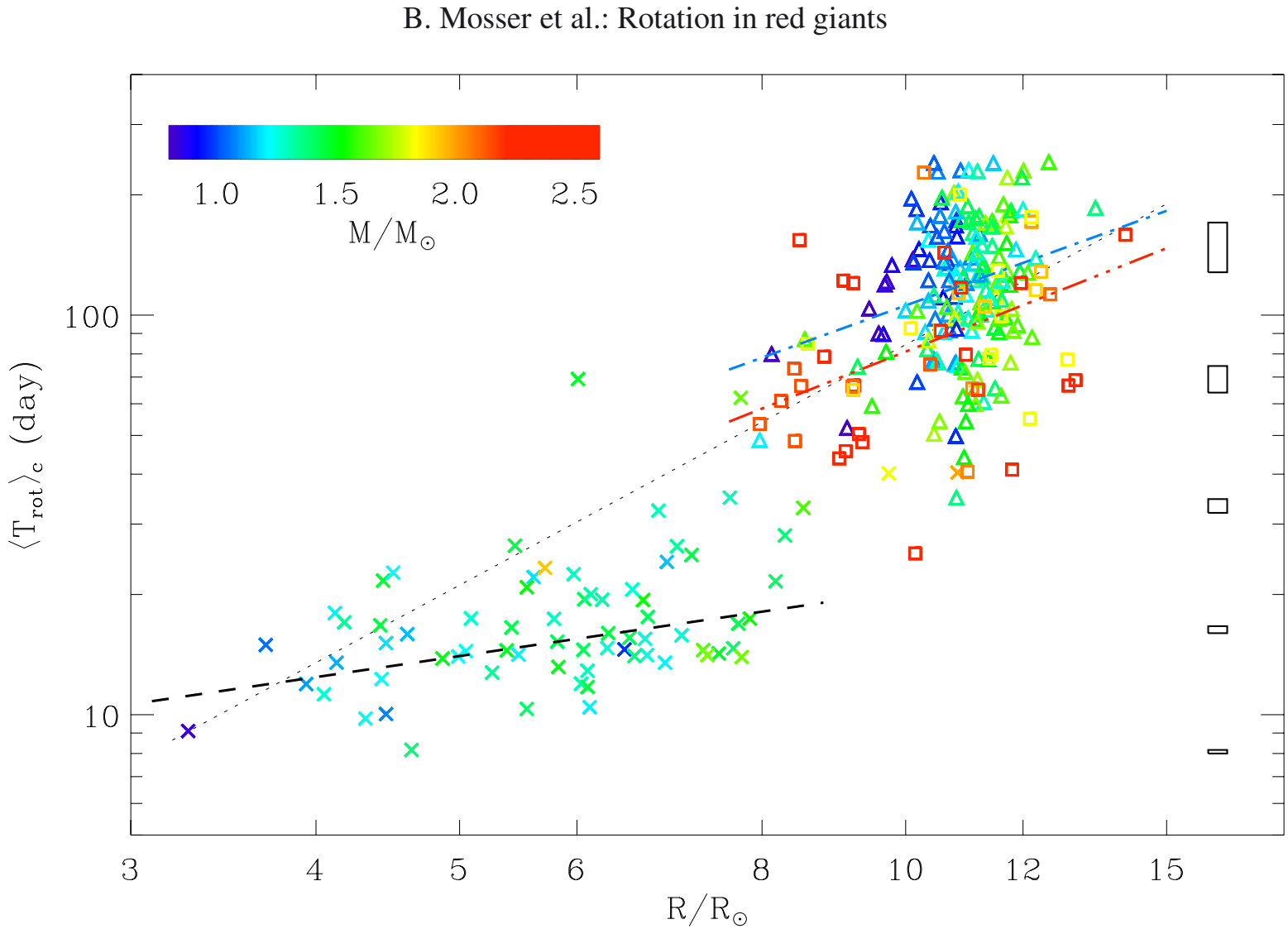

Fig. 9. Mean period of core rotation as a function of the asteroseismic stellar radius, in log-log scale. Same symbols and color code as in Fig. 6. The dotted line indicates a rotation period varying as R^2. The dashed (dot-dashed, triple-dot-dashed) line indicates the fit of RGB (clump, secondary clump) core rotation period. The rectangles in the right side indicate the typical error boxes, as a function of the rotation period.

Pulsations of Other Classes of Stars

- white dwarf stars:
  - DOV, DBV, and DAV stars
- sdB pulsators (EC14026 stars)
- classical Cepheids
- roAp stars
- β Cephei stars
- δ Scuti stars
- γ Doradus stars
- Solar-like pulsators

(Christensen-Dalsgaard 1998)

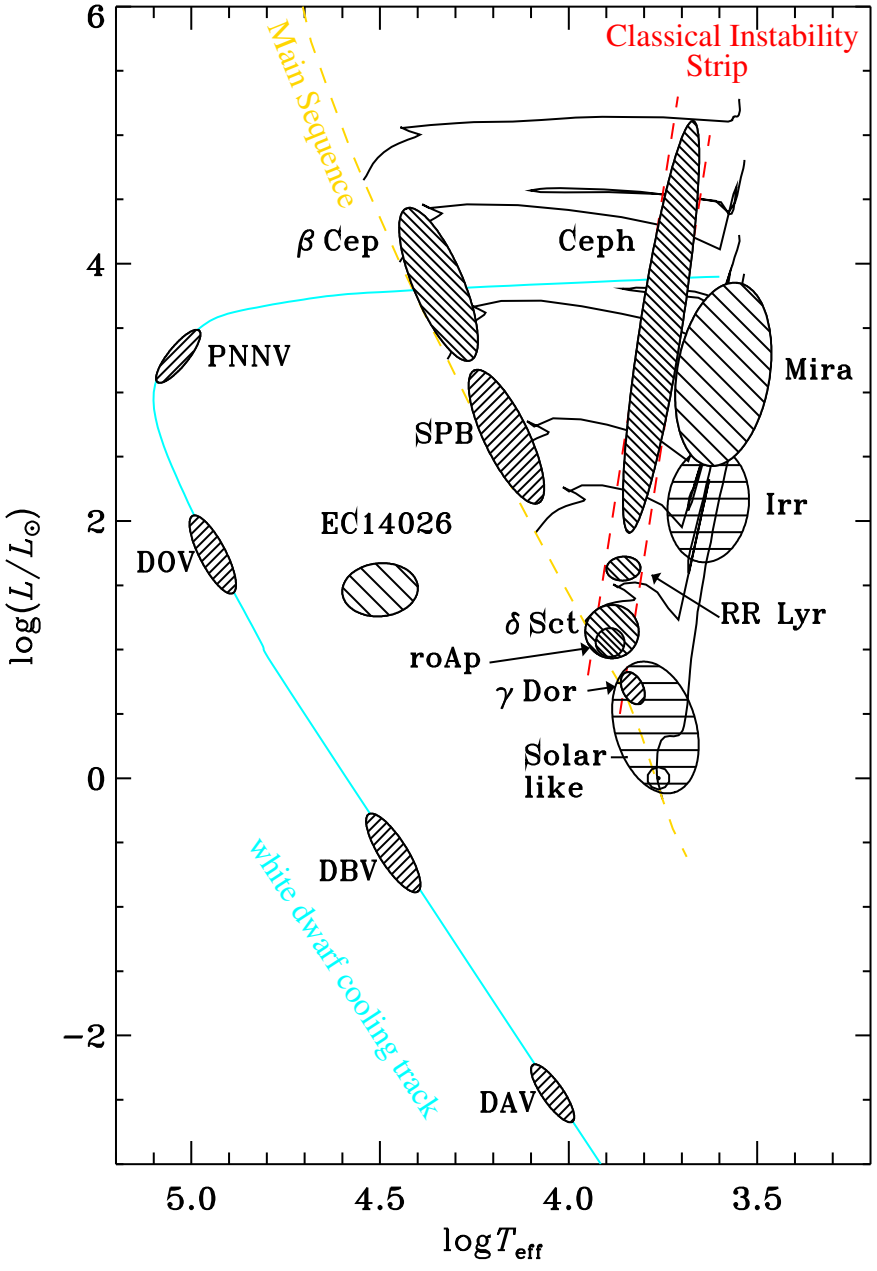

White Dwarf Pulsators

- richest pulsators other than the Sun (many modes simultaneously present)
- many are *large* amplitude pulsators ($\delta I/I \sim 0.05$ for a given mode, nonlinear)
- pulsations are due to g-modes, periods of $\sim$ 200–1000 sec
- pulsations are probably excited by "convective driving" (Brickhill 1991, Goldreich & Wu 1999), and possibly also by the kappa mechanism

  DAVs: pure H surface layer, driving due to H ionization zone

  DBVs: pure He surface layer, driving due to He ionization zone (predicted to pulsate by Winget et al. 1983, ApJ, 268, L33 *before* they were observed)

White Dwarf Pulsators (cont.)

- asymptotic formula for g-mode periods is

$$P_{n\ell} = \frac{2\pi^2 n}{[\ell(\ell+1)]^{1/2}} \left[\int_{r1}^{r2} \frac{N}{r} dr \right]^{-1}$$

$\Rightarrow$ *Periods* (not frequencies) are evenly spaced in n ($n = 1, 2, 3 \ldots$)

- as for p-modes, solid-body rotation splits degenerate modes into $2\,\ell + 1$ components:

  $\ell = 1 \longrightarrow 3$ distinct frequencies
  $\ell = 2 \longrightarrow 5$ distinct frequencies

- in many cases, asteroseismology of a particular object has led to an accurate determination of some subset of the following: the mass, temperature, rotation frequency, surface hydrogen or helium layer mass, and C/O abundance ratio in the core

A DOV star: PG 1159-035

- 125 individual frequencies observed
- both $\ell = 1$ and 2 modes observed

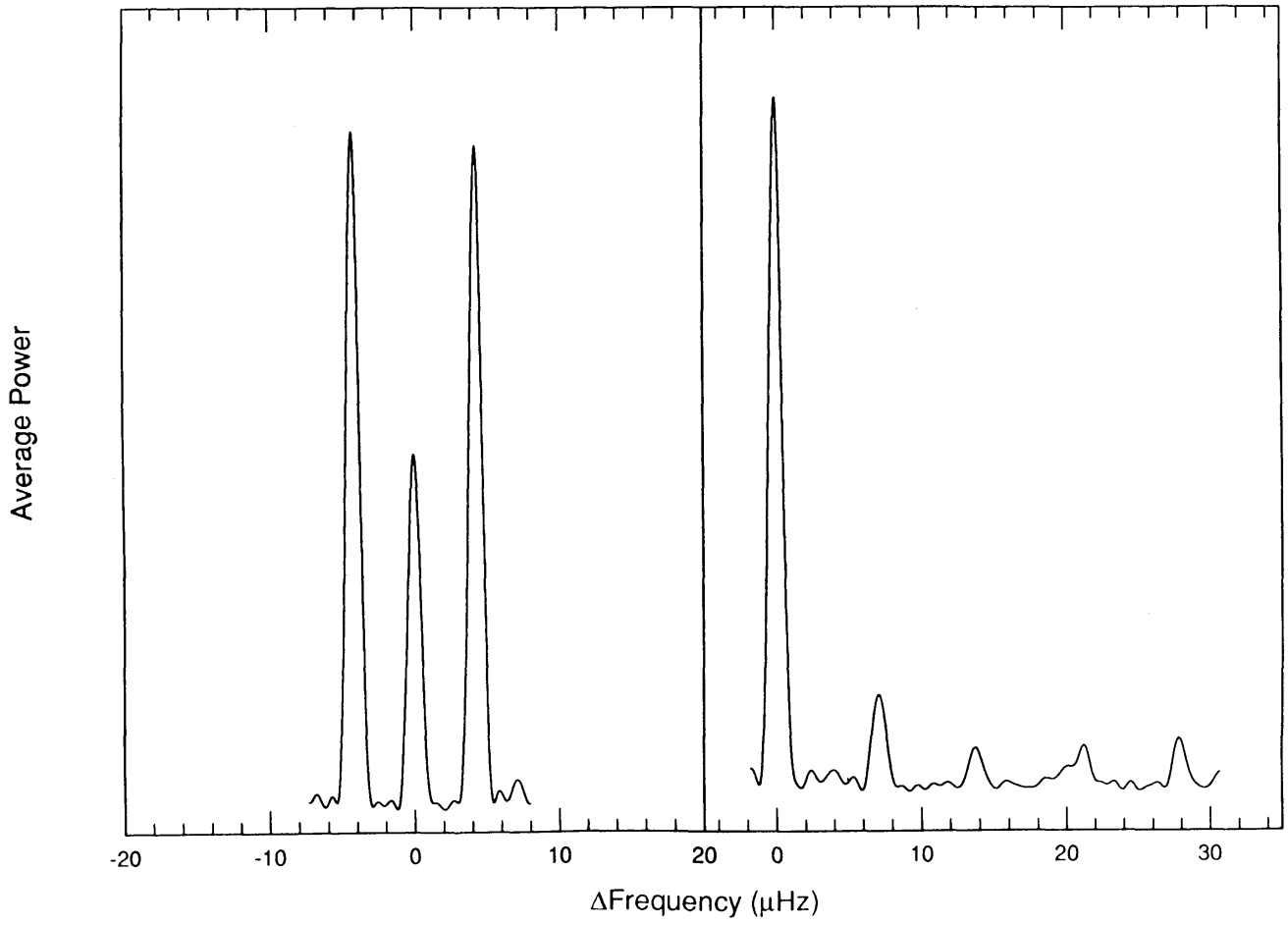

FIG. 6.—Average of the power in the multiplets shown in Fig. 4 for $l = 1$ (*left panel*) and $l = 2$ (*right panel*)

A DOV star: PG 1159-035 (cont.)

(Winget, D. E. et al. 1991, ApJ, 378, 326)

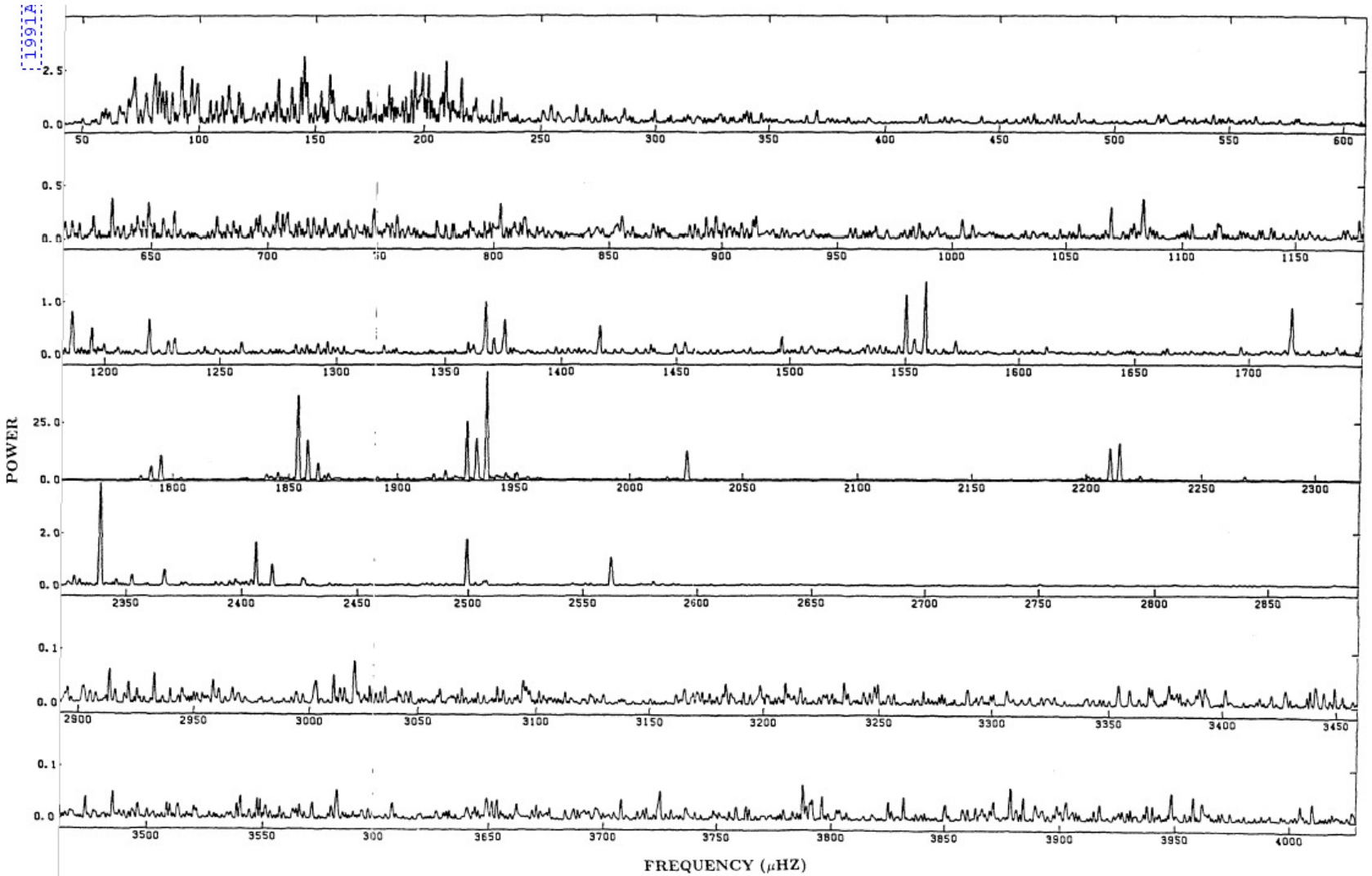

FIG. 4.—Power spectrum of the complete data set, shown as power in units of 10^{-6} vs. frequency in μHz. The vertical scale is different for each panel in an attempt to accommodate the dynamic range.

A DOV star: PG 1159-035 (cont.)

- proved beyond a shadow of a doubt that the modes were g-modes corresponding to $\ell = 1$, 2
- asteroseismologically derived parameters:

mass:	$0.586 \pm 0.003\ M_\odot$
rotation period:	1.38 ± 0.01 days
magnetic field:	$\lesssim 6000$ G

A DBV star: GD 358

10 consecutive $\ell = 1$ radial orders observed, with n=8–17

(Winget et al. 1994, ApJ, 430, 839)

IDENTIFIED FREQUENCIES FOR $\ell = 1$, 1000–2400 μHz

k	m	Frequency (μHz)	Power (μmp)	|Δ Frequency| (μHz)	Period (s)
17.....	−1	1291.00	24.5	6.58	774.59
	0	1297.58	210.7		770.67
	+1	1304.12	34.1	6.54	766.80
16.....	−1	1355.58	2.4	6.27	737.69
	0	1361.85	12.0		734.30
	+1	1368.50:	7.1	6.65	730.73
15.....	−1	1421.27	87.0	6.00	703.40
	0	1427.27	362.1		700.64
	+1	1434.04	82.4	6.77	697.33
14.....	−1	1512.72	12.6	6.23	661.06
	0	1518.95	69.7		658.35
	+1	1525.62	18.4	6.67	655.47
13.....	−1	1611.80	39.4	5.58	620.42
	0	1617.38	33.4		618.28
	+1	1623.49	29.8	6.11	615.96
12.....	0	1733.88:	1.8		576.76
11.....	−1	1840.46:	2.6	5.42	543.34
	0	1845.88:	1.8		541.75
	+1	1852.12	1.6	6.24	539.92
10.....	−1	1989.26:	0.3	4.42	502.70
	0	1993.68:	1.2		501.59
	+1	1998.83:	1.5	5.15	500.29
9.....	−1	2150.57:	2.1	3.53	464.99
	0	2154.10	20.5		464.23
	+1	2157.67	7.4	3.57	463.46
8.....	−1	2358.85	23.6	3.71	423.94
	0	2362.56	24.8		423.27
	+1	2366.46	12.3	3.90	422.57

Power spectrum of the white dwarf GD 358

(Winget, D. E. et al. 1994, ApJ, 430, 839)

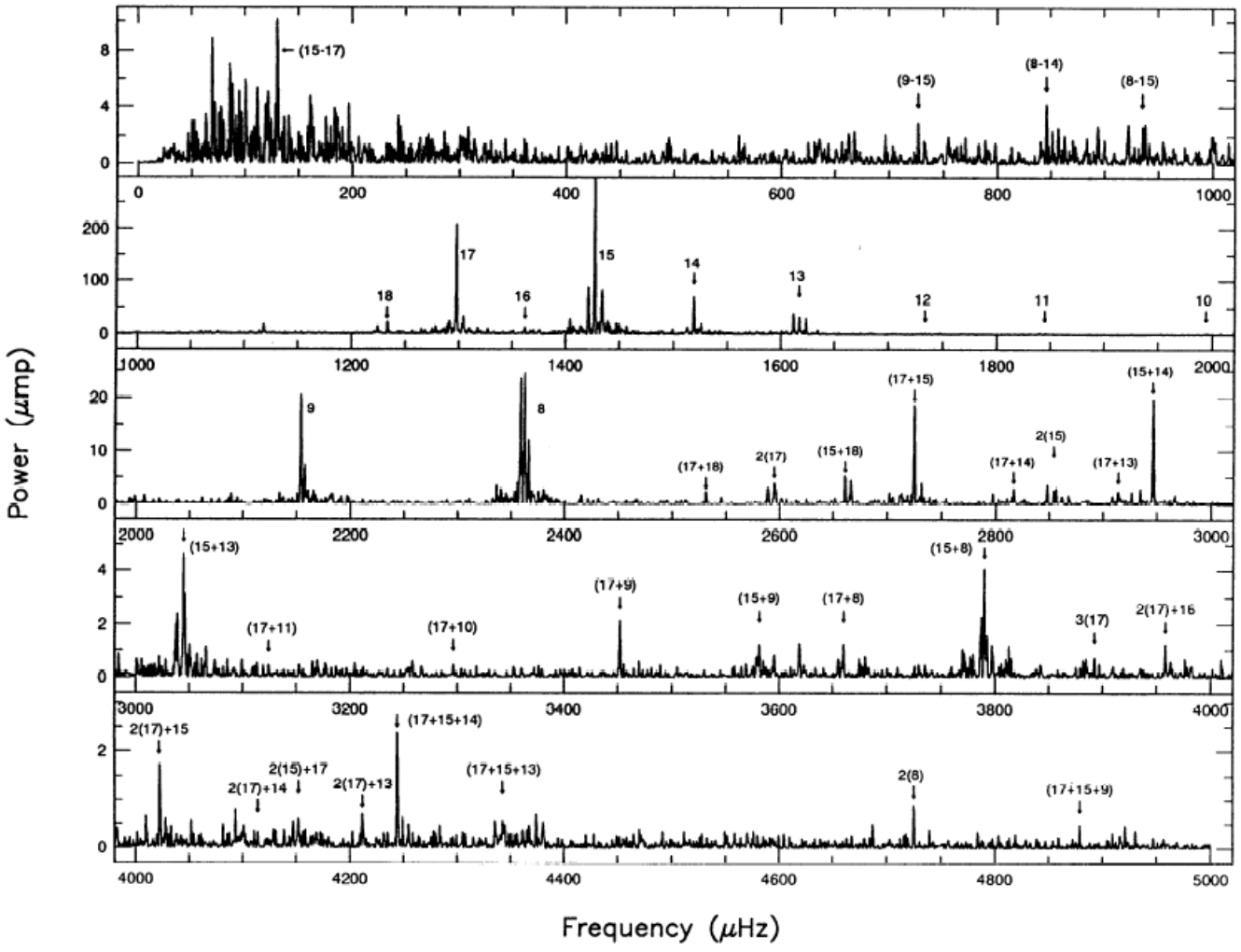

FIG. 7.—Full power spectrum of GD 358. The different scales for each panel attempt to accommodate the large dynamic range present. Triplets are labeled with their corresponding *k*-value, and the sum and difference frequencies are labeled with the *k*-values for the triplets which combine to form them.

GD 358 (cont.)

- asteroseismologically derived parameters
  (Bradley & Winget 1994, Winget et al. 1994):

mass:	$0.61 \pm 0.03\ M_\odot$
$M_{\rm He}$:	$2 \pm 1 \times 10^{-6}\ M_\star$
rotation period:	$\sim$ 0.9–1.6 days differential rotation implied
luminosity:	$0.05 \pm 0.012 L_\odot$
distance:	42 ± 3 pc

- measured parallax for GD 358 is 36 ± 4 pc

$\Rightarrow$ agrees with asteroseismologically derived distance

However, looking more carefully reveals *two* classes of asteroseismological fits…

GD 358 (cont.)

Models with a changing C/O profile in the core (Metcalfe 2003)

Models with a uniform core and a two-tiered helium profile in the envelope (Fontaine & Brassard 2002)

[the data are solid lines, filled circles, models are dashed lines, open circles]

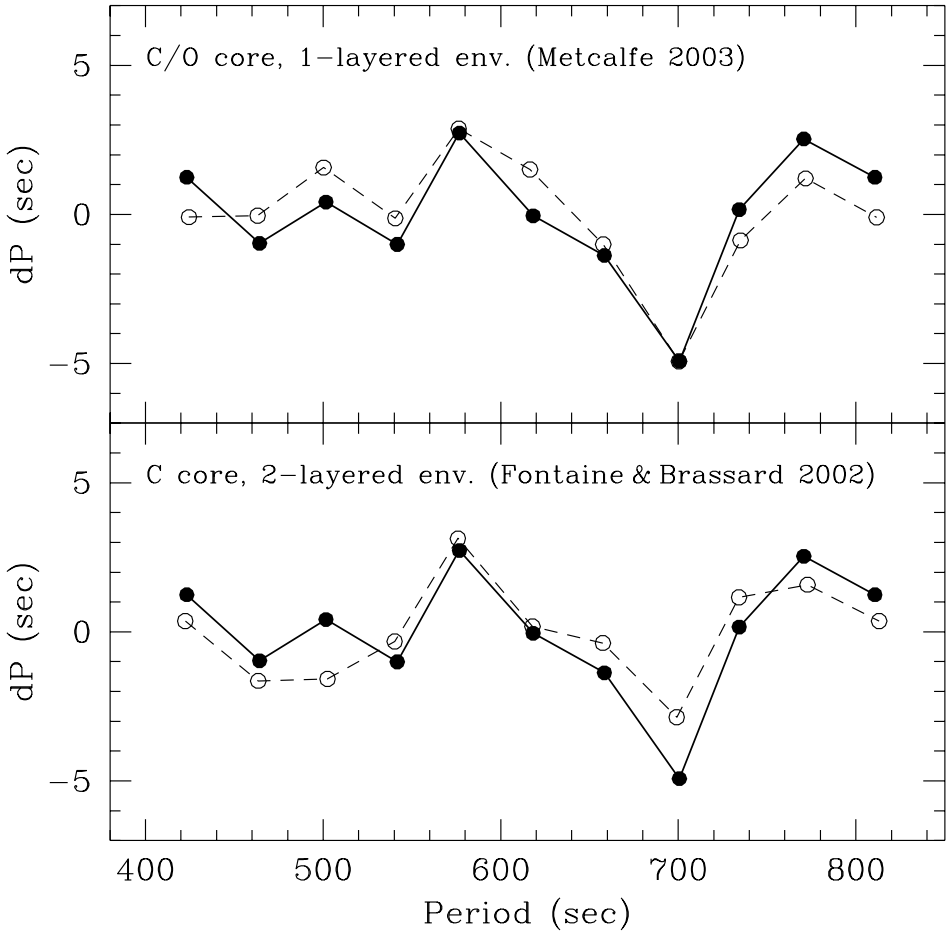

This can be explained as an example of the “core/envelope” symmetry in pulsating white dwarfs that we discussed previously.

GD 358 (cont.)

Genetic algorithm fitting techniques have recently been applied to white dwarf modeling (e.g., Metcalfe et al. 2000, ApJ, 545, 974, Metcalfe, Montgomery, & Kawaler 2003):

- explore possibility of a ^{3}He layer

  (Montgomery, Metcalfe, & Winget 2001, ApJ, 548, L53)
- constrain the $^{12}\mathrm{C}(\alpha,\gamma)^{16}\mathrm{O}$ reaction rate

  (Metcalfe 2003)
- constrain the mass fraction of oxygen in the core: $X_\mathrm{O} = 67$–76 %

  (Metcalfe 2003; Metcalfe, Winget, & Charbonneau 2001, ApJ, 557, 1021)
- constrain neutrino emission rates, compare with Standard Model of particle physics

  (Winget et al. 2004, ApJ, 602, L109)

A DAV: BPM 37093

- White dwarfs predicted to crystallize as they cool (Abrikosov 1960, Kirzhnitz 1960, and Salpeter 1961)
- crystallization delays cooling, adds ~ 2 Gyr to Galactic disk ages based on white dwarf cooling
- promise of deriving the crystallized mass fraction *asteroseismologically*

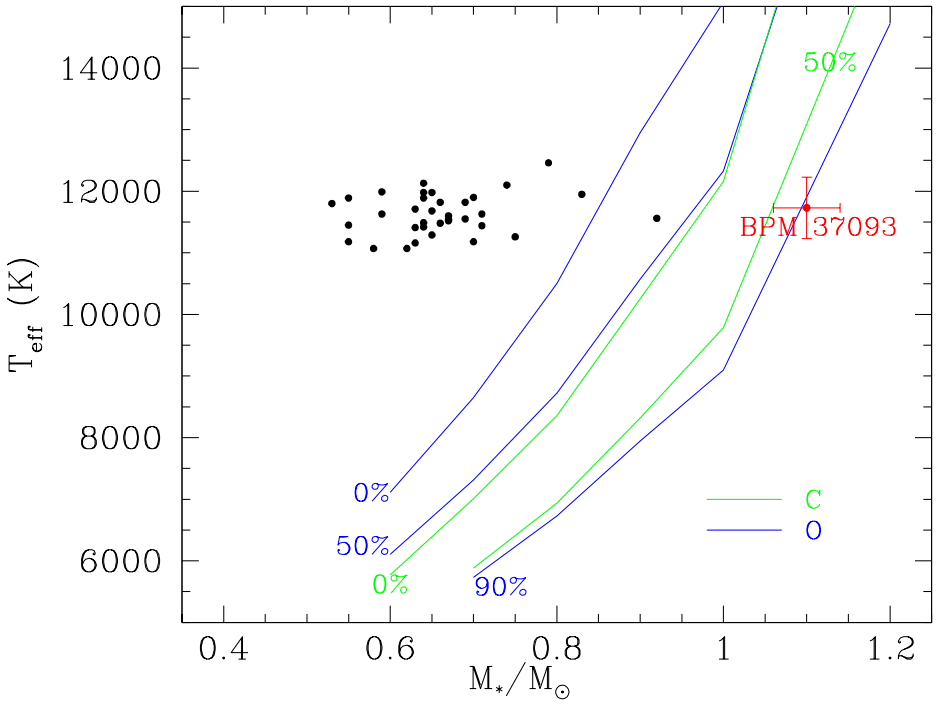

High mass $\Rightarrow$ crystallized

(Montgomery & Winget 1999, ApJ, 526, 976)

BPM 37093 (cont.)

- BPM 37093 has been extensively observed with the Whole Earth Telescope (WET)

The effect of the crystallized core is to exclude the pulsations from it (Montgomery & Winget 1999)

Preliminary results:

BPM 37093 is ~ 90 % crystallized by mass

(Metcalfe, Montgomery, & Kanaan 2004)

This would be the first "detection" of the crystallization process in a stellar interior.

As a cross-check of our approach, we will do a similar analysis for a low-mass star which should be uncrystallized, and we will check if we do indeed find a best fit having 0% crystallization.

The Classical Cepheids

Yellow giants and supergiants, radial pulsators, 1 or 2 modes excited, periods $\sim 1 - 50$ days. This is

- great for Period-Luminosity relationship (purely empirical)
- bad for seismology – not enough modes!

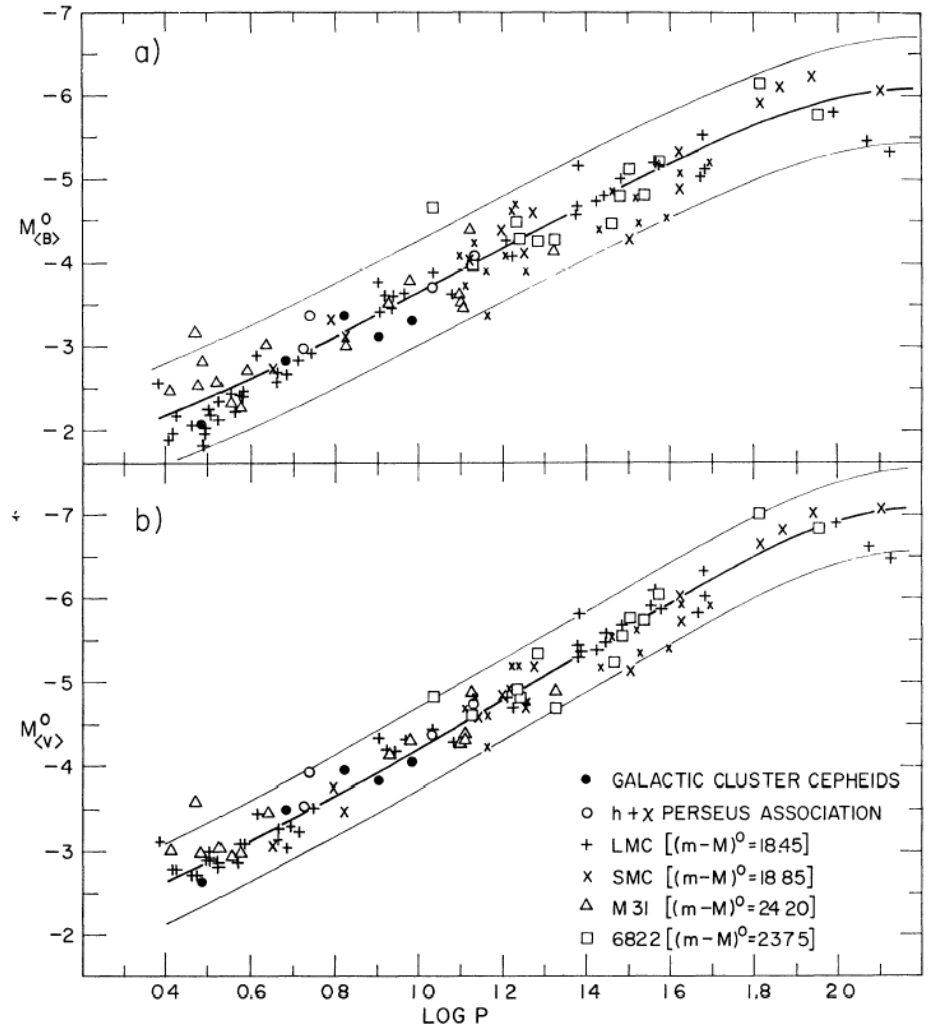

FIG. 1.—The composite period-luminosity relation at mean intensity in *B* and *V* wavelengths derived from the sources indicated at the lower right. The absolute calibration was made by using the nine Cepheids of the galactic system shown as open and filled circles. The photographic data from the SMC are plotted with smaller crosses than the Gascoigne and Kron photoelectric data.

(Sandage & Tammann 1968)

Subdwarf B/EC 14026 stars

- are Extreme Horizontal Branch (EHB) stars
- recently predicted and *then* observed to pulsate (Charpinet et al. 1996, ApJ, 471, L103)
- $T_{\rm eff} \sim 35,000$ K, $\log g \sim 5.9$
- driving is due to an opacity bump due to metals (in this case, mainly Fe), as in the β Cephei stars
- gravitational settling and radiative levitation work to increase the abundance of Fe in regions of the envelope, enhancing the driving effect

Subdwarf B/EC 14026 stars

Typical lightcurves of pulsating sdB stars

(Charpinet et al. 2009, AIP Conf. Proc. 1170, 585)

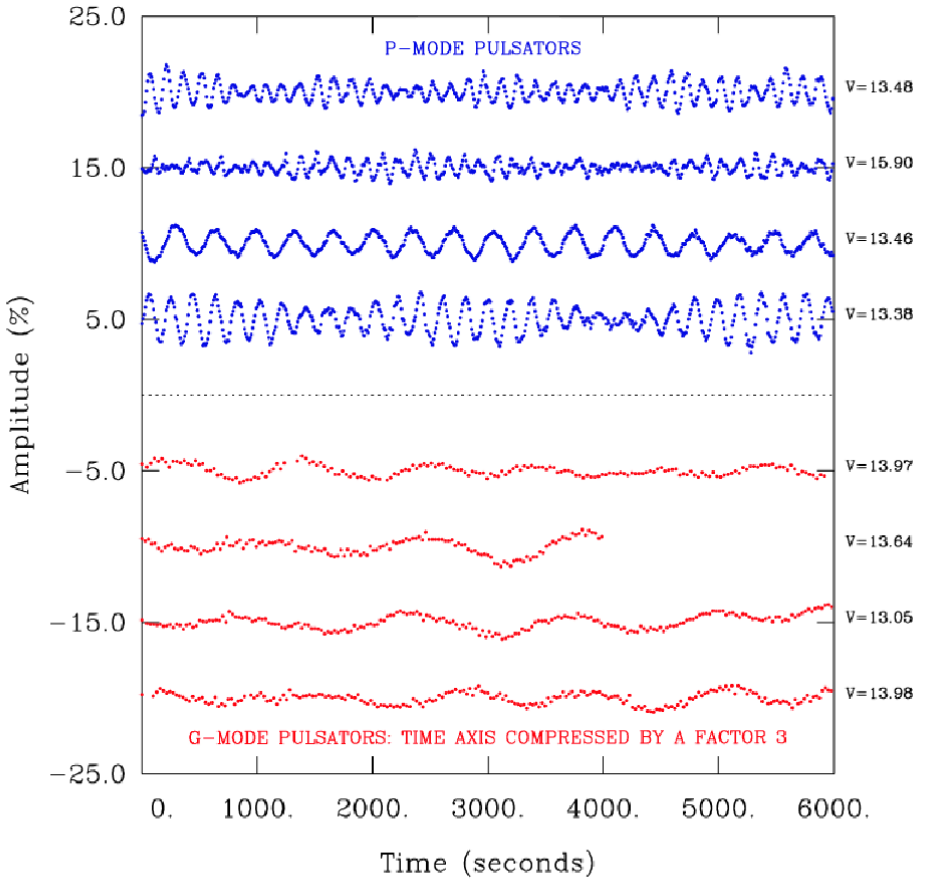

FIGURE 5. Typical lightcurves for pulsating sdB stars. The upper part (in blue) shows sections of lightcurves obtained for four rapid sdB pulsators (the V361 Hya stars) through PMT broadband photometry using a uniform sampling of 10 s. The lower part (in red) shows lightcurves obtained for four long period sdB pulsators (the V1093 Her stars) through CCD R-band photometry using a nearly constant sampling time of ~ 80 s.

Subdwarf B/EC 14026 stars

(Charpinet et al. 2009, AIP Conf. Proc. 1170, 585)

TABLE 2. Structural parameters from asteroseismology for a sample of 11 p-mode sdB pulsators.

Name	$T_{\rm eff}$	$\log g$	$\log M_{\rm env}/M_*$	M_*	References
PG 1047+003	33150 ± 200	5.800 ± 0.006	-3.72 ± 0.11	0.490 ± 0.014	[11]
PG 0014+067	34130 ± 370	5.775 ± 0.009	-4.32 ± 0.23	0.477 ± 0.024	[10]
PG 1219+534	33600 ± 370	5.807 ± 0.006	-4.25 ± 0.15	0.457 ± 0.012	[8]
Feige 48	29580 ± 370	5.437 ± 0.006	-2.97 ± 0.09	0.460 ± 0.008	[9]
PG 1325+101	35050 ± 220	5.811 ± 0.004	-4.18 ± 0.10	0.499 ± 0.011	[7]
EC 20117–4014	34800 ± 2000	5.856 ± 0.008	-4.17 ± 0.08	0.540 ± 0.040	[43]
PG 0911+456	31940 ± 220	5.777 ± 0.002	-4.69 ± 0.07	0.390 ± 0.010	[40]
BAL 090100001	28000 ± 1200	5.383 ± 0.004	-4.89 ± 0.14	0.432 ± 0.015	[46]
PG 1336–018	32780 ± 200	5.739 ± 0.002	-4.54 ± 0.07	0.459 ± 0.005	[5]
EC 09582–1137	34806 ± 233	5.788 ± 0.004	-4.39 ± 0.10	0.485 ± 0.011	[38]
PG 0048+091	33335 ± 1700	5.711 ± 0.010	-4.92 ± 0.20	0.447 ± 0.027	in prep

Other Pulsators

roAp stars: "rapidly oscillating Ap stars"

- have magnetic fields and peculiar chemical abundances
- p-mode oscillators (~ 5 minute periods) with the pulsation axis inclined relative to the magnetic axis
- driving mechanism not yet established

delta Scuti stars:

- ~ 1.6–$2.5\,M_{\odot}$
- p-mode oscillators, periods of hours
- driven by the standard Kappa mechanism

Other Pulsators (cont.)

Gamma Doradus Stars:

- g-mode oscillators, periods of one to several days
- probably driven by “convective driving”
- long periods make it difficult to do asteroseismology

Solar-like stars:

- p-mode oscillators
- stochastically driven (by convection zone)
- periods of several minutes

Observed frequencies in beta Hydri (Bedding et al. 2001, cyan curve) compared to a scaled solar spectrum (yellow curve)

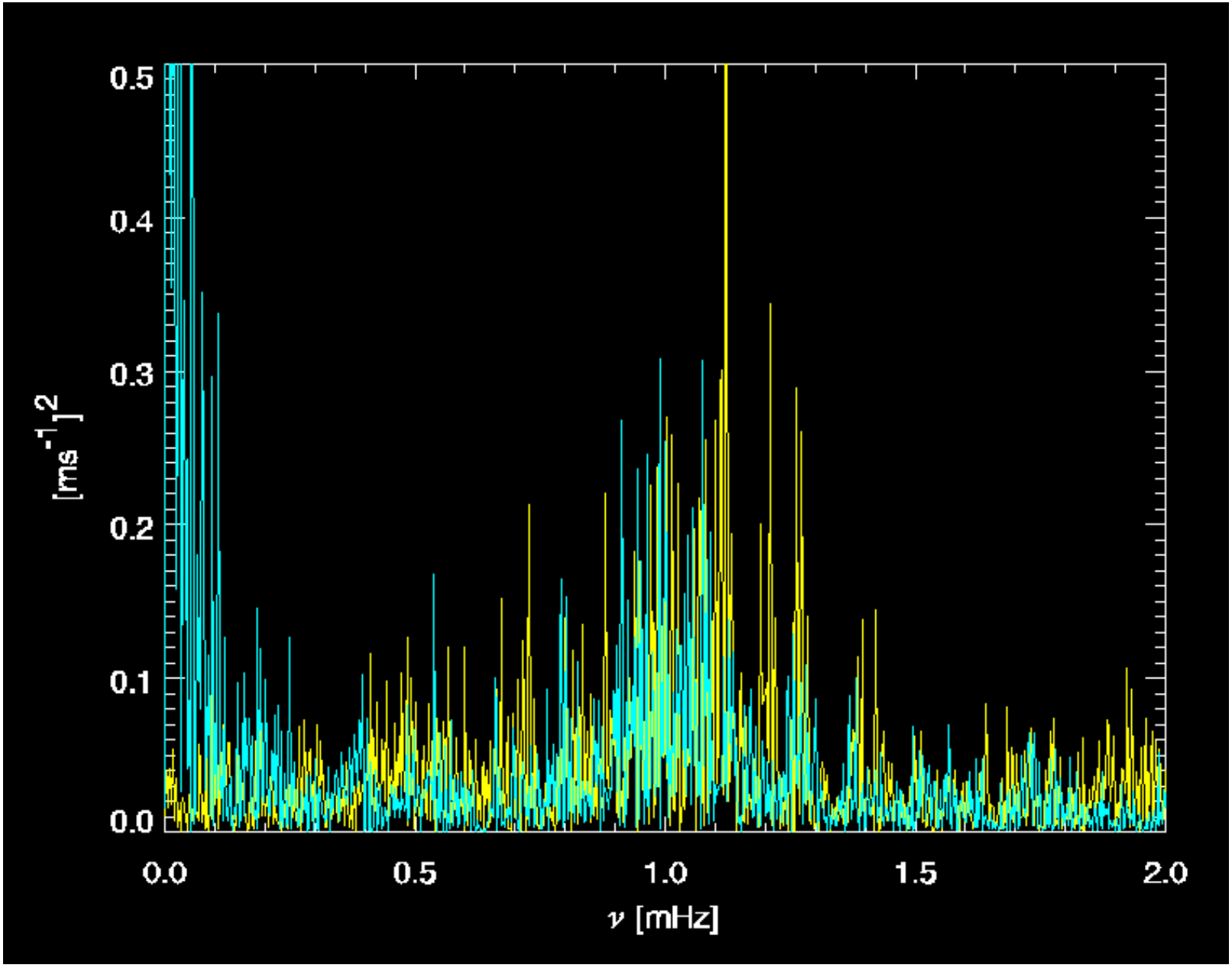

Electronic copies of these notes (in living color) can be found at:

www.as.utexas.edu/~mikemon/pulsations.pdf

Good luck!